



University
of Glasgow

Thomson, Douglas G. (1987) *Evaluation of helicopter agility through inverse solution of the equations of motion*. PhD thesis.

<http://theses.gla.ac.uk/4927/>

Copyright and moral rights for this thesis are retained by the author

A copy can be downloaded for personal non-commercial research or study, without prior permission or charge

This thesis cannot be reproduced or quoted extensively from without first obtaining permission in writing from the Author

The content must not be changed in any way or sold commercially in any format or medium without the formal permission of the Author

When referring to this work, full bibliographic details including the author, title, awarding institution and date of the thesis must be given

EVALUATION OF HELICOPTER AGILITY THROUGH INVERSE
SOLUTION OF THE EQUATIONS OF MOTION

by

Douglas G. Thomson, B.Sc.

Dissertation submitted to the Faculty of Engineering, University of
Glasgow, for the Degree of Doctor of Philosophy

May, 1987

© D.G. Thomson, 1987.

CONTENTS

Acknowledgements	i
Abstract	ii
Nomenclature	iii
Chapter 1 Introduction : Methods of Quantifying Agility	1
1.1 Introduction	1
1.2 Overall and Inherent Agility	3
1.3 Methods of Studying Agility	4
1.4 A General Method of Quantifying Helicopter Inherent Agility	7
Chapter 2 Inverse Solution of Helicopter Equations of Motion	12
2.1 Introduction	12
2.2 Definition of an Inverse Solution	16
2.3 Defining the Flight Path	18
2.4 The Numerical Algorithm	35
2.5 Some Examples	46
2.6 Validation of Results	51
2.7 Discussion and Analysis of Inverse Algorithm	55
2.8 Conclusions	64
Chapter 3 An Analytic Method of Quantifying Helicopter Inherent Agility	65
3.1 Introduction	65
3.2 Relating Agility to Inverse Solutions	66
3.3 The Agility Performance Index (API)	67

3.4	Selection of Maximum State Values	73
3.5	Selection of Weighting Constants	75
3.6	Agility Ratings	87
3.7	Example Calculations of Agility Ratings	94
3.8	Alternative Methods of Quantifying Agility Using Inverse Solutions	95
3.9	Conclusions	97
Chapter 4	Configurational Studies Using the Agility Evaluation Program	98
4.1	Introduction	98
4.2	The Influence of Tailplane Area on Inherent Agility	99
4.3	The Configurational Design of an "Advanced Rotor Helicopter"	104
4.4	Conclusions	107
Chapter 5	Conclusions	108
	Appendices	111
Appendix 1	Helicopter Equations of Motion	111
Appendix 2	Transformation Between Axes Systems	112
Appendix 3	Calculation of Turn Rate from Flight Path Geometry	115
Appendix 4	The Helicopter Mathematical Model	116
Appendix 5	Calculation of $\dot{\psi}$ and $\dot{\chi}$ in Sideslip Constrained Flight	131
Appendix 6	Numerical Differentiation	133
Appendix 7	Rotational Velocities and Accelerations	135
Appendix 8	Linearised Approach to Inverse Problem	136

Appendix 9	Calculation of the Volume Under an Agility Surface	146
	References	148
	Tables	152
	Figures	157

Acknowledgements

The author wishes to express gratitude to the following individuals: Mr Roy Bradley and Dr Alistair Caldwell, for their guidance and encouragement whilst supervising the project; Dr Gareth Padfield of Flight Systems Division, Royal Aircraft Establishment, Bedford, for his role as external supervisor; Professor Bryan Richards for his support; and Dr Stewart Houston, for his assistance in the early stages of the project.

Thanks are also due to Mrs Linda McCormick of the Glasgow University Computer Aided Engineering Centre, Miss Margaret Simpson, Aeronautics and Fluid Mechanics departmental secretary, and Mr Stephen Bryce, who proof read the manuscript.

The project was funded by the Science and Engineering Research Council as a Co-operative Award in Science and Engineering, with the Ministry of Defence (RAE Bedford) as external collaborating body.

Abstract

Helicopter agility in nap-of-the-earth flight is widely recognised to be of great importance. Despite this, a general method of quantifying agility does not exist. All previous attempts to quantify agility have been restricted either to flight tests or to simple kinematic modelling - both with obvious disadvantages. A method of quantifying helicopter inherent agility, the agility of the configuration independent of the pilot, utilising inverse solutions of the equations of motion has been developed.

A value for the inherent agility of a helicopter is given by studying its performance over a series of standard manoeuvres. The manoeuvres used represent typical tasks undertaken by the configuration under study. The combination of these tasks represent the helicopter's operational role. The helicopter's performance over these standard manoeuvres is found by using an inverse solution of the equations of motion - calculation of the control, and resulting state, time histories needed to fly a given flight path. A six degrees of freedom non-linear mathematical model is used to simulate single main and tail rotor helicopter flight dynamics. The helicopter's performance over each manoeuvre is rated by a quadratic performance function of the state and control variables. The performance function is weighted in such a manner as to penalise undesirably large displacements in the state and control variables of particular importance to that manoeuvre (e.g. large nose down attitude changes in accelerated flight are heavily penalised). An Agility Rating is awarded to a helicopter on the basis of its performance over a wide range of similar manoeuvres, a measure of total inherent agility being a function of the agility ratings for all the manoeuvres relevant to the helicopter's role.

The method is illustrated by applying it to two agility studies. Firstly, it is used to show how an optimum tailplane area can be calculated for manoeuvres in the longitudinal plane. Then an "Advanced Rotor Helicopter" is compared with a contemporary battlefield helicopter.

NOMENCLATURE

List of Symbols

a_{xb}, a_{yb}, a_{zb}	components of acceleration of blades
a_{otp}	lift curve slope of tailplane section
a_{otr}	lift curve slope of tail rotor blade section
b	number of main rotor blades
b_{tr}	number of tail rotor blades
c	chord of main rotor blades
c_{tr}	chord of tail rotor blades
C_{Mf}, C_{Nf}	fuselage aerodynamic moment coefficients
C_Q	main rotor torque coefficient
C_T	main rotor thrust coefficient
C_{Ttr}	tail rotor thrust coefficient
C_{Xf}, C_{Yf}, C_{Zf}	fuselage aerodynamic force coefficients
C_{Yfin}	fin sideforce coefficient
C_{Ztp}	tailplane lift coefficient
g	acceleration due to gravity
h	altitude
h_{fin}	height of fin centre of pressure above fuselage reference point
h_R	height of main rotor hub above fuselage reference point
h_{tr}	height of tailrotor centre line above fuselage reference point

$I_{xx}, I_{yy}, I_{zz}, I_{xz}$	moments, and product of inertia
I_{β}	blade flapping inertia
K_{β}	blade flapping stiffness spring constant
L, M, N	external rolling, pitching and yawing moments
L_A, M_A, N_A	aerodynamic components of external moments
l_{fin}	fin centre of pressure location aft of fuselage reference point
L_{TR}, M_{TR}, N_{TR}	components of external moments from main rotor
l_{tp}	tailplane centre of pressure location aft of fuselage reference point
l_{tr}	tail rotor centre line distance from fuselage reference point
L_{TR}, N_{TR}	components of external moments from tail rotor
n	normal load factor
n_{β}	blade inertia number
p, q, r	roll, pitch and yaw rates
p_w, q_w, r_w	roll, pitch and yaw rates in hub-wind axes
r_b	radial location on main rotor blade
R	rotor radius
R_c	radius of curvature of track
R_{tr}	tail rotor radius
s	solidity of main rotor
s	distance along track
S_{fin}	area of fin
S_{tp}	area of tailplane
s_{tr}	solidity of tail rotor

s_{β}	stiffness number
t	time
U_T, U_P	inplane and normal velocities at blade element
u, v, w	translational velocities along the x, y, z body axes
V	flight velocity
X, Y, Z	external forces along the x, y, z body axes
x, y, z	flight path co-ordinates relative to a earth fixed axis system
$\dot{x}, \dot{y}, \dot{z}$	velocity components along x, y, z earth fixed axes
$\ddot{x}, \ddot{y}, \ddot{z}$	acceleration components along x, y, z earth fixed axes
X_A, Y_A, Z_A	aerodynamic components of external forces
x_{cg}	centre of gravity position forward of fuselage reference point
X_R, Y_R, Z_R	rotor components of external forces
Y_{TR}	tail rotor sideforce
Z_{Hw}	force on rotor hub in z -direction, in hub-wind axes
α	fuselage incidence angle
α_{tp}	incidence of tailplane
α_{otp}	fixed incidence of tailplane
β	fuselage sideslip angle
β_0	coning angle
β_{1c}	main rotor longitudinal flapping angle
β_{1cw}, β_{1sw}	main rotor longitudinal and lateral flapping angles in hub-wind axes

β_{1s}	main rotor lateral flapping angle
γ	angle of climb
γ_s	forward shaft angle
δ	main rotor blade profile drag coefficient
δ_0, δ_2	coefficients of blade profile drag law
θ	fuselage pitch attitude angle
θ_{tw}	twist of rotor blade
θ_0	main rotor collective pitch angle
θ_{1c}	main rotor lateral cyclic pitch angle
θ_{1s}	main rotor longitudinal cyclic pitch angle
θ_{otr}	tail rotor collective pitch angle
λ_0	normalised main rotor uniform normal downwash velocity component
λ_{otr}	normalised tail rotor downwash velocity
$\lambda_{1cw}, \lambda_{1sw}$	normalised harmonic components of main rotor downwash velocity in hub-wind axes
λ_β	rotor flapping frequency ratio
μ	normalised rotor hub velocity
μ_{tr}	normalised tail rotor hub velocity
μ_x, μ_y, μ_z	normalised components of rotor hub velocity
μ_{ztr}	normalised z-component of tail rotor hub velocity
ρ	density of air
ϕ	fuselage roll attitude angle
χ	track angle
ψ	fuselage yaw attitude angle
ψ	azimuth position of rotor blade

γ_w	rotor sideslip angle
ω_x, ω_y	angular velocities in rotating co-ordinates
Ω	rotational speed of main rotor
Ω_{tr}	rotational speed of tail rotor

Sign Conventions

Fuselage Attitude

Pitch	+ve	nose up
Roll	+ve	bank to right
Azimuth	+ve	yaw to right

Cyclic Pitch Angles

<i>Longitudinal</i>		+ve	stick back
	BATTLEFIELD configuration	+ve	stick right
<i>Lateral</i>			
	TRANSPORT configuration	+ve	stick left

Tail Rotor Collective Pitch

	BATTLEFIELD configuration	LEFT Rudder
For +ve values :		
	TRANSPORT configuration	RIGHT Rudder

Rotor Direction

	Anticlockwise	BATTLEFIELD
When viewed from above rotor rotates:		
	Clockwise	TRANSPORT

Graph Labels and Dimensions

All time histories plotted from HELINV are given in seconds from the start of the manoeuvre, and are plotted as displacements from the trim value. Graphical output from HELINV uses the following abbreviations as axes labels :

THTO : θ_0 : Main rotor collective pitch : degrees
 THT1S : θ_{1s} : Main rotor longitudinal cyclic pitch : " "
 THT1C : θ_{1c} : Main rotor lateral cyclic pitch : " "
 THOTR : θ_{otr} : Tail rotor collective pitch : " "
 THT : θ : Fuselage pitch attitude : " "
 PHI : ϕ : Fuselage roll angle : " "
 PSI : ψ : Fuselage yaw attitude : " "

U,W : Translational velocities : m/s
 P,Q,R : Rotational velocities : deg/s

NOTE.

All matrix properties are written in **bold type**.

All vector quantities have the symbol " \sim " below the variable.

All normalised quantities have a bar " $\bar{}$ " above the variable.

CHAPTER 1

INTRODUCTION : METHODS OF QUANTIFYING AGILITY

1.1 Introduction

In recent years the role fulfilled by the military helicopter has grown from a purely utility and transportation vehicle to include ground attack and anti-armour duties. This puts the helicopter at ever increasing risk from ground-to-air fire, missile attack and air-to-air assault. In this hostile environment nap-of-the-earth (NOE) flight is used to improve survivability. This mode of flight lets the pilot use local terrain features to avoid detection and deny would-be aggressors the opportunity to lock-on weapon guidance systems.

The term "agility" has been loosely used to describe the helicopter's overall performance under these conditions. Although recognised as an important factor in helicopter design for many years, few attempts have been made to define formally and exactly what agility is, many authors confusing it with performance or manoeuvrability. Agility is a function of aircraft performance (maximum sustained load factor, turn rate, acceleration etc.) but must also include handling qualities - good performance is useless unless pilots have the confidence to use it. A more formal definition of agility might be : *agility is the ease with*

which a helicopter can change its position and state with precision and speed.

A method of quantifying the agility of a given helicopter configuration is of obvious value as a design tool. Configurational parameters could be varied and their influence on the agility of the helicopter studied. This would prove useful for the investigation of new configuration designs with respect to improvements in agility performance.

1.2 Overall and Inherent Agility

From the definition given in the introduction it is clear that agility is a function of many parameters. The use of words such as "ease" and "safety" implies that agility must be a function of handling qualities and pilot workload, thus involving control system performance. The word "precision" underlines the importance of control system design in helicopter agility. It is intuitive that "speed" is also of importance. Since pilot workload and handling qualities cannot, as yet, be fully quantified by analytic methods, it follows that agility also cannot be fully quantified using analysis.

However, a distinction can be made between the overall agility of a helicopter system (taking into account performance, handling qualities, pilot workload, control system performance etc.) and the "configuration" or "inherent" agility of a particular helicopter design. Inherent agility is dependent on a number of well defined configurational parameters (e.g. rotor stiffness, installed power etc.) and is therefore dependent only on design. It is a potential agility - the agility before any human influences have been added to the system. Due to the importance of pilot workload and handling qualities overall agility is best assessed by flight tests or piloted simulation (by using a Cooper-Harper style opinion rating, for example). Inherent agility (of the configuration), however, may be quantified analytically provided that it is taken as being independent of any pilot influence.

1.3 Methods of Studying Agility

Few attempts have been made to quantify agility (inherent or overall). Some of the more successful studies are discussed in this section. Agility studies can be separated into two types, flight testing, including piloted simulation (Refs. 1-5), and analytic methods (Refs. 6-10).

a) Studies of Agility by Flight Tests and Piloted Simulation

Recent studies at the Royal Aircraft Establishment (Refs. 1 and 2) have used results from flight tests to assign agility factors to helicopters flying specific classes of manoeuvres. An agility factor is calculated by comparing an theoretical maximum performances to actual performances achieved in flight tests. Brotherhood and Charlton (Ref. 1), use results from flight tests where the pilot has been instructed to fly a constant speed ninety degree bend between specified entry and exit points. A Turn Agility Factor is then defined as the ratio of the radius of a theoretical steady turn, performed at the maximum bank angle reached in the test, to the effective radius of the achieved turn. This Turn Agility Factor remained sensibly constant over a range of velocities and take-off weights for a single helicopter. Padfield and Charlton (Ref. 2) have extended this method to other manoeuvres. The agility of a helicopter performing a bob-up (vertical height change from the hover), for example has been defined as the ratio of minimum possible time to reach a fixed height (the time taken if the whole manoeuvre were performed at maximum vertical velocity) to the actual time taken.

Other agility studies using flight tests have tended to concentrate on qualitative analyses of agility rather than trying to quantify it. Tomlinson and Padfield (Ref. 3) used flight simulation to investigate the influence of rotor stiffness and blade flapping inertia on helicopter agility. They concentrated on the handling qualities aspect of agility and made no attempt to quantify it. Gerdes (Ref. 4) and Stewart, Dominick and Smith (Ref. 5) also concentrate on the handling qualities area of agility.

b) Studies of Agility by Analysis

Analytic methods are mainly used to study the effect of a particular configurational parameter on agility. Houston and Caldwell (Ref. 6) used a reduced order linear model to study the effects of an active tailplane in longitudinal manoeuvring flight. An agility rating is awarded to the most severe pop-up manoeuvre the helicopter can perform without exceeding its maximum rotor moment. In one respect this analysis is similar to that performed by Brotherhood and Charlton (Ref. 1), where agility is assessed by flight path geometry rather than aircraft performance.

Other analysts have mainly used kinematic helicopter mathematical models to study agility. Legge, Fortescue and Taylor (Ref. 7) used a simplified kinematic model to study the effects of longitudinal auxiliary thrust. A performance index is awarded to a helicopter configuration performing an acceleration-cruise-deceleration manoeuvre. It is calculated as an integral of a weighted function of pitch attitude w.r.t. time. Agility is related to a single variable and does not include rotor effects. A different approach is taken by Merkley (Ref. 8) and Wrestler

(Ref. 9) who use an energy balance method to calculate performance characteristics for helicopters in manoeuvring flight. Both relate agility to manoeuvre time without actually defining any sort of agility rating or factor. In effect, this reduces agility simply to a measure of excess power and the rate at which it can be summoned.

Flight tests are not the best way to study inherent agility since they depend largely on pilot opinion and skill. Pilots in general are better suited to study workload and handling qualities aspects of agility, and therefore flight tests are best used to assess the overall agility of a helicopter. Flight testing is not possible at the design stage and can be expensive during development. A general analytic method of calculating the inherent agility of a helicopter using simulation techniques would therefore be of great use.

1.4 A General Method of Quantifying Helicopter Inherent Agility

The methods described by the authors of References 6-9, have been developed to suit a particular application, no general method exists to measure or calculate the inherent agility of a helicopter. This thesis describes the development of such a method. The following discussion is intended to outline some of the most important aspects of the method.

i) The Importance of Manoeuvre Type

The value calculated for the inherent agility of a helicopter will be dependent on manoeuvre type. A helicopter which shows qualities indicating high agility in, for example, a turning manoeuvre, may show poor agility in an acceleration manoeuvre. If a value for the inherent agility of a helicopter is to be calculated, then it must be found by studying its performance over a series of standard manoeuvres. These manoeuvres would represent typical tasks performed by the configuration under study, and the combination of them might simulate missions within the helicopter's operational role. A value for agility would be given to a configuration for each class of manoeuvre.

The choice of manoeuvre is of importance. Houston and Caldwell (Ref. 6) assess agility on the basis of a single manoeuvre at the limit of the helicopter's flight envelope. A more complete measure of agility would be found if the helicopter's performance over a range of manoeuvres, of varying severity, was used. They should be flown at representative speeds over realistic flight paths. Some authors (Refs 8,9, and 15, for example) specify boundary conditions with the helicopter free to optimise

its performance between given entry and exit points. By defining the manoeuvres precisely, direct comparisons of the agility of various configurations can be made. The manoeuvres should be standardised by precise definition to allow any number of configurations to be tested under the same conditions. For this purpose, a series of algorithms have been developed (described in Chapter 2, section 2.3) which allow standard flight path elements to be defined. The flight paths have been chosen to represent typical NOE type manoeuvres (pop-up, turns etc.), and are defined by specifying altitude changes and turn rates as functions of time.

ii) Relating Inherent Agility to Helicopter Dynamics

Basing a method of quantifying agility on a helicopter's performance while flying a series of standard manoeuvres simplifies the definition of agility given in the Introduction. If, when comparing the inherent agility of various configurations, the change in position is exactly the same for each, then the "position" and "precision" aspects of the above definition are accounted for. Inherent agility is then defined as the ease with which a helicopter can change its state, and is a function of the aircraft's dynamics. The time histories of the body axes velocities and fuselage attitude angles over a manoeuvre are a direct measure of a change of state. The corresponding time histories of control angles give an indication of the ease with which state has been changed. It can then be surmised that inherent agility, for a given configuration over a fixed manoeuvre, can be evaluated by examination of its state and control time histories. A configuration with less control displacements and smaller changes in state variables over a fixed manoeuvre, has greater inherent agility.

iii) Use of an "Inverse Solution"

The problem then is to calculate state and control time histories for a configuration flying a precisely defined flight path. This is not possible to do using conventional simulation techniques where a flight path is calculated from a given control sequence. This is the opposite of what is required. It is therefore logical that an *inverse method* should be employed. An inverse solution of the equations of motion involves specifying a flight path and velocity, then calculating the control and state time histories needed to fly it. The flight path can be defined rigidly, and the calculation of control and state time histories repeated for any number of configurations. The main advantage in using an inverse method is that manoeuvres are repeatable. When using a conventional simulation to compare the response of several configurations it is possible to repeat a set control sequence. The aircraft's responses will give different flight paths. With inverse solutions, control sequences and attitude responses may be compared over a precisely defined flight path. This makes inverse methods particularly useful when studying helicopter performance during tightly defined manoeuvring flight, such as in nap-of-earth missions or air-to-air combat manoeuvres. Few attempts have been made to solve the helicopter equations of motion inversely, the authors of Reference 6, 14 and 15 all having success with methods developed to suit their particular application. If a wide range of manoeuvres (i.e. a wide range of flight states) are to be simulated in the agility evaluation process, then a more general inverse solution is required. Since such a method was not available, in fact has never been attempted, a large portion of this thesis is concerned with the development of a general inverse algorithm. It is believed that the

method presented in Chapter 2 is the first successful inverse solution of nonlinear helicopter equations of motion.

iv) Choice of Mathematical Model

The type of mathematical model used is of great importance. There are always advantages to be gained by making an analysis as simple as possible, in the understanding of the problem as well as in computational time. However, simple mathematical models have limitations which precludes their use in this analysis of inherent agility. The limitations of using kinematic models, as discussed by Curtiss and Price (Ref. 10), are poor prediction of dynamic behaviour at low speed and, since these basic simulations do not include a rotor model, any consequent analysis of agility will not highlight undesirably large values of rotor parameters encountered during manoeuvring flight. Reduced order dynamic models have the problem of poor (if any) prediction of coupling effects when simulating hingeless rotor helicopters. As noted by Gerdes (Ref. 4), in severe manoeuvres, coupling between rotor collective pitch and fuselage pitch attitude can be excessive. Linearised models are also of limited use since they only predict the helicopters flight state for small disturbances from its trim condition. Use of any of the models mentioned above would impose limitations on the severity of the manoeuvres over which inverse solutions are to be sought. A nonlinear six degrees of freedom model will be used to allow a wide range of manoeuvres to be simulated.

v) Application of a Method of Evaluating Helicopter Inherent Agility

A method of calculating helicopter inherent agility on its own could not be considered as a complete "design package". For example, the inherent agility evaluation method might predict that particular changes made to a configuration would make it more agile. These changes may however cause new instabilities to appear in the modified aircraft, which in turn may have adverse effects on its handling qualities. A method of quantifying agility would, therefore, have to be used in conjunction with other flight mechanics studies in order to ensure adequate stability, controllability and handling qualities.

From the considerations listed above, it is apparent that the first task is to develop an inverse method of solving the helicopter equations of motion. A description of an inverse algorithm, HELINV, incorporating a six degrees of freedom mathematical model, HELISTAB, and a series of standard flight paths is given in Chapter 2. The development of HELINV as an agility evaluation algorithm is detailed in Chapter 3, whilst examples of its use are presented in Chapter 4.

CHAPTER 2

INVERSE SOLUTION OF HELICOPTER EQUATIONS OF MOTION

2.1 Introduction

Studies of helicopter performance in nap-of-earth (NOE) flight conditions are usually based on conventional flight simulation or on test flying, both of which are expensive in time and money. A useful tool in such studies might be an 'inverse simulation'. This type of simulation can be used to calculate the control time history (and the resulting attitude and velocity time histories) required to fly a given flight path, and the helicopter's performance assessed on the basis of these time histories. An inverse method would be particularly useful for NOE simulation since the most important manoeuvres (pop-up, hurdle-hop etc.) performed in this type of flying are well understood, and can be easily simulated.

Most attempts at solving aircraft equations of motion inversely have been based on simulations of fixed wing aircraft. Some of the first attempts used very basic low order linearised models, for example Jones (Ref. 11) used an analytic technique to solve inversely the equations of motion to study gust effects. As mathematical models grew more complex inverse solutions became more difficult to achieve by analytic methods.

It is only recently that flight dynamicists have shown greater interest in this form of solution. There are two main reasons for this resurgence in interest. Firstly, the increased availability of low cost and powerful computing facilities has allowed numerical solutions to be found for complex models – obviously more desirable than the earlier limited analytic solutions. Secondly, control system designers have found inverse methods useful in the development of Automatic Flight Control Systems (AFCS), Ref. 12, for example. More specifically inverse solutions have found applications in the design of controllers for dynamic systems possessing highly coupled non-linearities, which may require multivariable control. This implies that inverse solutions will be of use in helicopter flight mechanics where linear system theory is of limited use due to the large degree of coupling between the longitudinal and lateral dynamics of the aircraft.

Most recent work on inverse solutions has been applied to fixed wing aircraft control system design. For example Meyer and Cicolani (Ref. 12) use an inverse solution to design an automatic flight control system for a V/STOL aircraft in an air traffic control environment. Recently, Kato and Sugiura (Ref. 13) have developed a more general method which, in theory, should allow them to compute control and state time histories for a general commanded flight path (although the only example they cite is a straight and level flight path with a continuous 360 degree roll along it). Although similar to the method described in this thesis, Kato and Sugiura use fuselage attitude time histories as the starting point of their solution rather than specifying a flight path.

Few attempts have been made to solve helicopter equations of motion

inversely. A recent attempt by Houston and Caldwell (Ref. 6) used a reduced order linearised model of a helicopter's longitudinal dynamics (the solution of which involves matrix manipulation) to study the use of an active tailplane in longitudinal manoeuvring flight. The method used relies on a linearised mathematical model and hence suffers from the restriction of being valid only for small perturbations from the trim state.

A less direct method of finding control and state time histories is employed by Haverdings (Ref. 14). Haverdings makes an initial guess at what the control time history should be for a given flight path, then uses a conventional time response solution to find what flight path this control sequence actually produces. This flight path is compared with the desired one, and the control time history is modified until the two flight paths converge. This category of indirect inverse solution (an inverse solution by successive time responses) is effective although inefficient in terms of computer time, but is probably the most widely used method (also used by Meyer and Cicolani, Ref.12).

A completely different approach to inverse solutions has been implemented by Wood et al (Ref. 15). This method (the computer program designated MCEP; Manoeuvre Criteria Evaluation Program) uses energy balance to calculate the helicopter's attitude and trajectory for a given task. The main difference in solution between this method and the others is that the start point is a task (e.g. pedal turn or return to target) rather than a flight path defined as a series of co-ordinates. The task is optimised within a series of boundary conditions (load factor and velocity limits etc.) with the flight path, the fuselage pitch and roll

attitude time histories calculated on the basis of excess energy available. The kinematic mathematical model used is relatively basic, the fuselage attitude being calculated by a semi-empirical function of velocity, and the main rotor is modelled by simple two dimensional momentum theory. MCEP has two major drawbacks. Firstly, although it is possible to compare the performance of two helicopter configurations undertaking the same task, it is not possible to compare their performance over exactly the same manoeuvre. The second drawback is the simplified nature of the rotor model. This type of model does not allow calculation of the rotor conditions during manoeuvring flight and therefore the control displacements cannot be calculated. Thus, although a helicopter's performance may seem to be favourable, it could be exceeding control limits. This program is probably the most successful inverse type solution applied to helicopters to date.

The inverse method described herein uses a nonlinear six degrees of freedom mathematical model, and so has no restriction on the allowable displacement from trim. The mathematical model also allows control displacements and rotor conditions to be calculated. The starting point for the solution is a tightly defined flight path, and this flight path may be "flown" with any number of configurations. The algorithm has been implemented on computer with the package being named HELINV.

2.2 Definition of an Inverse Solution

Aircraft equations of motion (eqns. A1, Appendix 1) are usually solved in order to find an aircraft's response to a given control input. This is achieved in the following manner :

- i) Define control input(s) as a function of time.

- ii) At time point i calculate the components of the external (aerodynamic and thrust) forces and moments (X,Y,...N) and the gravitational force components which are functions of the pitch and roll attitude angles θ_i and ϕ_i (as well as the other state and control variables).

- iii) Solve the nine simultaneous non-linear ordinary differential equations A1.1,2,3 from time t_i to t_{i+1} for the aircraft's body axis translational and rotational velocities and attitude ($u,v,w,p,q,r,\theta,\phi,\psi$).

- iv) The aircraft's component velocities in earth-fixed axes can then be found by transformation through the Euler (attitude) angles (see Appendix 2).

- v) The aircraft's position in the earth-fixed reference frame can thus be calculated by integrating the components of the earth axis velocities.

Hence, a conventional *forward* algorithm calculates the flight path

produced by a given control time history and is an integration process. The *inverse* method presented here can be described as the calculation of a control time history required to fly a given flight path and is a process of differentiation. A forward algorithm consists of the solution of nine differential equations (Appendix 1) for nine unknowns ($u, v, w, p, q, r, \theta, \phi, \psi$) usually by a Runge-Kutta integration method. The inverse method described in this thesis involves the solution of the six equations of motion for seven unknowns : the control angles ($\theta_0, \theta_{1S}, \theta_{1C}, \theta_{0Tr}$) and the attitude angles (θ, ϕ, ψ). A further equation may therefore be added (see section 2.5) to give a unique solution.

The algorithm for the inverse solution can be declared as :

- i) Define a flight path in earth-axes and calculate the velocities and accelerations along the path.
- ii) Transform velocities and accelerations to the body-fixed axes system.
- iii) Calculate external forces and moments for equations of motion.
- iv) Solve equations of motion for fuselage attitude angles and rotor condition and hence calculate the control angles.

The starting point for the inverse solution is therefore the calculation of the flight path and the velocities and accelerations along it.

2.3 Defining the Flight Path

The flight paths modelled in this section were chosen, after discussion with the Royal Aircraft Establishment, Flight Systems Division, to represent manoeuvres most frequently flown in NOE conditions. To date, no previous attempts have been made to define mathematically this sort of manoeuvre. The following section describes a series of algorithms developed to make such manoeuvres available for use in an inverse solution.

The flight paths can be divided into three distinct categories : longitudinal flight paths (performed in the x-z plane), turning manoeuvres (performed in the x-y plane) and three-dimensional manoeuvres. The flight path is taken to be the trajectory of the helicopter's centre of gravity and the flight velocity is defined as being the velocity vector tangential to the flight path. The flight path is described by a track in the horizontal (xy) plane with altitude displacement around it (see Fig 2.1). The altitude is given in the (s,h) plane where s is the distance along the track and h is the altitude at s. The origin of the earth axes system is taken as the entry point of the manoeuvre and the helicopter is assumed to be pointing in the direction of the x-axis (see Fig 2.1). The flight path is defined by one of three methods depending on type :

- i) specify the altitude and the flight velocity as a functions of time;
- ii) specify the turn rate and the flight velocity as functions of time;
- iii) specify the turn rate, flight velocity and altitude as functions of time.

The first method is used for purely longitudinal manoeuvres (pop-up,

hurdle-hop etc.). The second is used for turning flight where attempts to define the flight path as an analytic function of the c.g. position w.r.t. time can result in discontinuities where straight lines join curves. By specifying turn rate as a function of time it is possible to have a smooth transition from rectilinear to turning flight. A mixture of the two methods is used to define three-dimensional manoeuvres (e.g. climbing turn). Each of these methods is now described.

2.3.1 General Description of Manoeuvres

a) Flight Path Defined Using (z,V) : Longitudinal Flight

Here the flight path is defined as :

$$\left. \begin{aligned} z &= f_1(t) \\ \dot{y} &= 0 \\ V &= f_2(t) \end{aligned} \right\} \dots (2.1)$$

Thus, using the expression (z-velocity being found by differentiating the first of equations 2.1) :

$$v^2 = \dot{x}^2 + \dot{y}^2 + \dot{z}^2 \dots (2.2)$$

it is possible, by integration, to define fully the flight path in terms of (x,y,z,V).

b) Flight Path Defined Using (x,V) : Turning Flight

Here the flight path is defined by :

$$\left. \begin{aligned} z &= \text{const.} \\ \dot{x} &= f_3(t) \\ V &= f_4(t) \end{aligned} \right\} \dots (2.3)$$

The velocities \dot{x} and \dot{y} are functions of the track angle x and velocity (the track angle being found by integration of function f_3). Hence, since $z = \text{constant}$ therefore, $\gamma = 0$:

$$\left. \begin{aligned} \dot{x}(t) &= V(t) \cos x(t) \\ \dot{y}(t) &= V(t) \sin x(t) \end{aligned} \right\} \dots (2.4)$$

The flight path co-ordinates (x,y) can then be found by integration of equations (2.4).

c) Flight Path Defined Using (z,x,V) : Three-Dimensional Flight Paths

Here the flight path is defined by :

$$\left. \begin{aligned} z &= f_5(t) \\ \dot{x} &= f_6(t) \\ V &= f_7(t) \end{aligned} \right\} \dots (2.5)$$

Referring to Fig. 2.1 it is apparent that the components of velocity in the earth axes system are given by :

$$\left. \begin{aligned} \dot{x} &= V \cos y \cos x \\ \dot{y} &= V \cos y \sin x \\ \dot{z} &= - V \sin y \end{aligned} \right\} \dots (2.6)$$

and the accelerations are found to be, by differentiation :

$$\left. \begin{aligned} \ddot{x} &= \dot{V} \cos\gamma \cos\alpha - V \dot{\gamma} \sin\gamma \cos\alpha - V \dot{\alpha} \cos\gamma \sin\alpha \\ \ddot{y} &= \dot{V} \cos\gamma \sin\alpha - V \dot{\gamma} \sin\gamma \sin\alpha + V \dot{\alpha} \cos\gamma \cos\alpha \\ \ddot{z} &= -\dot{V} \sin\gamma - V \dot{\gamma} \cos\gamma \end{aligned} \right\} \dots (2.7)$$

The flight path angle γ is found from the third of equations (2.6) :

$$\gamma = -\sin^{-1} \left[\frac{\dot{z}}{\dot{V}} \right] \dots (2.8)$$

from which (with manipulation) :

$$\dot{\gamma} = -\frac{\ddot{z} V - \dot{V} \dot{z}}{V^2 \cos\gamma} \dots (2.9)$$

The track angle is found by integration of the second of equations (2.5) and the flight acceleration found by differentiation of the third. It is then possible to find all of the velocities and accelerations in the earth axes system and therefore, by integration, the flight path co-ordinates.

2.3.2 Description of Some Specific Manoeuvres

Each of the available manoeuvres is now described in turn.

a) Longitudinal Flight Paths

Longitudinal manoeuvres (those in which the acceleration along the earth y-axis is zero) include altitude change manoeuvres for obstacle clearance and acceleration and deceleration. These manoeuvres can be defined by using the first of the above general methods.

i) The Pop-up Manoeuvre

This height change manoeuvre (see Fig 2.2a) is used in NOE flight for obstacle avoidance. It is performed over a mid-speed range (40 - 100 knots) and takes the helicopter from one level, trimmed condition to another. The height of, and the distance to, the obstacle (h_1, s_1) and the entry and exit velocities (V_1, V_2) are all that are required to define the flight path. The first step is to examine the boundary conditions of the flight path :

$$\left. \begin{array}{l} \text{a) } t = 0, z = 0, \dot{z} = 0, \ddot{z} = 0 \\ \text{b) } t = t_1, z = -h_1, \dot{z} = 0, \ddot{z} = 0 \end{array} \right\} \dots (2.10)$$

where t_1 = the manoeuvre time (an unknown).

By making the velocity \dot{z} equal to zero equation (2.8) gives the angle of climb to be zero. This ensures level flight at entry to and exit from the manoeuvre. The acceleration \ddot{z} , is also made zero for a trimmed flight condition at entry and exit. There are six boundary conditions and therefore the most simple function for z is a 5th order polynomial:

$$z = at^5 + bt^4 + ct^3 + dt^2 + et + f \dots (2.11)$$

Expressions for the velocity and acceleration \dot{z} and \ddot{z} are found by differentiating equation (2.11). Applying the boundary conditions (2.10) to equation (2.11) (and its derivatives) gives the following :

$$\left. \begin{aligned} d = e = f = 0 \\ -h_1/t_1^3 = at_1^2 + bt_1 + c \\ 0 = 5at_1^2 + 4bt_1 + 3c \\ 0 = 20at_1^2 + 12bt_1 + 6c \end{aligned} \right\} \dots (2.12)$$

The flight velocity is given as a polynomial function of time (see Fig. 2.2b). A cubic polynomial is suitable since it can satisfy the four boundary conditions :

$$\left. \begin{aligned} \text{a) } t = 0, V = V_1, \dot{V} = 0 \\ \text{b) } t = t_1, V = V_2, \dot{V} = 0 \end{aligned} \right\} \dots (2.13)$$

This gives a change of velocity from V_1 to V_2 but still retains the no-acceleration trim states at entry and exit. The expression for velocity is then :

$$V = a_1t^3 + b_1t^2 + c_1t + d_1 \quad \dots (2.14)$$

Substitution of the boundary conditions (2.13) into the equation (2.14) and its first derivative gives :

$$\left. \begin{aligned} d_1 = V_1 \\ c_1 = 0 \\ V_2 - V_1 = a_1t_1^3 + b_1t_1^2 \\ 0 = 3a_1t_1^2 + 2b_1t_1 \end{aligned} \right\} \dots (2.15)$$

Noting that :

$$\dot{s}^2 = \dot{x}^2 + \dot{y}^2 \quad \dots (2.16)$$

where s is the distance along the track, we have, from (2.2) :

$$s_1 = \int_0^{t_1} \sqrt{(V^2 - \dot{z}^2)} dt \quad \dots (2.17)$$

There are now six unknowns (a, b, c, a_1, b_1, t_1) and six non-linear simultaneous equations (2.12, 2.15, 2.17) which can be solved by a numerical iterative method as follows :

1. Values for $s_1, h_1, V_1,$ and V_2 are supplied as user inputs.
2. An initial guess of the manoeuvre time is taken to be the straight line distance between the entry and exit points divided by the average velocity, i.e.

$$t_i = \frac{2\sqrt{(s_1^2 + h_1^2)}}{V_1 + V_2}$$

3. Equations 2.12 can now be solved for the coefficients $a, b,$ and $c,$ whilst equations 2.15 can be solved for a_1 and $b_1.$
4. The integration 2.17 can now be performed using the Trapezoidal Rule (Ref. 16).
5. The calculated value of s_1 is then compared with the inputted value. If there is a difference (greater than a set tolerance) between these values then the value of t_1 is altered and the process continues from (3).

Example. Using the above equations to define a pop-up to height $h_1=30m,$ over a distance $s_1=200m,$ at a constant velocity $V_1 = V_2 = 80$ knots, gives a manoeuvre taking 4.93 seconds, with maximum climb angle of $16',$ and load factor varying between 0.27 and 1.73.

ii) The Hurdle-Hop Manoeuvre

This manoeuvre (see Fig 2.3a) is used in NOE flight for obstacle clearance where, once the obstacle (perhaps a tree-line) has been cleared, the helicopter returns to its initial altitude to avoid detection. Again it is performed over the mid-speed range (40 - 100 knots), and takes the helicopter from one level trimmed condition to another. The height of the hurdle, h_1 , and the distance to the exit of the manoeuvre, s_2 are required to define the flight path. The obstacle is taken to be at half the total distance. The method is the same as that described for the pop-up above except that a seventh order polynomial is required to satisfy an extra two boundary conditions ($z = -h_1$ and $\dot{z} = 0$) at the hurdle. A fifth order polynomial velocity change (see Fig. 2.3b) is also included. This gives the user an option to vary the flight velocity from V_1 at entry to V_2 at the hurdle then V_3 at exit with zero acceleration at entry and exit.

Example. Using a seventh order polynomial to define a hurdle-hop over an obstacle of height $h_1=30\text{m}$, from a distance $s_2=500\text{m}$, at a constant velocity of 80 knots, gives a manoeuvre taking 12.25 seconds with the flight path angle varying between limits $\pm 11.6^\circ$ and load factor varying between 0.5 and 1.4.

iii) Accelerations and Decelerations

In NOE flight it is important to be able to move as quickly as possible between areas of cover. Good deceleration performance is as important as acceleration to avoid overshooting the cover. Constant height must be maintained to avoid tail rotor or main rotor ground strike

at high positive and negative fuselage angles of attack. In the HELINV program speed variations are defined either by a cubic polynomial function of time, as in the pop-up or by a constant acceleration (or deceleration) with transients (see Fig 2.4). The second of these methods is basically the same as that used to define turn rate in the turning manoeuvres (described below). In both cases the manoeuvre is defined by specifying a speed change to be achieved over a given distance at constant height.

Example. Accelerating from 40 to 60 knots in a distance of 150m takes 5.8s and the maximum acceleration is 0.27g. Decelerating from 40 to 20 knots in 100m takes 6.5s and the maximum deceleration is 0.24g.

b) Turning Manoeuvres

The manoeuvres performed in purely turning flight (constant height) are defined using the second of the above methods.

Turn with Speed Change

This manoeuvre is used to change direction without any loss (or gain) in height by rolling the helicopter through an unsteady transition section to a circular main section, and then as the exit from the manoeuvre is approached, the helicopter is rolled back to a straight and level flight state (see Fig. 2.5a). The manoeuvre is defined by specifying the turn rate around the manoeuvre as a function of time :

$$\left. \begin{aligned}
 \dot{x}_1 &= a_1 t^3 + b_1 t^2 + c_1 t + d_1 & 0 < t < t_1 \\
 \dot{x}_2 &= V(t)/R_c & t_1 < t < t_2 \\
 \dot{x}_3 &= a_2 t^3 + b_2 t^2 + c_2 t + d_2 & t_2 < t < t_3
 \end{aligned} \right\} \dots\dots (2.18)$$

where R_c is the radius of the circular section. Turn rate can be found by dividing velocity by radius of curvature (see Appendix 4). The resulting turn rate function is shown in Fig. 2.5b. Cubic polynomial functions of time are chosen for the transients, to allow second order derivative continuity when joining the circular section to the straight line entry and exit trajectories. The user has to specify the amount of the manoeuvre spent in the transients (defined by the parameter k) where, if x_1 and x_2 are the track angles at the start and end of the circular section, and x_e is the track angle at the exit from the manoeuvre (also specified by the user) then :

$$x_1 = kx_e \quad \text{and} \quad x_2 = (1-k)x_e \quad \dots\dots (2.19)$$

The value of k is usually set between 0.1 and 0.2 i.e. the transients occupy the first and last 10-20% of the manoeuvre. The equivalent radius of the turn R_e must also be specified by the user. This is the radius of circular arc needed to give the required co-ordinates and track angle at exit from the turn (x_e, y_e, x_e). When the transients are taken into account the equivalent radius is greater than the radius of the circular section. The exit co-ordinates are found to be :

$$x_e = R_e \sin x_e \quad \text{and} \quad y_e = R_e (1 - \cos x_e) \quad \dots\dots (2.20)$$

Calculation of the parameters for this flight path are performed in

three sections.

The Entry Transient. The boundary conditions for the entry transient are :

$$\left. \begin{array}{l} \text{a) } t = 0, \dot{x} = 0, \ddot{x} = 0 \\ \text{b) } t = t_1, \dot{x} = V(t_1)/R_C, \ddot{x} = 0 \end{array} \right\} \dots (2.21)$$

where t_1 = time to reach the circular section. Substitution of these boundary conditions into the first of equations 2.18 (and its first derivative) gives four nonlinear simultaneous equations (similar to equations 2.12) in six unknowns (the four coefficients of the cubic, the time t_1 , and the radius of the circular section R_C). The track angle can be found as a function of time by integrating this cubic. Hence the track angle at the end of the transient is given by :

$$x_1 = kx_e = \int_0^{t_1} \dot{x}_1(t) dt \dots (2.22)$$

This, when expanded, gives a nonlinear equation in terms of the four coefficients of the cubic and the time t_1 .

The Circular Section. Flight velocity may be varied in the circular section as a cubic function of time :

$$V = at^3 + bt^2 + ct + d \dots (2.23)$$

The boundary conditions for the velocity change are :

$$\left. \begin{array}{l} \text{a) } t = t_1, V = V_1, \dot{V} = 0 \\ \text{b) } t = t_2, V = V_2, \dot{V} = 0 \end{array} \right\} \dots (2.24)$$

This gives a change of velocity from V_1 to V_2 but still retains the no acceleration condition at entry and exit from the circular section. The track angle swept out in the constant radius main section of the turn is given by :

$$x_2 - x_1 = (1-2k)x_e = \int_{t_1}^{t_2} \dot{x}_2(t) dt \dots (2.25)$$

Expansion of this integral gives a nonlinear equation in terms of the coefficients a, b, c, d and the times t_1 and t_2 . Substitution of the boundary conditions 2.24 into equation 2.23 and its first derivative adds four nonlinear equations in these coefficients and times.

The Exit Transient. The boundary conditions for the exit transient are :

$$\left. \begin{array}{l} \text{a) } t = t_2, \dot{x} = V(t_2)/R_C, \ddot{x} = 0 \\ \text{b) } t = t_3, \dot{x} = 0, \ddot{x} = 0 \end{array} \right\} \dots (2.26)$$

On substitution into the third of equations 2.18 (and its first derivative), these boundary conditions give four nonlinear simultaneous equations in another six new unknowns (t_2, t_3 and the four coefficients of the cubic). The track angle as a function of time is found by integrating the cubic. Thus the track angle covered in the exit transient x_3 , is given by :

$$x_3 = kx_e = \int_{t_2}^{t_3} \dot{x}_3(t) dt \dots (2.27)$$

Again, this reduces to a nonlinear function of the coefficients of the cubic and the times t_2 and t_3 .

There are now two conditions still to be fulfilled - the correct exit co-ordinates x_e and y_e must be reached (equations 2.20). From equations (2.6), with $\gamma=0$:

$$\dot{x}(t) = V(t) \cos x(t) \quad \text{and} \quad \dot{y}(t) = V(t) \sin x(t) \quad \dots (2.28)$$

The track angle, as functions of time, is known (with unknown coefficients). The exit co-ordinates are then given by :

$$x_e = \int_0^{t_3} \dot{x}(t) dt \quad \text{and} \quad y_e = \int_0^{t_3} \dot{y}(t) dt \quad \dots (2.29)$$

The problem now consists of sixteen unknowns (the cubic coefficients $a, b, c, d, a_1, b_1, c_1, d_1, a_2, b_2, c_2, d_2$; the times t_1, t_2, t_3 ; and the radius of the circular section R_C) and seventeen nonlinear simultaneous equations (four each from the boundary conditions 2.21, 2.24 and 2.26 plus integral equations 2.22, 2.25, 2.27 and two from 2.29). These equations can be solved numerically as follows.

1. The inputs from the user are : k, x_e, V_1, V_2, R_e .
2. The track angles x_1 and x_2 are found from equations 2.19 and the exit co-ordinates are found from equations 2.20.
3. An initial guess of the radius of the circular section, R_C , is made.
4. Substitution of boundary conditions 2.21 into the first of equations 2.18 gives two simultaneous linear equations in a_1, b_1 and t_1 ($c_1=d_1=0$), from which :

$$a_1 = -2\dot{x}(t_1)/t_1^3 \quad , \quad b_1 = 3\dot{x}(t_1)/t_1^2$$

5. Equation 2.22 can be expanded to a fourth order polynomial in terms of a_1, b_1, t_1 , which can be solved for t_1 by substitution of the above values of a_1 and b_1 :

$$t_1 = 2\dot{x}(t_1)/x_1$$

6. The series of five simultaneous nonlinear equations (formed by substitution of boundary conditions 2.24 into equation 2.23 and the expansion of equation 2.25) are solved using a routine from a numerical algorithm package (Ref. 17) for the five unknowns a, b, c, d, t_2 .
7. The series of five simultaneous nonlinear equations (formed by substitution of boundary equations 2.26 into the third of equations 2.18 and the expansion of equation 2.27) are solved (using the same routine as above) for the five unknowns a_2, b_2, c_2, d_2, t_3 .
8. The track angle time history can now be found for the whole turn by integrating equations 2.18.
9. Integrations 2.29 are performed (using the Trapezoidal Rule - Ref.16) to give the exit track co-ordinates corresponding to the the latest estimate of R_C .
10. These exit co-ordinates are compared with their desired values. If they are not within a set tolerance, then the process continues at stage 4 with an updated estimate of the radius R_C .

Although the problem is over defined (i.e. seventeen equations to be satisfied and only sixteen unknowns), a solution can be found provided the required tolerance is not too severe (an error of less than 1% in the

values of x_e and y_e is taken to be sufficient).

Example. If the user inputs give a 90° right hand turn (i.e. $x_e = \pi/2$) of effective radius $R_e=200m$, at a constant velocity ($V_1=V_2$) of 80 knots, with the first and last 10% of the manoeuvre spent in transients (i.e. $k=0.1$), then the above equations give a manoeuvre of duration (t_3) 7.91s, and a load factor in the circular section (of radius $R_c=173m$) of 2g. The required exit co-ordinates were $x_e=y_e=200m$. The exit co-ordinates calculated were $x_e=y_e=200.5m$.

c) Three-Dimensional Manoeuvres

Such flight paths are defined using a mixture of the two methods used to define longitudinal and turning manoeuvres.

Turn with Height Change

Here the turn is performed with a height change during the circular section of the manoeuvre (similar to the flight path in Fig. 2.1). The solution is very similar to that of the constant height turn described above, except that a height variation is incorporated instead of a velocity change. This height change is specified in the same manner as the pop-up (i.e. a fifth order polynomial giving a height change h_1 over the circular section), but could just as easily have been the same as the hurdle-hop if required. The height change is therefore defined as :

$$z = a_3t^5 + b_3t^4 + c_3t^3 + d_3t^2 + e_3t + f_3 \dots (2.30)$$

and the boundary conditions are :

$$\left. \begin{array}{l} \text{a) } t = t_1, z = 0, \dot{z} = 0, \ddot{z} = 0 \\ \text{b) } t = t_2, z = -h_1, \dot{z} = 0, \ddot{z} = 0 \end{array} \right\} \dots (2.31)$$

The turn rate is given by the same equations and boundary conditions as the level turn above (2.18, 2.21 and 2.26). The solution now has an extra six unknowns (the coefficients of the height change law), but an extra six equations arise when the boundary conditions (2.31) are applied to the equation (2.30) and its derivatives. The only other alteration required for solution is the inclusion of terms in γ (see equations 2.6) in the velocity expressions (2.28) where γ , the flight path angle, is found from equation (2.8). The numerical solution of these equations is similar to that described for the level turn.

Example. A height change of 25m around a 90° right hand turn of effective radius $R_e=200\text{m}$, at a velocity of 80 knots, with the first and last 10% of the manoeuvre spent in transients, gives a manoeuvre of duration of 8s and a maximum load factor of 2.12g.

2.3.3 Alternative Methods of Defining Flight Paths

The methods described in the previous sections allow manoeuvres, with load factor limits far in excess of any likely to be encountered by real helicopters, to be defined. The pop-up algorithm, for example, can calculate all of the required parameters (earth axis accelerations and velocities) for manoeuvres with maximum load factors greater than 6, whilst the turn algorithm is capable of defining turns with maximum load

factor greater than 4, before the solution fails to converge. The resulting flight paths may not precisely match those of real helicopters, although the resemblance is close enough for this study. If precise simulation of manoeuvres flown in flight tests were required, then new methods of defining flight paths might be necessary. If only flight path co-ordinates were available, then a curve fitting method would have to be used, the accelerations and velocities along the flight path being found by differentiation of the approximating function. If the aircraft's velocity and acceleration components were known at a series of points in time then a look-up table would be sufficient.

2.4 The Numerical Algorithm

The success of any solution of the equations of motion relies on the accuracy and validity of the mathematical model used. Work at Glasgow University on inverse solutions has been supported by the Royal Aircraft Establishment who made their own mathematical model for the study of helicopter flight mechanics available. This model forms the basis of the simulation package "HELISTAB" (Ref. 18 and 19). An outline of the HELISTAB model is given in Appendix 4 and a more detailed description is given by Padfield (Ref. 19).

The section of HELISTAB used is the routine for calculating the helicopter's trim state. In its original form this routine can calculate the trim attitude and rotor conditions for a general steady flight state. This is accomplished by setting the acceleration terms in the equations of motion (A1.1,2) to zero and solving the resulting six non-linear algebraic equations. For rectilinear steady flight the equations of motion become :

$$\left. \begin{aligned} X - mg \sin\theta &= 0 \\ Y + mg \cos\theta \sin\phi &= 0 \\ Z + mg \cos\theta \cos\phi &= 0 \\ L = M = N &= 0 \end{aligned} \right\} \quad (2.32)$$

Expressions for the external forces and moments are given in Appendix 4. For steady turning flight, the terms involving products of translational and rotational velocities must be included since the rotational velocities are non zero. These equations are solved simultaneously for six unknowns (chosen to be the fuselage attitude angles θ, ϕ , the main and tail rotor thrust coefficients C_T, C_{Ttr} , and the longitudinal and lateral flapping

angles β_{1c}, β_{1s}). The control angles can then be calculated as described in Appendix 4.

A trim algorithm calculates the control angles needed to maintain a defined steady flight state. It can therefore be considered as a basic form of inverse solution. A standard trim algorithm is of limited use in an agility study, the only significant steady manoeuvre performed in NOE flight being the level turn. Modification of equations (2.32) to include the acceleration and inertial terms will allow inverse solutions to be found for any unsteady manoeuvre. The resulting equations of motion, from Appendices 1 and 4, are :

$$m\dot{u} = -m(wq - vr) + X_A + \rho(\Omega R)^2 \pi R^2 [C_T(\beta_{1c} + \gamma_s) - \delta s\mu_x/4] - mg \sin\theta \quad (2.33)$$

$$m\dot{v} = -m(ur - wp) + Y_A + \rho(\Omega R)^2 \pi R^2 [-C_T \beta_{1s} - \delta s\mu_y/4] + \rho(\Omega_{tr} R_{tr})^2 \pi R_{tr}^2 C_{Ttr} + mg \cos\theta \sin\phi \quad (2.34)$$

$$m\dot{w} = -m(vp - uq) + Z_A - \rho(\Omega R)^2 \pi R^2 C_T + mg \cos\theta \cos\phi \quad (2.35)$$

$$I_{xx} \dot{p} = (I_{yy} - I_{zz}) qr + I_{xz} (\dot{r} + pq) + L_A - b/2 K_\beta \beta_{1s} + \rho(\Omega R)^2 \pi R^2 h_R [-C_T \beta_{1s} - \delta s\mu_y/4] + \rho(\Omega_{tr} R_{tr})^2 \pi R_{tr}^2 h_{tr} C_{Ttr} \quad (2.36)$$

$$I_{yy} \dot{q} = (I_{zz} - I_{xx}) rp + I_{xz} (r^2 - p^2) + M_A - [b/2 K_\beta \beta_{1c}] - \rho(\Omega R)^2 \pi R^2 [h_R C_T (\beta_{1c} + \gamma_s) - h_R \delta s\mu_x/4 - x_{cg} C_T] \quad (2.37)$$

$$\begin{aligned}
I_{zz} \dot{r} = & (I_{xx} - I_{yy}) pq + I_{xz} (\dot{p} - qr) + N_A + \rho(\Omega R)^2 \pi R^3 C_Q + \\
& \gamma_s [-b/2 K_\beta B_{1s} + \rho(\Omega R)^2 \pi R^2 h_R (-C_T B_{1s} - \delta s \mu_y / 4)] - \\
& (l_{tr} + x_{cg}) \rho(\Omega_{tr} R_{tr})^2 \pi R_{tr}^2 C_{Ttr}
\end{aligned} \tag{2.38}$$

The aerodynamic components (X_A, \dots, N_A) as functions of $u, v, w, p, q, r, \theta, \phi, \psi$, are given by expressions A4-3. The method used to solve the foregoing equations for unsteady flight will also be described in this section.

The inverse solution is algebraic in nature, the external force and moment, gravitational, inertial and acceleration terms in the equations of motion being complicated non-linear functions of the unknown attitude angles, body velocities and rotor parameters. For example, the external force X (in the u equation of motion) includes a term due to the drag of the fuselage, which in turn is a function of the fuselage angle of incidence, α , where:

$$\alpha = \tan^{-1} (w/u). \tag{2.39}$$

The velocities w and u are in the body fixed axes system (functions of the direction cosines of the earth/body transformation matrix - see Appendix 2). They are therefore trigonometric functions of the helicopter's attitude angles (θ, ϕ, ψ) , and the earth axis velocities. This example shows the coupling between flight path and attitude. The complexity of the functions rules out any analytic solution : an iterative procedure must be used.

In its original form the trim algorithm used nested iterative loops to solve equations 2.33-2.38. As well as being expensive in computer

time, this solution was very sensitive to initial condition, and numerically unstable when solving for turning flight. For these reasons, when the trim algorithm was modified to include acceleration and inertial forces and moments, it was also restructured to allow solution using a faster, and more reliable Newton-Raphson iterative scheme (Ref.21). Using a Newton-Raphson iteration, a system of n non-linear equations :

$$f(x) = \begin{bmatrix} f_1(x_1 \dots x_n) \\ \vdots \\ f_n(x_1 \dots x_n) \end{bmatrix} = 0 \quad (2.40)$$

can be solved where, if x_0 is an estimate of the solution, and J is the Jacobian of the system, then a better estimate, x_1 , is given by :

$$x_1 = x_0 - J^{-1} f(x_0) \quad (2.41)$$

This inverse solution requires six equations (2.33-2.38) to be solved for six unknowns ($\theta, \phi, C_T, C_{Ttr}, \beta_{1c}, \beta_{1s}$). Examination of the equations shows that, if used in a specific order, the problem can be reduced to two nonlinear equations, with the attitude angles θ, ϕ as the unknowns. If estimates of the attitude angles have been made then :

1. the thrust coefficient, C_T , can be found from 2.35,
2. the longitudinal flapping angle, β_{1c} , can be calculated from 2.37,
3. the tail rotor thrust coefficient, C_{Ttr} , and the lateral flapping angle, β_{1s} , can be found by simultaneous solution of equations 2.36 and 2.38.

These steps are described more fully in section 2.4.3 and 2.4.4 below. This leaves equations 2.33 and 2.34 to be solved for θ and ϕ . The algorithm used is outlined graphically in block diagram form in Figures

2.6 and 2.7. This algorithm has been implemented on a DEC VAX 11/750 computer, the package being named HELINV. Each step in the numerical process is now described.

2.4.1 Definition of Manoeuvre

a) The Flight Path

The starting point of the process is to define a manoeuvre. As described in section 2.3, the manoeuvre is defined as a time history of the helicopter's earth-axis velocities and accelerations. Since numerical differentiation is used to calculate attitude rates at points throughout the manoeuvre, these velocities and accelerations should ideally be calculated at a series of equally spaced time intervals.

b) Sideslip Constraint

The inverse method can be described as the solution of six equations of motion with seven unknowns, these being the three fuselage attitude angles; θ, ϕ, ψ and the four control angles; $\theta_0, \theta_{1S}, \theta_{1C}, \theta_{0tr}$. If a unique solution is to be found then one further condition must be added. Specifying the sideslip angle is the most realistic constraint which can be imposed on the solution. In NOE flight, control of this degree of freedom is important not only for the pilot's vision, but also for fuselage pointing, for example, large angles of sideslip are often used to decelerate the helicopter. Specifying sideslip allows calculation of the azimuth angle (Appendix 5). The number of unknowns is then decreased to six. Sideslip angle is expressed as a function of time :

$$\beta = \beta(t)$$

The sideslip velocity and acceleration are given by :

$$v = V \sin\beta \quad (2.42)$$

and

$$\dot{v} = \dot{V} \sin\beta + \dot{\beta} V \cos\beta \quad (2.43)$$

Sideslip angle can be kept at a constant value (usually zero) or varied as a function of time depending on the required manoeuvre.

The following steps are carried out at each point in time along the manoeuvre.

2.4.2 Initial Guesses of Attitude Angles

The solution for a straight and level trim state is not sensitive to initial value variation, therefore a single fixed initial value allows solution over the complete range of velocities. The solution in unsteady flight is very sensitive to initial value. This sensitivity is directly related to the severity of the manoeuvre i.e. as the manoeuvre becomes more severe, the difference in the values of the attitude angles between successive time steps increases, hence better first guesses are required. A cubic polynomial function is fitted through the previous five points in the θ and ϕ time histories (Ref. 22). Better initial values are then found by extrapolation (i.e. by evaluating the two cubics at the latest time point). This reduces computing time by ensuring rapid convergence. Over the first few time points, where there are too few points to fit a polynomial, the initial guesses are found by linear extrapolation.

2.4.3 Solution Using a Newton-Raphson Iteration

A Newton-Raphson iteration is used to solve equations 2.33 and 2.34 (the u and v equations) for θ and ϕ . When rewritten these equations become :

$$\left. \begin{aligned} F_1(\theta, \phi) &= -m(\dot{u} + wq - vr) + X - mg \sin\theta = 0 \\ F_2(\theta, \phi) &= -m(\dot{v} + ur - wp) + Y + mg \cos\theta \sin\phi = 0 \end{aligned} \right\} \quad (2.44)$$

At a point, i , in the iteration, a better estimate of the solution is given by :

$$\begin{bmatrix} \theta_{i+1} \\ \phi_{i+1} \end{bmatrix} = \begin{bmatrix} \theta_i \\ \phi_i \end{bmatrix} - \begin{bmatrix} \frac{\partial F_1}{\partial \theta} & \frac{\partial F_1}{\partial \phi} \\ \frac{\partial F_2}{\partial \theta} & \frac{\partial F_2}{\partial \phi} \end{bmatrix}^{-1} \begin{bmatrix} F_1(\theta_i, \phi_i) \\ F_2(\theta_i, \phi_i) \end{bmatrix} \quad (2.45)$$

It would be possible to formulate expressions for the partial derivatives, although this would be a time consuming and tedious task. The resulting expressions would be cumbersome and require changing each time the mathematical model was updated. Instead, a two step, central difference, numerical differentiation technique (Ref. 23 and Appendix 6) is used. The partial derivatives are calculated by first calculating the values of F_1 and F_2 using the current values of θ and ϕ . The next stage is to perturb θ by increments of $(1 \pm h)$ and $(1 \pm 2h)$, holding the value of ϕ constant, and calculating the resulting four values of the functions. This is repeated, perturbing ϕ by the same increments, and holding θ constant. Values of both functions are therefore calculated for nine possible combinations of θ and ϕ (denoted : $F_1(1), \dots, F_2(9)$) :

- | | | |
|----|-------------------------------|---------------------------|
| 1. | $\theta_1 = \theta_i$ | $\phi_1 = \phi_i$ |
| 2. | $\theta_2 = \theta_i(1 + h)$ | $\phi_2 = \phi_i$ |
| 3. | $\theta_3 = \theta_i(1 + 2h)$ | $\phi_3 = \phi_i$ |
| 4. | $\theta_4 = \theta_i(1 - h)$ | $\phi_4 = \phi_i$ |
| 5. | $\theta_5 = \theta_i(1 - 2h)$ | $\phi_5 = \phi_i$ |
| 6. | $\theta_6 = \theta_i$ | $\phi_6 = \phi_i(1 + h)$ |
| 7. | $\theta_7 = \theta_i$ | $\phi_7 = \phi_i(1 + 2h)$ |
| 8. | $\theta_8 = \theta_i$ | $\phi_8 = \phi_i(1 - h)$ |
| 9. | $\theta_9 = \theta_i$ | $\phi_9 = \phi_i(1 - 2h)$ |

After experimentation with a range of values, h was set at a value of 0.0001. This produces values of the functions which differ by small amounts. To avoid rounding errors in the subtraction of similar values, the Fortran computer code is written in double precision.

The required sequence of calculations to allow evaluation of the functions, given in the next section, is performed nine times, once with each of the above combinations of θ and ϕ . The Jacobian is calculated from the nine values of each function.

2.4.4 Calculation of Functions F_1 and F_2

The process of calculating the functions is shown in Figure 2.7. Each step in the process is now discussed.

- i) Azimuth angle and rate are calculated from the constrained values of sideslip velocity and acceleration, as described in Appendix 5.

ii) The attitude rates and accelerations are calculated using numerical differentiation. A backward difference method (Ref. 23) is used. The derivative of each attitude angle is calculated on the basis of the latest estimate of the angle, and the value at the last calculation time point (see Appendix 6). For example, pitch rate at time point k, is given by :

$$\dot{\theta}_k = \frac{\theta_k - \theta_{k-1}}{t_k - t_{k-1}} \quad (2.46)$$

iii) The body-axis translational velocities and accelerations can now be calculated using the transformation given in Appendix 2. The rotational velocities and accelerations are calculated using the expressions given in Appendix 7. The inertial and acceleration force and moment components of the equations of motion can now be calculated.

iv) The angles of incidence are calculated (eqns. 2.39 and 2.42) and, using the helicopter's configurational data, the aerodynamic forces and moments can be calculated from equations A4-3, Appendix 4.

v) Using configurational data, the main rotor thrust coefficient, C_T , can now be calculated by rearrangement of equation 2.35 (the z-force equation), and the longitudinal flapping angle, β_{1C} , from the pitching equation, 2.37.

vi) With the thrust coefficient C_T known, it is possible to calculate the induced velocity through the rotor by first evaluating the components of rotor hub velocity (equations A4-7), then solving equation A4-10 (Appendix 4).

vi) An iterative scheme is now used to calculate the tail rotor thrust coefficient, C_{Ttr} , and the lateral flapping angle, β_{1s} , from equations 2.36 and 2.38. This scheme can be summarised as follows.

- a) Make an initial guess of the lateral flapping angle, β_{1s} (the final value at the last time point is suitable).
- b) Calculate the longitudinal flapping angle in wind-axes, β_{1cw} , and the main rotor torque coefficient, C_Q , from equations A4-9 and A4-8, Appendix 4.
- c) The tail rotor thrust coefficient is calculated by manipulation of equation 2.38, the yawing equation.
- d) A new value of β_{1s} is then found by rearranging equation 2.36, the rolling equation.
- e) This value is compared with the last estimate, and adjusted if necessary. The process continues from stage (b) until there is convergence of the β_{1s} values.

Values for all parameters in equations 2.44 are now known and the functions F_1 and F_2 can be evaluated.

2.4.5 New Estimate of Attitude Angles

With the nine values of F_1 and F_2 calculated, the elements of the Jacobian can be evaluated. For example, from Appendix 6,

$$\frac{\partial F_1(\theta_1, \phi_1)}{\partial \theta_1} = \frac{2 [F_1(2) - F_1(4)] - [F_1(3) - F_1(5)] / 4}{3h\theta_1}$$

The other entries in the Jacobian are found from similar expressions. A new estimate of the attitude angles can then be found from equation 2.45. The next step is to test for convergence. The solution is assumed to have converged when the following two conditions are satisfied.

$$1 - \left[\frac{\theta_{i+1}}{\theta_i} \right] \leq 0.0001 \quad , \quad 1 - \left[\frac{\phi_{i+1}}{\phi_i} \right] \leq 0.0001$$

Once these conditions are fulfilled the control angles can be computed (as described in Appendix 4) and the solution continues at the next time point. The values of the attitude angles are stored to enable a good first estimate to be made at the next time point.

The performance of the algorithm is discussed in section 2.7 after some results, obtained using the HELINV program, have been presented.

2.5 Some Examples

The HELINV program allows control time histories to be calculated for several classes of flight path. They can be split up into three categories (as described in section 2.3) - longitudinal, turning and three-dimensional manoeuvres. Results from calculations of the state and control time histories, for helicopters flying manoeuvres from each of these categories, are presented in the following section.

Two sets of configuration data have been used in the mathematical model, the first set representing a conventional battlefield helicopter (henceforth referred to as the B configuration) and the second representing a conventional transport helicopter (T configuration). Some configurational data is given in Table 1. The B configuration has a semi-rigid rotor with high stiffness in flapping, whilst the T configuration has a fully articulated rotor. This is accounted for by the large difference in the values of the rotor flapping stiffness (K_p) shown in Table 1. The B configuration has more control power than the T configuration due to this difference in flapping stiffness. This should be evident when comparing their responses and control displacements flying identical manoeuvres.

All of the manoeuvres are "flown" with sideslip constrained to be zero (i.e. $\beta = 0$), and all variables are plotted as displacements from their trim value.

2.5.1 The Pop-up Manoeuvre

This manoeuvre is used to clear obstacles. In this example the obstacle is 25m high and the manoeuvre is started from a distance of 200m. At a constant speed of 80 knots the manoeuvre time is 4.9s and the load factor varies between the limits $0.4 \leq n \leq 1.6$. A time interval of 0.05s was used for the calculation. The control, attitude and velocity time histories are shown in Fig. 2.8

The control angle plots show the difference in control power available to the helicopters. The B configuration, with its very much stiffer hingeless rotor, requires smaller control deflections to perform the same manoeuvre as the T configuration, with its less stiff articulated rotor. Collective pitch (THT0) is used to vary the helicopter's rate of change of height as indicated by its graph (increasing height rate in pull-up then decreasing at push-over, with a small over-shoot to level off to the new trim state). Since the manoeuvre is performed with sideslip constrained to be zero, the tail rotor collective pitch (THOTR) follows the same trend as main rotor collective (tail rotor is used simply to balance the main rotor torque, and not to point the fuselage). The tail rotor collective pitch angles of the B and T configurations have opposite sign because the main rotors rotate in opposite directions. This also explains why the helicopters roll in opposite directions when cyclic and collective pitch changes are applied. Longitudinal cyclic pitch (THT1S) is used to control the forward speed of the helicopter - negative values showing a stick (and disc) forward condition. The helicopter's nose pitches up (positive values of fuselage pitch attitude - THT) in the pull-up at the start of the manoeuvre, as would be expected, but as the

helicopter pushes over, the nose is pointed down sharply to maintain constant speed. Towards the exit from the manoeuvre the disc tilts back to ensure that the commanded forward speed is not exceeded and the pitch angle returns to its trim value. Due to coupling, the large displacements in longitudinal cyclic pitch cause smaller displacements in lateral cyclic pitch (TH1C), which in turn causes significant roll displacements. The attitude graphs clearly indicate the large degree of coupling between pitch and roll experienced in helicopter flight.

The pitching moment produced by a helicopter is made up of two components; the moment due to the offset of the tilted main rotor thrust vector from the centre of gravity, and the moment due to the elastic stiffness of the rotor. Since the B configuration has a much stiffer rotor than the T, the required disc tilt to produce a particular control moment is less. This results in a much smaller fuselage pitch displacement. This effect is discussed by Attlefellner and Sardanowsky (Ref. 24).

The results presented for this manoeuvre are calculated on the basis of the manoeuvre being flown at constant speed. As discussed above, this causes large excursions in longitudinal (and hence lateral) cyclic pitch angles. In reality a pilot is more likely to allow his speed to drop as he climbs. The time histories shown in Fig 2.9 are for the same manoeuvre described above, but with a reduction of 10 knots between entry and exit. Since it is no longer necessary to tilt the disc to maintain speed, there is a large reduction in the required longitudinal cyclic pitch displacements. This has the effect of reducing lateral cyclic variation and hence roll displacement. Since the power required to perform the

manoeuvre has been reduced, there is a large reduction in the amount of collective pitch required.

2.5.2 The Level Turn

Time responses for a 90 deg. right-hand level turn with an effective radius of 250m are given in Fig. 2.10. The transition sections occupy the first and last 10% of the track. The manoeuvre time at a constant 80 knots was 9.8s and the calculation step length was 0.1s. Again an indication of relative control power is given by the control plots, the T configuration requiring much larger control deflections to perform the same task. The primary control for this manoeuvre is lateral cyclic, which is used to roll the helicopter to the required bank angle through the entry transient, then maintain this attitude until rolling back to level through the exit transient. The plot of lateral cyclic shows the T configuration requiring almost twice as great a deflection in the transients to produce the required roll rate. Tail rotor collective follows main rotor collective as the turn is performed with zero sideslip. To maintain height during a turn, thrust has to be increased to compensate for the weight balancing component which is reduced as the aircraft banks and the thrust vector is tilted. This is achieved by increasing main rotor collective.

2.5.3 The Climbing Turn

The time responses for a 90 degree right hand climbing turn are shown in Figure 2.11. The effective radius of the turn was 250m and a height change of 25m was commanded. The transient sections of the turn

occupied the first and last 10% of the track. The manoeuvre time at a constant 80 knots was 10s and a step length of 0.1s was used. This manoeuvre can be considered as a combination of the previous two examples - the transients in the climbing turn being flown at constant height (as in the level turn) and the height change (in the form of a pop-up) being superimposed over the steady circular turn section.

2.6 Validation of Results

Although the time histories generated by HELINV appear intuitively to be sensible in size and trend, it is still of importance to be able to verify these results. This section describes the method used.

2.6.1 The Use of a Time Response Solution

The HELINV program gives control angles required to fly a given flight path for a helicopter independent of pilot and control system i.e. the solutions achieved are based only on the dynamics of the aircraft. This means that any attempt to compare directly control time histories generated using the program, with actual flight data is pointless from the point of view of program validation. A pilot flies a manoeuvre with a certain amount of foresight and acts as a sensor in a feedback loop making corrections to his control inputs as he progresses along the flight path. When the computer "flies" the simulated helicopter along the same trajectory, it can draw only on information at, and before, its present location on the flight path. Therefore it is unlikely that, even with a control system included in the mathematical model, HELINV results would closely match those of a flight test. The only method of verifying whether accurate results are being calculated is by comparison with an existing simulation. This involves performing a forward time response solution, using the mathematical model from the original HELISTAB program, to find what flight path a HELINV generated control time history produces. By comparing this control generated flight path with the commanded flight path it is possible to see how accurate the inverse method is. If the two flight paths are identical (to within a reasonable

numerical tolerance) then the inverse method is supplying accurate solutions and the validity of these solutions depends on that of the mathematical model.

A general description of a forward type solution is given in section 2.2. The program used for validation is based on this method. Control angle values are supplied (by HELINV) at equally spaced time intervals. They are then joined by ramps to give the simplest form of continuous function. The same expressions are used to calculate the external forces and moments (Appendix 4) of the aircraft for use in the equations of motion in both forward and inverse solutions. This ensures that the same equations are being solved in the forward and inverse directions. The equations of motion are integrated using a Runge-Kutta-Merson technique (Ref. 25) to give body velocity and attitude time histories which, when transformed to the earth fixed axes system, can be used to find the control generated flight path.

2.6.2 Results

The above method has been used to find control generated flight paths for both helicopters over all three manoeuvres described in the previous section. The results for the B and T configurations are shown in Figures 2.12 and 2.13 respectively.

The results for the pop-up manoeuvre are particularly good with an almost perfect match in altitude (only a very small divergence at the exit) and a drift from the required track of less than 0.15m for the B configuration and 0.4m for the T configuration data.

The comparison of flight paths for the B configuration in the level turn is also very accurate (the tracks are almost indistinguishable and there is a maximum change in altitude of only 0.75m over the 400m of track). The level turn comparison for the T configuration is not quite so accurate with a height gain of about 5m, and a noticeable cumulative error building around the track.

The comparison of flight paths for the B configuration data shows an almost exact agreement between forward and inverse solutions for the track in the climbing turn manoeuvre. The altitude plots show a small error at the entry transient where the helicopter levels off. The comparison for the T configuration again shows good correlation in the track plots but a large error in the altitude plots towards the exit.

2.6.3 Cause of Discrepancies

One of the problems encountered when comparing a forward with an inverse solution is that different numerical processes are used in each. The inverse solution uses a first order backward differentiation technique (equation 2.46), whilst the forward solution is based on a fourth order integration. The truncation error, caused by the omission of higher order terms from an approximating series or function, associated with each of these methods is different. As the time step used in the calculations tends to zero, the truncation errors should also tend to zero. The following test was performed to investigate what effect truncation errors have on the forward solution.

Firstly, HELINV was run for the pop-up described above ($s=200m$,

h=25m, V=80 knots), using data for the B configuration, but with a calculation time step of 0.005 seconds. The attitude and control time histories are shown in Figure 2.14. The resulting control time histories were used in a forward solution, producing the flight path comparison given in Figure 2.15 (a). A "thinned" series of control time histories were then extracted from those of the original inverse solution, values from every tenth time point being removed. This has the effect of increasing the time step used for the forward solution by a factor of ten. The forward solution is then performed with the reduced control time histories, the results plotted on Figure 2.15 (b). If the truncation error associated with the forward solution was significant, then increasing the time step, in this case by thinning the time histories, would produce an increased truncation error. Examination of Figure 2.15 shows this is clearly not the case.

It can be concluded that the forward solution is consistent, and that the use of dissimilar numerical methods cannot be blamed for the discrepancies in the comparisons of flight paths. Hence, the cause of errors and inaccuracies in the HELINV results must come mainly from within the inverse algorithm itself. Comparison of the time histories plotted in Figures 2.8 and 2.14 gives some insight into the reason for the errors. Both sets of plots are for the same manoeuvre, the time histories in Figure 2.14 being calculated using a time step one tenth as small as that used to produce the plots for Figure 2.8. The main difference between the two sets of plots is that with the time step reduced, the solutions become oscillatory in nature. This is most clearly observed in the graphs of "THTIS" and "P". This effect is analysed and discussed fully in the next section.

2.7 Discussion and Analysis of Inverse Algorithm

Examination of the above comparisons of forward and inverse solutions shows that the results for the B configuration would tend to indicate an accurate and valid solution, only very small errors being visible between the commanded flight path and the control generated flight path. The much larger differences present in the T configuration comparisons seem to contradict this. The plots obtained using HELINV presented in the previous sections (Figures 2.8-2.14) also exhibit other features which require explanation. In particular, oscillations are visible in many of the plots (the graph of "P" in Figure 2.9, and most of the graphs in Figure 2.10, amongst others). There is also the problem of attaining the commanded trim condition at the exit from the manoeuvres (all of the plots should return to zero). These features of the inverse algorithm are analysed and discussed in the following section.

2.7.1 A Linearised Approach

It is often useful to analyse the behaviour of a nonlinear dynamic system by linearising its equations of motion. The equations can be written in a convenient matrix form and simple matrix algebra used to determine the dynamic characteristics of the system. For this reason it would seem logical that a linearised version of the mathematical model would be of use in the investigation of the irregularities present in the HELINV solutions. For convenience, a linearised version of the HELISTAB mathematical model was used. A description of the linearising process and the resulting equations are given in Appendix 8, section 1. The aerodynamic derivatives of the helicopter are calculated by numerical

differentiation of equations A4.1.

2.7.2 The Oscillatory Nature of the Inverse Solution

The linearised equations, when arranged in the form given by equation A8.1, can be used to describe the unconstrained motion of a helicopter in response to an applied series of control inputs. The eigenvalues of the helicopter are found from the system matrix, hence the period and damping of any oscillatory modes can be calculated. Calculation the system matrix and eigenvalues for the B configuration at a velocity of 80 knots, gives oscillatory modes of period 2.8 and 16.7 seconds. These do not correspond to those observed in the inverse solution for a pop-up at a constant speed of 80 knots, given in Figure 2.14. In Figure 2.14 the oscillations have a period of approximately 1.15 seconds for "THT1S" and 0.75 seconds for "P". The oscillations observed in the inverse solution are not therefore due to the modes of the unconstrained helicopter. An explanation of these oscillations is found by examining the fundamental nature of the inverse solution.

The inverse method detailed in this chapter solves the equations of motion for a helicopter constrained to fly a rigidly defined manoeuvre. Section 2 of Appendix 8 shows that by grouping together the state variables which are under constraint (u, v, w from the flight path definition, and r from the sideslip function), and partitioning the system matrix, a new representation of the helicopter's dynamics is found (equation A8.6). The modes of the new, constrained system are found from the modified system matrix A_C , the method of calculation of which is given in section 3 of Appendix 8. Using the constrained system matrix A_C , it is

possible to predict the oscillatory form of the solution.

Using the case given in Figure 2.14 as an example, calculation of the matrix A_C , and its associated eigenvalues for a trim flight velocity of 80 knots, gives the following two modes. The first is a divergent oscillation of period 0.7 seconds and time to double amplitude of 116 seconds. The second mode is a convergent oscillation of period 1.19 seconds and a time to half amplitude of 2.9 seconds. These periods show good correlation with those measured from the graphs on Figure 2.14 (0.75 and 1.15 seconds). A more comprehensive example, using both B and T configurations, is given by considering a different manoeuvre. The plots in Figure 2.16 are for a pop-up to a height of 20m over a distance of 300m, performed at a constant speed of 120 knots. The calculation step size was 0.01 seconds. The matrix A_C predicts oscillations of period 0.76 and 1.21 seconds for the B configuration and 1.27 and 2.49 seconds for the T configuration. The graphs in Figure 2.16 exhibit oscillations of approximately these periods.

It can be concluded that the oscillatory nature of the results from the inverse algorithm is due to the application of constraints. The constraints modify the dynamics of the helicopter thereby causing new oscillatory modes to dominate its response. The periods of the oscillatory modes are predicted by the theory given in Appendix 8. The damping of the oscillations is linked to the time step chosen for the calculation, as the time step is reduced, damping is reduced (Figures 2.8 and 2.14).

2.7.3 Displacement from Trim State at Exit from Manoeuvre

The displacement from the commanded trim condition at the exit from the manoeuvre can be explained by consideration of the flight path geometry at this point. At the exit, the polynomial representation of the flight path is, in effect, joined to a linear steady section. In the case of the pop-up, there is only continuity in the flight path up to the second derivative at the join (i.e. the boundary conditions allow for zero acceleration). There are similar discontinuities in all of the flight paths. It is the discontinuity of higher order derivatives which causes the error in the trim state at the exit. In an inverse solution, a discontinuity in the higher order flight path derivatives (i.e. a discontinuity in the "input signal") is analogous to a step input to a control variable in a conventional time response solution. The helicopter can therefore be expected to respond in a similar manner. The analysis given above predicts that the dynamics of a helicopter, constrained to fly a precisely defined flight path, are dominated by two oscillatory modes. The response of the helicopter, after encountering the discontinuity at the exit from the manoeuvre, will therefore be to oscillate about the commanded trim state. This is most clearly demonstrated by the following example.

Figure 2.18 shows time histories for the previously described pop-up manoeuvre (Figure 2.8) but with a 200m linear section added at the exit. The calculation step size has also been reduced to 0.025 seconds. The solutions are identical up to the exit from the pop-up section (after about 5 seconds), thereafter all of the state and control variables oscillate towards their trim values. The period of these oscillations are as predicted by the theory in Appendix 8. It is noticeable that the

oscillations of the B configuration are more heavily damped. This is consistent with the analysis and with the relative properties of the helicopters rotors, the high elastic stiffness of the B configuration's rotor supplying significantly more damping to the helicopter than the articulated rotor of the T configuration.

2.7.4 Difference Between Control Generated and Commanded Manoeuvres

Comparisons of commanded and control generated flight paths for the previous two pop-up manoeuvres (Figures 2.16 and 2.18) are given in Figures 2.17 and 2.19. It is apparent from these plots that using a small time step does not produce good correlation between the flight paths. In Figure 2.19, the difference between the flight paths up to the exit from the pop-up are similar to those in Figures 2.12a and 2.13a. It is only in the linear section that large differences occur, especially in the plots of the track (x vs. y). Since in this phase of the manoeuvre the oscillatory modes are dominant, it can be surmised that the oscillations are the major cause of the discrepancies between the flight path plots. Further, comparing Figure 2.12a with 2.15a, it is apparent that as the computational time step used for a given manoeuvre is reduced, the difference between the control generated and commanded flight paths increases. Again, this is a consequence of the oscillations in the inverse solution, as the time step is reduced the amplitude of the oscillations is increased. Although the difference between the flight paths will be reduced as the time step is increased, there is an upper limit where a large time step will produce errors in the numerical differentiation process. This implies that an optimum time step might exist for each manoeuvre.

2.7.5 Numerical Differentiation

The use of small time steps may also cause inaccuracies in the calculation of attitude angle rates. Over a small time step the value of a particular attitude angle may only change by a small amount. This may produce rounding errors in the numerical differentiation process when subtracting similar numbers. This condition is most likely to occur when computing the attitude rates for gentle manoeuvres using small time steps.

2.7.6 Limitations in the Mathematical Model

The time histories in Figure 2.20 are calculated using the data for the B configuration performing a pop-up manoeuvre to clear a 40m obstacle, from a distance of 200m, at a constant velocity of 80 knots. The normal load factor in this manoeuvre varies between zero and 2g. Although this is a fairly severe manoeuvre it is still within the envelope of a real battlefield helicopter. The control time histories show values far in excess of the control limits (shown by the broken lines). The attitude plots also show very large deviations from trim (over 50 degrees of roll at one point). Figure 2.21 shows the comparison of flight paths for forward and inverse solutions. These graphs show only very small differences. This suggests that the inverse algorithm is able to calculate accurate and valid solutions for severe manoeuvres, but that the mathematical model is not predicting accurate values for the control angles.

The existing mathematical model has a major limitation when used to find inverse solutions for severe manoeuvres, namely the calculation of

the aerodynamic forces and moments of the fuselage and empennage. The aerodynamic force and moment coefficients of the fuselage are given as empirical functions of the incidence angles (equation A4.2), whilst those of the tailplane and fin are calculated on the basis of two-dimensional aerodynamic theory. In both cases the coefficients are only accurate over the range $-20^\circ < \alpha, \beta < 20^\circ$. For the fuselage coefficients, polynomial functions are fitted through wind tunnel data measured over the above limits. Beyond these limits the functions increase (or decrease) rapidly without any levelling off. This behaviour is not consistent with that of a real helicopter where, outside these limits, the flow would be expected to separate from the fuselage. Prediction of the flow pattern in these conditions is obviously extremely difficult due to the presence of the downflow from the rotor. The fin and tailplane coefficients will also be inaccurate outside these limits as the surfaces are likely to have entered the stall region. As the downwash effects on the tailplane are not modelled, prediction of the pitching moment from the tailplane may not be accurate. This may have implications when calculating the pitch attitude of the helicopter. It is apparent that under certain flight conditions the aerodynamic forces and moments of the helicopter are not adequately modelled. Outside the incidence limits quoted above, unrealistically large values are predicted, which in turn cause poor prediction of the control and attitude angles.

An improved mathematical model already exists which incorporates a more comprehensive rotor model with individual blade degrees of freedom. Inclusion of this model into the inverse program may improve accuracy in the prediction of the control angles. A more significant improvement would be a better representation of the fuselage aerodynamic properties. The

current limits of ± 20 degrees angle of attack is inadequate for certain severe manoeuvres. A possible solution might be some sort of look-up table for the fuselage aerodynamic coefficients, which might also include the effects of fuselage pitching velocity.

2.7.7 Improved Flight Paths

Gaps exists in the range of available flight paths, possibly the most significant being the bob-up manoeuvre. This is a height change from the hover and is of importance in the battlefield role for target acquisition in the hover whilst remaining under cover of a tree line (perhaps using a mast mounted sight) then weapons firing once the cover has been cleared. This manoeuvre would be defined as a velocity change along the earth z-axis from zero in the hover to some maximum value then back to zero at the firing height. Consequently the velocity components along the x and y earth axes are zero. Referring to Appendix 5 equation A5.2 reduces to :

$$\dot{z} \sin\phi \cos\theta = 0$$

since the coefficients a and b of expressions A5.3 and velocity V, are all zero.

The above expression is independent of yaw attitude ψ , and thus it is impossible to find the body axes velocities using an Euler angle transformation, however changing the frame of reference would overcome this problem. This discontinuity in the transformation causes problems in fixed wing aircraft flight mechanics in the vertical dive flight state.

Other flight paths such as the wing-over and side-step might also be added to produce a more complete set of NOE manoeuvres.

2.8 Conclusions

The requirements for a general method of quantifying helicopter inherent agility are outlined in section 1.4 of Chapter 1. The main requirement was the development of an inverse method for solution of the helicopter equations of motion. A description of such a method has been given in this chapter. The algorithm is based on an established six degrees of freedom, nonlinear mathematical model, HELISTAB. A series of standard manoeuvres have been defined to represent tasks relevant to the NOE environment. It has been shown that by constraining a helicopter to fly a precisely defined manoeuvre with a fixed sideslip, its dynamic characteristics are significantly altered. Despite this, the inverse algorithm, HELINV, is robust and free from numerical instabilities, its limitations being governed by those of the mathematical model. Although the limitations of the model impose boundaries on the severity of the possible manoeuvres, it has been shown that accurate and valid inverse solutions can be found, for various configurations, performing a wide enough range to allow progress in an agility study.

CHAPTER 3

AN ANALYTIC METHOD OF QUANTIFYING HELICOPTER INHERENT AGILITY

3.1 Introduction

In Chapter 1 (section 1.4) some of the qualities necessary for an agility evaluation method are discussed. It was shown that an inverse solution of the helicopter equations of motion would be of great use. The development of an algorithm, HELINV, capable of performing this type of solution was described in Chapter 2. The expansion of HELINV into an Agility Evaluation Program (AEP) is presented in this chapter. The preliminary stage of the development is to determine ways in which the results from HELINV can be related to helicopter inherent agility.

3.2 Relating Agility to Inverse Solutions

A simple definition of inherent agility, given in Chapter 1, is "inherent agility is the ease with which a helicopter can change its state". The inherent agility of several helicopter types can thus be compared if each is forced to change its state by a prescribed amount, and the ease with which this is achieved is measured. The inverse solutions produced by HELINV are ideal for this purpose. It was shown in the previous chapter (section 2.7), and in Appendix 8, that precise definition of a manoeuvre effectively applies constraints on certain states (namely u, v, w, r). It follows that if a number of different helicopters are simulated performing the same manoeuvre, using HELINV, then the change in the constrained states will be equivalent for each helicopter. Further, as azimuth angle, ψ , is calculated directly from the constrained sideslip velocity (see Appendix 5), changes in this state will also be equivalent for a given manoeuvre. The inherent agility is therefore the ease with which the remaining states (p, q, θ, ϕ) are changed. The state changes can be measured by their time histories, whilst the ease of change can be found from the control time histories. For a given manoeuvre, the more agile the helicopter, the smaller will be the control and unconstrained state displacements. This is the basis of the method of quantifying agility developed in this thesis.

3.3 The Agility Performance Index (API)

3.3.1 Use of Performance Indices to Evaluate Agility

A method of quantifying inherent agility based on its control and unconstrained state displacements will allow values to be calculated based on the helicopter's performance flying a single manoeuvre. This value will be calculated from the resulting state and control time histories produced by HELINV. Standard techniques of quantifying the performance of dynamic systems already exist (Ref. 27), the most common being the use of performance indices. They are generally written in the form :

$$J = \int_0^t F(\underline{x}, \underline{u}) dt \quad (3.1)$$

where : J = performance index,

F = cost function,

\underline{x} = the state vector,

\underline{u} = the control vector.

The use of performance indices to evaluate helicopter agility was first demonstrated by Legge, Fortescue, and Taylor (Ref. 7). Legge et al used a simple kinematic helicopter model to calculate pitch attitude displacements for a dash/stop manoeuvre (an acceleration from the hover to a finite speed, followed by a deceleration back to the hover). Agility was then calculated as the integral of a cost function based on these pitch angles. A simple analysis such as this relates agility simply to excess power and fuselage drag (rotor thrust was assumed constant). No account was taken of the helicopter's dynamic state during manoeuvre. The

six degrees of freedom, nonlinear model used in this analysis has two major advantages when used in conjunction with performance theory to evaluate agility. Firstly, all of the states and control variables may be incorporated into the cost function, and secondly, valid simulations of helicopters flying a much wider range of manoeuvres can be performed.

For this agility study, small state and control displacements (which indicate high inherent agility) integrated over the manoeuvre time, will give lower values of the performance index. Optimum agility performance is found when the index is a minimum. A quadratic cost function has been used, and can be expressed, in general terms, as :

$$F(\underline{x}, \underline{u}) = q_1 x_1^2 + \dots + q_i x_i^2 + \dots + q_{n_s} x_{n_s}^2 + r_1 u_1^2 + \dots + r_j u_j^2 + \dots + r_{n_c} u_{n_c}^2$$

where :

- q_i = the weighting constant of state i ,
- r_j = the weighting constant of control j ,
- n_s = number of unconstrained states,
- n_c = number of controls.

(3.2)

This function heavily penalises large values of any state or control variable by squaring them. Using a quadratic cost function also has the advantage of simplicity and ensures positive values for the performance index. By careful selection of the weighting constants the more important variables can have greater influence over the value of the performance index than other less important variables. Each weighting constant will reflect the importance of each variable to the agility of the helicopter. Since each control or variable has its own particular significance in each type of manoeuvre (large displacements in lateral cyclic are expected in

turning flight but undesirable in accelerations, for example) the values of q_i and r_j will be dependent on the type of manoeuvre being performed. The weighting constants for a turning manoeuvre are different from those in a pop-up or hurdle-hop manoeuvre.

3.3.2 Definition of an Agility Performance Index

The general form of cost function given by equation 3.2 is insufficient to quantify agility. An Agility Performance Index (API) more suitable for quantifying the inherent agility of a helicopter for a single manoeuvre, can be defined as :

$$API = t' \cdot \left\{ \sum_{i=1}^{n_s} q_i \cdot \int_0^{t_m} \left[\frac{x_i(t) - x_{it}}{x_{im} - x_{it}} \right]^2 dt + \sum_{j=1}^{n_c} r_j \cdot \int_0^{t_m} \left[\frac{u_j(t) - u_{jt}}{u_{jm} - u_{jt}} \right]^2 dt \right\} \quad (3.3)$$

where :

- t_m = manoeuvre time,
- t_{max} = maximum manoeuvre time (see below),
- t' = t_m / t_{max}^2 ,
- n_s = number of states,
- q_i = weighting constant of state i ,
- $x_i(t)$ = time history of state i ,
- x_{it} = trim value of state i ,
- x_{im} = maximum allowable value of state i ,
- n_c = number of controls,
- r_j = weighting constant of control j ,

- $u_j(t)$ = time history of control j ,
- u_{jt} = trim value of control j ,
- u_{jm} = limit of control j .

The API has been expressed in this form for the following reasons.

a) The standard form of cost function, equation 3.2, uses the absolute value of each state and control. Since agility is a measurement of performance in unsteady flight, it is more desirable to use displacements from trim in the cost function.

b) In order to quantify what fraction of potential performance has been used, the instantaneous displacement from trim of each variable is divided by its maximum allowable displacement. The maximum allowable values of the state variables are set by consideration of design limits, pilot comfort, and safety (see section 3.4). Control limits are dependent on rotor design. The control limits of the B and T configurations are given in Table 2. Using a ratio of instantaneous to maximum allowable displacement has the effect of normalising the cost function, as well as measuring what fraction of the allowable displacements have been used to achieve a commanded flight state. An agile helicopter will require smaller displacements, and have available larger allowable displacements (i.e. higher limits), therefore giving smaller fractions in the cost function and lower API values.

c) It is essential that the cost function be formulated in the above manner if comparisons between different helicopters are to be made. If absolute values were used instead of displacements from trim, then a

configuration with large trim state or control values might be awarded a high API value (indicating poor agility) even if it performed a manoeuvre with small displacements from its trim state. If the maximum allowable values of each state were not included, then it would be possible for two helicopters to be awarded the same API value, by performing the manoeuvre using the same state and control displacements, although one of them may be flying close to its limits. Using a cost function of the form given by equation 3.3, as the limits are approached, the ratios tend towards unity, which when squared, can give high values of API. Thus, a helicopter which performs a manoeuvre close to its limits will be graded as having poor inherent agility, whilst one which still has the potential to perform a more severe manoeuvre before its limits are reached, will be graded as having better inherent agility.

d) The theory developed in this chapter will be used to compare the agility of different helicopters over several series of standard manoeuvres. Each series of manoeuvres will consist either of a single flight path flown at various velocities, or a series of similar flight paths, varied by altering a single dimension (the distance to an obstacle of fixed height in the case of the pop-up, for example), all flown with the same velocity. In both cases, a series of manoeuvres of varying severity will be formed. Although unlikely, there is a possibility that a helicopter may be awarded the same API for its performance in two manoeuvres of completely different severity (by merit of performing both manoeuvres with similar state and control displacements). If comparisons between a helicopters performance over a series of manoeuvres are to be made, then the manoeuvres must be weighted. Good performance (i.e. small state and control displacements) in more severe manoeuvres must have a

higher grading (lower API values) than similar performance in a less severe manoeuvre. This is achieved by multiplying the cost function by manoeuvre time. Severe manoeuvres will be performed in a shorter time, hence multiplying the cost function by a smaller number.

e) The maximum value of each state or control ratio in the cost function is unity. If the weighting constants are given the property :

$$\sum_{i=1}^{n_s} q_i + \sum_{j=1}^{n_c} r_j = 1$$

then the maximum possible value of API is t_m^{-2} . To assist in its interpretation, the expression for API has been divided by the square of the "maximum manoeuvre time". This is the time taken to perform the least severe manoeuvre within a defined series. As well as having a non-dimensionalising effect, this ensures the maximum possible value of API is one, corresponding to the poorest possible agility. This value is unlikely ever to be reached since it could only occur if the least severe manoeuvre of a series (where $t_m = t_{max}$), was performed with all states and controls at their limiting value. Similarly, best possible agility is indicated by an API value of zero. This is impossible to achieve since it would require the whole manoeuvre to be flown without any displacement of the states or controls.

Before equation 3.3 can be used to calculate Agility Performance Indices values must be set for the state limits, and the weighting constants.

3.4 Selection of Maximum State Values

The maximum value of the states depends on the manoeuvres being performed. A trivial illustration of this is the value chosen for maximum roll angle, a value of 10° might be suitable for the pop-up manoeuvre, but totally unacceptable for a turning manoeuvre. The maximum state values chosen for each type of manoeuvre are given in Table 3, and the reasons for their choice are now discussed.

a) Roll Rate, p

During manoeuvres in the longitudinal plane (the pop-up, for example) large roll rates, in conjunction with inevitable pitch excursions, might cause pilot disorientation, as well as difficulties in tracking obstacles or targets. A low limit has therefore been set for these manoeuvres, whilst much higher limits have been set for turning manoeuvres.

b) Pitch Rate, q

A similar situation arises here - large pitch rates are unavoidable in longitudinal manoeuvres, but are undesirable in turning flight. This is reflected in the choice of maximum values.

c) Roll Angle, ϕ

Large roll displacements can cause height loss, which can be dangerous in low level flight. Roll displacements occur in longitudinal

manoeuvres as well as in turns. During severe longitudinal manoeuvres (e.g. rapid pull-ups) the cross coupling of pitch and roll with main rotor collective and cyclic pitch can cause large roll displacements. The resultant potential height loss has to be accounted for by increased collective pitch and hence increased pilot workload. For this reason, a low value of maximum allowable roll angle is set for longitudinal manoeuvres. The limiting value for roll angle in turning flight was set at 70° because of limits in the HELINV algorithm. This is still a realistic value since, in NOE flight in close proximity to the ground, helicopters are unlikely to fly at high enough speeds to allow roll angles greater than this to be achieved.

d) Pitch Angle, θ

Rapid acceleration causes the nose of a helicopter to pitch down as the rotor disc tilts forward. This has two implications. Firstly the tail rotor (a major noise source) may appear above a covering tree line and secondly there is danger of an advancing blade ground strike. Similarly severe deceleration causes large nose up attitudes as the rotor disc tilts back. There is then the danger of tail rotor ground strike. A limit of 20° has been set for longitudinal manoeuvres. Model limitations had some influence on the choice of this value. Outside this limit the validity of the expressions for the aerodynamic forces and moments of the helicopter is in doubt.

3.5 Selection of Weighting Constants

3.5.1 The Need for Weighting Constants

Large displacements of each state or control variable has a different significance in each class of manoeuvre. For example, large nose-up fuselage pitch angles can hamper a pilot's vision - of obvious importance in descending flight at low level. Large nose up pitch attitude is therefore undesirable in the descending portion of the hurdle-hop manoeuvre. However, large pitch displacements are of less importance during turning flight where the pilots vision is governed by the roll attitude which the helicopter adopts. If the contributions of each variable to the cost function were simply added without weighting, then a large displacement of a relatively unimportant variable might influence the calculated value of API. This can be show by the following example.

Figure 3.1 shows plots of API for both B and T configurations flying a single pop-up manoeuvre (height 25m, distance 250m) over a range of velocities (60-80 knots). The maximum manoeuvre time is 8.15 seconds, which is the time taken to fly the pop-up manoeuvre at 60 knots. In this example, all weighting constants have been given the value of 1. It is intuitive that the B configuration will be more agile than the T, by merit of its stiffer rotor. This is reflected in the plots, the curve for the T configuration being above that for the B. Figure 3.2 shows the contribution made by each variable to the total API. In both cases main rotor collective is the dominant variable. This is no surprise since large displacements in this control can be expected during a height change

manoeuvre. However, the manoeuvre was performed at constant forward speed implying that longitudinal cyclic control is at least as important as collective. This is not reflected by the plots. The degree to which collective dominates the API is also questionable, its contribution being three times that of the next largest contributor, roll angle ϕ . Examination of Figure 3.2 underlines the need to develop a method of selecting values for the weighting constants.

3.5.2 A Method of Selecting Weighting Constants

Weighting constants are chosen to ensure that the contributions made by each variable to the total API reflects the consequence, on the helicopter's agility, that large displacements of the variable might have. For example, large nose down displacements in pitch can cause main rotor ground strikes in low level accelerated flight. An agile helicopter will be able to perform this manoeuvre with small pitch changes. The weighting constant chosen for pitch displacement should reflect the importance of this variable by making its contribution to the total API large, in relation to the contributions of the other variables. Each of the other variables will have its own implications on the agility of the helicopter, and the weighting constants should be chosen to exhibit this.

No standard technique exists for the selection of weighting constants. However, performance functions are often used in optimal control theory (Ref. 28) where an accepted method of selecting weighting constants does exist. The technique consists of selecting initial values for the constants, then studying the resultant system response. The constants are then modified until the required response is achieved. The

initial value of a weighting constant is often taken as the reciprocal of the square of the maximum expected value of the state or control. This method has been adapted to allow selection of the weighting constants of the agility performance function.

In order to find good initial values, and to reduce the effort needed to find suitable final values, a strategy to find the level of importance of the contribution from each variable, in a particular manoeuvre, has been devised. The methodology adopted is as follows.

1. Answer the follow questions for each variable.
 - a) Can weighting constant be set to zero ?
 - b) In an agile helicopter, is a large displacement in this variable likely ?
 - c) In an agile helicopter, is a large displacement in this variable acceptable ?
2. For all states and controls, award a whole number grading, representing the implications on the agility of a helicopter that a large displacement this variable will have.
3. Find the initial value of each weighting constant by expressing its relative importance grading as a fraction.
4. Select a test range of manoeuvres, and calculate API values for each manoeuvre within this range.

5. Examine the contributions of each variable to the total API over all of the test manoeuvres.

6. If the contributions do not reflect the relative importance of each variable to the helicopter's agility, then this series of constants is unsuitable.

7. The weighting constants should be altered, in turn, until a suitable series is found.

Some explanation of this method is given below.

i) It may be possible to give the value zero to some of the weighting constants. In particular, in turning flight the roll attitude adopted by the helicopter is mainly a function of velocity and radius of turn, the assymetry of the vehicle having only small effect. Since agility is to be assessed over a series of standardised manoeuvres, the contribution from roll angle will be approximately equal for all helicopters. There seems little need to include the roll angle term for turning manoeuvres.

ii) The nature of a manoeuvre may make large displacements in certain variables inevitable (lateral cyclic in turns, for example). These displacements may not indicate poor agility but, if they are incorrectly weighted, they might give large values of API. Large displacements in some variables, provided they are not accompanied by large excursions in others, may be acceptable to pilots without necessarily being detrimental to the helicopter's agility. An example of this is lateral cyclic in

turning flight. Large changes in this control, for turning manoeuvres, might be acceptable, provided they are not accompanied by large changes in collective pitch (to maintain height) or longitudinal cyclic (to maintain forward speed).

iii) The questions posed in section 1 are answered in tabular form (see Tables 4-7) to ease the process of grading the relative importance, to agility, of each variable. The answers to these questions are used as a guide for selecting the weighting constants. The simplest way to grade the variables is to define a value representing the total of all the contributions, then grade individual variables as components of this. For flexibility, the value adopted for "total of contributions" is taken to be twice the number of non-zero constants. Each variable is then graded by awarding a score reflecting its level of relative importance to the agility of the helicopter, flying a particular manoeuvre. The total of all the gradings should equal the value of "total contribution".

iv) Since the total value of all weighting constants is to be unity, an initial estimate of their values is found by expressing each variable's "relative contribution" grading as a fraction of the "total contribution".

v) A trial and error process is used to determine final values for the weighting constants. Finding initial values by the above process ensures that the time taken to arrive at suitable final values is small.

vi) It is possible that a series of constants might be found which produce appropriate contribution by each variable for one helicopter, but not for others. In an attempt to avoid this, the process is performed

with two sets of helicopter data. Since the Battlefield configuration is intuitively more agile than the Transport, data for these helicopters has been used to aid the selection of constants.

This method will be made clearer by examination of the following examples.

3.5.3 Selection of Weighting Constants

The rationale behind the choice of weighting constants, for each type of manoeuvre discussed in this thesis, is now presented. For each class of manoeuvre, a single flight path has been selected, and inverse solutions performed for the Battlefield configuration flying it at various velocities. Weighting constants are then selected using the method described above. The same series of manoeuvres are then performed using data for the Transport configuration, and API values are calculated using the newly selected series of weighting constants. This is performed to ensure that sensible values for the weighting constants have been selected. As a final check, API is plotted against velocity for both aircraft. This plot should show the agility of the B configuration is significantly greater than that of the T.

1. Pop-up and Hurdle-Hop Manoeuvres

The flight path chosen to represent these manoeuvres was a pop-up to height 25m, from a distance of 300m, over a range of velocities 60 - 100 knots. Table 4 was completed as part of the selection process, and the gradings (hence the initial values of the weighting constants) were set for the following reasons.

In a manoeuvre where height is constantly changing, large displacements in main rotor collective can be expected in all helicopters. Similarly, if constant speed is to be maintained during the manoeuvre (as in this case), then large displacements in longitudinal cyclic are inevitable. Displacements in these controls will be acceptable to pilots provided excursions in the other two are small. Since, numerically, the displacements of collective will be very much larger than those of the other controls, it has been given a lower grading. Both types of manoeuvre are performed in two dimensions hence displacements in roll and roll rate, due to coupling effects, will be small. Large roll rates have greater implications on the vehicle's agility (due to disorientation and problems trying to track targets or obstacles) particularly when accompanied by high pitch rates. Roll rate is therefore given a higher rating than pitch angle. High pitch rates are to be expected in this manoeuvre, and to avoid its domination of total API it has been given a low grading. The pitch angle adopted by the helicopter during the manoeuvre is of greater significance to agility. A more agile helicopter will perform this manoeuvre with smaller pitch changes, this variable is therefore given a higher grading.

Initial values of the weighting constants were then used in the API function to give the contributions shown of Figure 3.3. The most noticeable feature of this plot is the large contribution by collective (THTO), and the very much lower contributions by the other controls. As discussed above, the displacements of the other controls are of equal importance to the agility of the helicopter. To produce contributions which reflect this, the weighting constant for collective was reduced whilst those of the other controls were increased. The contribution made

by pitch angle (THT) was also too small and was increased to increase its influence on the total API. By trial and error, the contributions, for both configurations, shown on Figure 3.4 were obtained, and the resulting final values for the weighting constants, given in Table 4, were found. It is apparent from Figure 3.4 that the contribution made by the control variables is much greater for the T configuration. This difference can be explained by consideration of the type of rotor possessed by the vehicles. The B configuration with its semi-rigid rotor will require much smaller control displacements to fly a given manoeuvre than the T configuration with its articulated rotor. The greater agility of the Battlefield configuration is shown by Figure 3.5, over the whole series of manoeuvres its API values are much less than those of the Transport machine.

2. Acceleration and Deceleration Manoeuvres

A series of accelerations from an initial velocity varying between 20 and 40 knots, to a final velocity of 60 knots, over a distance of 150m, was used to select weighting constants. The contribution due to pitch angle should have the greatest influence on the API value calculated for this manoeuvre. In NOE operations large excursions in pitch attitude can cause problems particularly when flying close to the ground. Large pitch changes are inevitable, therefore a low grading will still produce a large contribution. Speed changes are achieved by tilting the rotor disc in the fore or aft direction. Large changes in longitudinal cyclic (THT1S) are therefore to be expected. In order to maintain height, collective pitch has also to be increased. As in the pop-up, the contribution from collective will be large due to the high trim value which is necessary to

overcome the weight of the vehicle. The large trim value means that the ratio used in the cost function (equation 3.3) is relatively large for this variable. A low grading is therefore necessary for this variable. Lateral cyclic (THT1C) and tail rotor collective (THOTR) will both have much smaller displacements, but since large excursions of these variables is undesirable in linear flight, they are given a high grading.

The contributions by each variable, for the B configuration, using the initial values of the weighting constants are given in Figure 3.6. The most obvious fault is that the fuselage pitch (THT) is much too dominant, and swamps all of the other variables. The weighting constant for this variable was reduced, increasing those of the controls, until the contributions given by Figure 3.7 a) were found. The new weighting constants give a more even distribution but pitch attitude and collective still dominate. Figure 3.7 b) gives the contributions for the T configuration. Collective gives a much greater contribution due to this helicopter's rotor type and weight.

3. Level Turn Manoeuvre

A series of 90° right-hand turns of effective radius 250m, performed at velocities varying between 40 and 80 knots, was used to select the weighting constants for this manoeuvre. The primary control in turning manoeuvres is lateral cyclic, small displacements of this control will indicate good agility. Relative to the other controls, large displacements in lateral cyclic will occur, therefore in order that the influence that its importance merits, a grading of 2 is appropriate. The other controls have all been given equal weighting since they are all of

equal importance to the agility of the helicopter : longitudinal cyclic to maintain speed, collective to maintain height, and tail rotor cyclic to satisfy the no sideslip constraint. Only small changes are likely in pitch attitude, and since large changes have little consequence on the agility of the helicopter in this manoeuvre, it has been given a grading of 1. Since high roll rate is desirable in turning flight, and are likely to occur, a grading of 1 is likely to be high enough to give a significant contribution.

Figure 3.9 gives the contributions made by each variable using using the initial values of the weighting constants. Surprisingly, the major contribution comes from pitch rate, possibly due to the maximum allowable value being too small. The weighting constant for this variable was reduced, increasing those of the controls to produce the contributions given on Figure 3.10 a). The contributions for the T configuration are given in Figure 3.10 b), again the differences can be accounted for by consideration of rotor type. Total API is plotted for the whole series of manoeuvres for both configurations, the B configuration again shown as more agile.

4. Climbing Turn Manoeuvre

A series of 90° right-hand turns of effective radius 250m, with a height change of 25m, performed with velocity varying between 40 and 80 knots, was used to select weighting constants. In this manoeuvre height changes very slowly hence large pitch angles and rates are unlikely, and are undesirable as large roll angles and rates are inevitable. Pitch angle and rate are therefore given a grading of 2. Large displacements in

all of the controls are likely since the manoeuvre is performed in three dimensions. Contributions of approximately the same size would therefore seem appropriate. To achieve this, collective and lateral cyclic have been given lower gradings since the largest displacements must be expected from these controls.

The contributions made by each variable using the initial values of the weighting constants are shown in Figure 3.12. The only major problem is that the contribution from collective is too high. The weighting constant for collective has therefore been reduced, increasing those of pitch attitude and longitudinal cyclic to produce the contributions shown in Figure 3.13 a). The contributions for the T configuration, Figure 3.13 b) show, as in the previous manoeuvres, much higher contributions for the control variables. Figure 3.14 show total API plotted for both configurations for the complete series of manoeuvres, the agility of the B configuration predicted as being greater than that of the T for the whole series.

3.5.4 Discussion of Method

The weighting constants selected in the previous section are by no means the only appropriate set. Their choice relies heavily on the author's interpretation of helicopter agility. An alternative set, equally as valid, might be found by someone with other ideas of what helicopter agility is. If the method of quantifying agility given in this thesis were to be adopted by other analysts, then a wider range of opinion would have to be sought before a definitive set of constants were proposed. However, Figures 3.6 - 3.14 all show sensible trends, which

indicate that the chosen values are appropriate. In particular, Figures 3.5, 3.8, 3.11 and 3.14 all show the distinct difference in the agility of the Battlefield and Transport configurations. It can be concluded that the choice of weighting constants made in this section will allow further development of this method.

3.6 Agility Ratings

It has been shown that Agility Performance Indices can be calculated for a series of manoeuvres, and the agility of various helicopters flying them compared. In doing this, a number of values for agility are calculated, but a single value, representing the helicopter's agility for a particular type of manoeuvre, is not defined. One method of defining this would be to nominate a single manoeuvre from within the series, and declare the corresponding API value as representing the helicopter's agility for that type of manoeuvre. This is not the best solution for two reasons. Firstly, there is the problem of choosing which manoeuvre to use : the helicopter will fly a wide range of manoeuvres in each class within its operational lifetime. The second, and more serious problem is that false results might be found where a helicopter is credited high agility for this single manoeuvre, but shows poorer agility in others. A more reliable method is to assess the helicopter's agility over as wide a range of manoeuvres as is possible. The manoeuvres should vary in severity from the most gentle to those which approach the helicopter's flight envelope limits. Such a method is developed in this section.

3.6.1 Definition of an Agility Rating

In section 3.5 it was shown that API can be plotted for a single flight path flown at various velocities. It is also possible to calculate API values for a series of similar flight paths, their geometry varied by altering one dimension (for example, distance to the obstacle for the pop-up), all flown at the same velocity. An example of this is given by Figure 3.15. This plot shows API calculated for a series of pop-ups, each

flown at 80 knots, to clear an obstacle of height 25m from a distance within the range 250 - 350m. Hence a standard series of manoeuvres can be defined by either specifying a representative flight path and flying it at a series of velocities within a set range, or specifying a representative velocity, and flying a series of geometrically similar flight paths. Since lower values of API indicate higher agility, the closer the API plot is to the x-axis, then the more agile is the helicopter. High agility would therefore be given by small areas under the API curve, therefore in both cases a single value for agility (i.e. an Agility Rating) could be found by integrating API with respect to the varied parameter. Thus Agility Ratings might be expressed in either of the following ways :

$$AR = \int_{V_{f\min}}^{V_{f\max}} API \, dV_f \quad \text{or} \quad AR = \int_{s_{\min}}^{s_{\max}} API \, ds$$

where :

- AR = Agility rating,
- s_{\max}, s_{\min} = Limits of a flight path variable
- $V_{f\max}, V_{f\min}$ = Limits of flight velocity
- API = Agility performance index.

Both methods would assess agility on the basis of performance over a series of manoeuvres of varying severity, however the problem of choosing a single representative velocity, or flight path, still exists.

The solution to this is to use both methods simultaneously, i.e. for a series of flight paths within the distance limits, calculate API's for each flight path flown at a series of velocities within the limits. Plotting the API values will produce a series of mutually perpendicular

contours which form a surface as shown in Figure 3.16. This surface has been plotted by calculating API values for the B configuration flying a pop-up manoeuvre to a height of 25m from distances varying between 250 and 350m, with velocities varying between 60 and 100 knots. This "Agility Surface" would represent the inherent agility of a configuration for a single type of manoeuvre. Greater agility is achieved when the surface is closer to the x-y plane (i.e. lower API values over the distance and velocity range). In other words, the less the volume under the surface, then the greater is the agility. The Agility Rating (AR) of the configuration is therefore taken to be the volume under this surface.

Agility rating is therefore defined as :

$$AR = \int_{s_{\min}}^{s_{\max}} \int_{V_{f\min}}^{V_{f\max}} API \, ds \, dV_f$$

The units of Agility Rating are m^2/s . Since Agility Ratings will only be used for comparisons, these units are of no real significance. This integral is evaluated numerically as described in Appendix 9.

3.6.2 Definition of Standard Manoeuvres

For the purpose of this study, six manoeuvres have been chosen to represent tasks common in NOE flight. Manoeuvres are standardised by setting upper and lower limits of velocity and an appropriate flight path parameter. The flight path parameter is always a distance - for the pop-up and hurdle-hop it is the distance to an obstacle of fixed height, for straight line accelerations and decelerations it is the distance over

which the speed change is to take place, and for turning flight it is the effective radius of the turn. Setting upper and lower limits of velocity and distance allows the Agility Rating to be awarded on the basis of a series of manoeuvres of varying severity. Ideally, the choice of limits would be made by studying distances and speeds for manoeuvres performed during flight tests under operational conditions. Unfortunately limitations in the mathematical model and in the inverse algorithm, as discussed in Chapter 2, mean that HELINV may not be able to compute state and control time histories for the most severe of these manoeuvres. Instead, the manoeuvre limits are chosen by studying results from HELINV, taking the upper limits to be those from the most severe manoeuvre from which valid inverse solutions can be found. This does not give a fully representative set of manoeuvres (since it does not include the most severe one likely to be encountered by the real aircraft), but will still allow an Agility Rating to be calculated based on a reduced range of manoeuvres. The most severe manoeuvres are unlikely to be flown very often and therefore the value given for inherent agility over the reduced range of manoeuvres is still likely to be realistic. As improvements are made to the HELINV program the upper limits of the manoeuvres can be increased.

The limits chosen for the manoeuvres are given below. All manoeuvres are performed with sideslip constrained to be zero. The upper and lower limits of load factor experienced over the range of manoeuvres is also given, along with the maximum manoeuvre time for the series.

a) Pop-up : height change $h_1 = 25\text{m}$ over a distance s_1 at constant forward velocity.

Velocity Limits : $60 \leq V \leq 100$ knots

Distance Limits : $250 \leq s_1 \leq 350$ m

Load Factor : $0.38 \leq n \leq 1.62$

t_{\max} : 11.4 s

b) Hurdle-Hop : obstacle clearance of height $h_1 = 25\text{m}$ with return to original height at distance s_2 with constant forward speed.

Velocity Limits : $60 \leq V \leq 100$ knots

Distance Limits : $500 \leq s_2 \leq 600$ m

Load Factor : $0.36 \leq n \leq 1.5$

t_{\max} : 19.5 s

c) Constant Height Turn : right hand 90° of radius R , turn at constant height and velocity. The turn is made of transient entry and exit components with a circular main section.

Velocity Limits : $40 \leq V \leq 80$ knots

Radius Limits : $200 \leq R \leq 300$ m

Load Factor : $1.2 \leq n \leq 2.0$

t_{\max} : 23.7 s

d) Acceleration : Velocity change from V_1 to 60 knots over a distance s_1 at constant height.

Velocity Limits : $20 \leq V_1 \leq 40$ knots

Distance Limits : $100 \leq s_1 \leq 200$ m

Load Factor : $1.2 \leq n \leq 1.65$

t_{\max} : 9.7 s

e) Deceleration : Velocity change from V_1 to 15 knots over a distance s_1 at constant height.

Velocity Limits : $30 \leq V_1 \leq 50$ knots

Distance Limits : $150 \leq s_1 \leq 200$ m

Load Factor : $0.7 \leq n \leq 0.93$

t_{\max} : 17.3 s

f) Climbing Turn : Right handed 90° turn of radius R to a height of 25m at a constant velocity.

Velocity Limits : $40 \leq V \leq 80$ knots

Radius Limits : $200 \leq R \leq 300$ m

Load Factor : $1.18 \leq n \leq 2.1$

t_{\max} : 23.9 s

The above flight paths and their limits have been chosen to represent as far as is possible, realistic manoeuvres performed by

battlefield helicopters in NOE operations. If a full measure of inherent agility was required, then other manoeuvres, and variations on the above manoeuvres, would be included. For example, the level turn manoeuvre can be expanded to include accelerating and decelerating turns in left as well as right hand directions (the response of a helicopter in turning flight depends on whether it is turning towards or away from the advancing blade - Ref. 1). Other manoeuvres such as the bob-up (a height change in the hover) and the wing-over might also be included.

3.7 Example Calculations of Agility Ratings

The Agility Ratings given in Table 8 have been calculated, using both T and B configurational data in the model, for all of the previously described manoeuvres. The weightings derived in section 3.5 and manoeuvre limits given in section 3.6.2 have been used. As would be expected, the results show the B configuration significantly more agile than the T for all manoeuvres. The question of how to interpret these results now arises. Since each class of manoeuvre has a different set of weighting constants and state limits, the Agility Ratings of a particular helicopter, for different manoeuvres are not directly comparable. Using the results in Table 8 as an example, the Agility Rating calculated for the B configuration performing the climbing turn manoeuvre is approximately half that of the same helicopter performing the hurdle-hop. The B configuration cannot be interpreted as being twice as agile in a climbing as in a hurdle-hop since Agility Ratings in both cases are calculated using different parameters in the performance function. However, for a given manoeuvre, the Agility Ratings of any number of configurations are directly comparable. Again, using the results in Table 8 for illustration, the B configuration is approximately twice as agile as the T in the pop-up manoeuvre.

It can be concluded that if a single value for the inherent agility of a helicopter were required, then an addition of all Agility Ratings might be used (in this case the T configuration scores 52.45 and the B configuration scores 21.36). In order to account for the relative importance of each manoeuvre type, a weighted sum of Agility Ratings is perhaps more appropriate.

3.8 Alternative Methods of Quantifying Agility Using Inverse Solutions

Although it has been shown that the method presented in this thesis is successful, it may be possible to use the HELINV program to develop other techniques of quantifying helicopter agility. Previous authors have used a measurement of limiting performance as a guide to the agility of a helicopter. Merkley (Ref. 8) and Wrestler (Ref. 9) both used the MCEP package (Ref. 15) to find the minimum time in which a particular task might be performed. It is not possible to use this method with HELINV since the manoeuvre, hence manoeuvre time, must be explicitly defined. Houston and Caldwell (Ref. 6) also used a performance limit, maximum allowable hub moment, to calculate the most severe pop-up manoeuvre possible. A value for agility is then awarded on the basis of the geometry of the manoeuvre. A method similar to this could be developed using HELINV.

Using the example of the pop-up, we note that the most severe manoeuvre possible could be found by firstly specifying the velocity and obstacle height. The distance to the obstacle would then be reduced in steps, effectively increasing the manoeuvre's severity, performing inverse solutions for each new flight path. The most severe manoeuvre possible is found when a control (or state) limit is exceeded. A value of agility, perhaps an integration w.r.t of load factor during the manoeuvre, could then be awarded to the helicopter. The problem then arises of which height and velocity should be used as representative. This might be solved, as in the existing method, by using various heights and velocities to produce an Agility Surface, the area under which is representative of the agility of the helicopter. In this case higher volumes, given by more

severe manoeuvres (higher load factors) will indicate greater agility.

A simpler approach might be to define, for each class, a single very severe manoeuvre. The helicopter is then forced to fly this manoeuvre using HELINV, and a value for agility awarded as a function of the amount by which each state and control has exceeded its specified limit. As well as the problem of choosing a flight path and velocity, the question of validity of the calculated control angles arises. It is possible that if the control limits are exceeded by a large amount then the pitch angle of the blade might be greater than the validity limits of the aerodynamics of the blade profile.

It is obvious that implementation of HELINV in other methods for quantifying agility might cause problems. At present the severity of manoeuvres over which inverse solutions can be found is restricted by limitations in the mathematical model. Since both methods require inverse solutions to be found for severe manoeuvres, neither is applicable at present. This problem is not encountered in the present method since the choice of manoeuvres is tailored to suit the limitations inherent in the inverse method.

3.9 Conclusions

A method of quantifying helicopter inherent agility using inverse solutions of the helicopter equations of motion, and performance theory, has been developed. This method has two drawbacks. Firstly, agility is quantified on the basis of performance over a series of standard manoeuvres representative of those flown by the helicopter in its operational role. These should include the most severe manoeuvres likely to be flown in a given class, but unfortunately HELINV is unable to supply inverse solutions for them. This restricts the range of manoeuvres over which configurations can be tested. As improvements to the mathematical model are made, this problem should be alleviated. The second, and more serious drawback is the necessity of selecting weighting constants for the agility function, the choice being dependent on the users interpretation of agility. Despite these drawbacks, the power of the method was demonstrated by comparing the agility of two different configurations. The use of this technique as a design tool is further demonstrated in the next chapter.

CHAPTER 4

CONFIGURATIONAL STUDIES USING THE AGILITY EVALUATION PROGRAM

4.1 Introduction

The Agility Evaluation Program (AEP) described in the Chapter 3, is used to measure the inherent agility of a defined helicopter configuration. It is therefore most suited to studies of how configurational parameters affect the agility of a helicopter. In the present chapter this method is applied, firstly to study the effect of tailplane size on agility during manoeuvres in the longitudinal plane, and then to investigate the agility of an "Advanced Rotor Helicopter" (ARH) based on the existing configurational data of the conventional Battlefield helicopter. The second of these studies was first presented at the 12th European Rotorcraft Forum (Ref. 29). It should be stressed that the AEP is not intended as a complete design package. Results obtained from it quantify only the possible improvements in agility gained by altering configurational parameters. It does not predict the influences on stability, handling performance etc. that these changes might have.

4.2 The Influence of Tailplane Area on Inherent Agility

4.2.1 Introduction

Fixed wing aircraft employ a horizontal tailplane to allow trimmed flight with its centre of gravity offset from its centre of lift. In helicopter flight, the moment due to this offset can be balanced if the fuselage (which can be considered, in simple terms, as a mass suspended below the main rotor thrust vector) adopts the correct pitch attitude. This implies that the tailplane, with its accompanying drag, could be removed from rotorcraft. Handling quality deficiencies, in particular the absence of pitch damping usually supplied by the tailplane, could be corrected using a Stability Augmentation System (SAS). Caldwell et al (Ref. 30) have shown that an actively controlled tailplane can be used to enhance agility and to make a further mode of flight i.e. the ability to point the fuselage independently from the flight path, possible. This would require a tailplane of larger surface area. Other difficulties may also be encountered when designing the mechanical systems required to achieve this type of control. The added weight and complexity may outweigh the benefits gained.

The question then arises as to whether a reduced area, fixed tailplane has any benefits other than the most obvious attribute of a lower trim drag. The only real disadvantage is that a more sophisticated Stability Augmentation System than currently employed may be required to correct for any handling deficiencies caused by the reduced pitch damping. By using the method described in this document it is possible to show that by reducing the tailplane area, inherent agility may be improved

and that an optimum value can exist.

4.2.2 Choice of Flight Paths and Configurations

Flight Paths

It is unlikely that any changes made to a configuration involving its tailplane will have any affect on performance in turning flight. It is also unlikely that performance in accelerations and decelerations will be greatly affected by modest changes in tailplane area. A large, controllable tailplane, such as that on the Sikorsky UH-60 Black Hawk, can be used in landing flares to correct for undesirable pitching moments due to main rotor wake impingement. However this document is more concerned with agility in NOE flight, this mode of flight being more important for transportation/commando missions. Benefits are most likely to be observed in pitching flight where the tailplane can aid or abet the pitching motion of the fuselage. This study therefore concentrates on improved agility in pitching flight and in particular during the pop-up and hurdle-hop manoeuvres. The limits chosen for the manoeuvres are those described in section 3.6 and the weighting coefficients given in Table 4 are used.

Configurations

Data for the B and T configurations have been used as standards. For each configuration Agility Ratings have been calculated for various values of tailplane area. It has been assumed that the tailplane is fixed at the same angle of attack relative to the fuselage, its lift curve slope is unaltered and that the position of its centre of lift remains at the

same distance from the c.g. of the aircraft.

4.2.3 Discussion of Results

Results are given in Tables 9 and 10, tailplane areas being quoted as fractions of those of the conventional aircraft. Negative values of the scale area indicate an upload from the tailplane as opposed to the usual download i.e. the tailplane fixed to fuselage upside down. This is not intended to be a practical proposition, it is simply meant to highlight the shape of the AR plots. The graphs in Fig. 4.1 a) show Agility Rating plotted against tailplane area for the B and T configurations in the pop-up manoeuvre. The plots for both aircraft show minimum values of Agility Rating. These can be interpreted as the tailplane areas which give maximum inherent agility. For both aircraft, the optimum tailplane area occurs at approximately half of its conventional value. The graphs in Fig. 4.1 b) show Agility Rating plotted against tailplane area for both configurations in the hurdle-hop manoeuvre. The plots show optimum agility achieved, for both aircraft, with a tailplane of approximately half its original area.

The download at the tail is helpful in the pull-up section of the pop-up manoeuvre since it produces a significant nose-up pitching moment, whilst it is a hindrance in the push-over section as this nose-up moment is tending to resist the motion of the helicopter. For a given manoeuvre, as the tailplane area is reduced the main rotor has to provide the extra pitching moment required to pull-up, whilst in the push-over it is required to provide a lower moment, as the resisting moment from the tail has been reduced. Hence, less control action is needed in the push-over,

making the helicopter more agile in that phase, and more control action is needed in the pull-up making that phase less agile. The opposite is true for increased tailplane area (i.e. more agile pull-up and less agile push-over). The above results have shown that an optimum value for tail area exists for the B and T helicopters (roughly about half their present size). This represents the tailplane area which gives the best compromise between the advantageous tail download in pull-ups and adverse download in push-overs.

The results for the B and T configurations both show improved agility with their tailplane area approximately halved. A reduction in tailplane area has implications in trimmed flight as well as in unsteady flight. Figures 4.2 and 4.3 show how reducing the tailplane area by half affects fuselage pitch attitude and main rotor longitudinal cyclic pitch setting for trimmed flight. The values are calculated using the Royal Aircraft Establishment's helicopter simulation package HELISTAB (Refs. 18 and 19). At lower speeds, where the lift (and hence the pitching moment) of the tailplane is small, there is very little difference. At higher speeds the tail produces a smaller download (i.e. a smaller nose up pitching moment), hence the aircraft adopts a more severe nose down attitude. The consequence of this is that less forward stick (i.e. since negative values of longitudinal cyclic indicate forward stick, the values shown in Figures 4.2 and 4.3 are greater) is required to produce the necessary component of thrust in the direction of flight.

4.2.4 Conclusion

The above analysis suggests that reducing the area of the tailplane

in both helicopters will make them more agile in certain types of longitudinal manoeuvring flight. Reducing the tailplane area does have adverse effects in trimmed and unsteady flight. In unsteady flight the reduction in pitch damping can be counteracted by the SAS, whilst the trim problems only occur at higher speeds. Since the duties of the Transport configuration would imply long periods flying at cruise speeds, it is unlikely that a smaller tailplane would have any overall operational benefits. A dedicated Battlefield helicopter might, however, utilise a small tailplane to aid agility in NOE flight, using Active Control or a sophisticated SAS to retain acceptable handling qualities.

4.3 The Configurational Design of an "Advanced Rotor Helicopter" (ARH)

4.3.1 A Description of the ARH

The ARH configuration is based on the conventional Battlefield helicopter with three major rotor parameters altered. These changes were an increase in the flapping stiffness and inertia of the rotor, and an increase in the solidity of the rotor by adding an extra blade. The ARH configuration is compared with the B and T in Table 1. The changes made to the rotor will improve agility for the following reasons.

The control moment produced by a helicopter rotor is made up of two parts : a thrust moment due to rotor tilt and a elastic moment due to the flapping hinge offset. The magnitude of the elastic moment depends on the flapping stiffness of the rotor, which in turn is a function of blade flapping inertia and effective hinge offset. A helicopter possessing a greater rotor stiffness (and hence larger elastic moment) will require a smaller thrust vector tilt to produce the same control power as a helicopter with a less stiff rotor. As pitch attitude is related to disc tilt, increased rotor stiffness gives lower pitch attitudes. Tomlinson and Padfield have shown the importance to agility of these rotor parameters (Ref. 3). The rotor stiffness has been increased from 166 to 300 kNm/rad and the blade flapping inertia increased from 680 kg m² to 800 kg m². It should be noted that these changes increase the effective flapping hinge offset from 0.161 to 0.228. This could cause problems in control system design since the effective offset affects the dynamic behaviour of the rotor (in particular the lag between pitching and flapping).

Rotor solidity can be increased by adding extra blades. The blades of the high solidity rotor require lower pitch displacements to produce the same lift as a similar rotor with fewer blades. The drag of each individual blade is reduced although the sum of the drag of all the blades may have increased. Since the high solidity rotor will require smaller control displacements, inherent agility should be improved.

It is assumed that these modifications do not affect the position of the centre of gravity or the mass and inertias of the aircraft. The above modifications would require major changes to the control system (to deal with the stiffer rotor) and a redesigned rotor, although few changes to the airframe would be required. A more complete investigation of this configuration would involve calculating performance figures, trim values for rotor parameters (as well as attitude angles) over a range of steady flight conditions, and, possibly of greatest importance, a study of the dynamic stability of the aircraft (response calculations, eigenvalues etc.). Although the tools to do this are available (the simulation package HELISTAB), it was decided to concentrate on the Agility aspect of the design. It is therefore assumed that the above changes to the B configuration would result in an aircraft with dynamic characteristics which are sufficiently stable to ensure that the aircraft handleable (perhaps using Active Control).

4.3.2 Discussion of Results

Agility Ratings have been calculated for the series of manoeuvres described in section 3.6 and using the limits and weighting coefficients given in Tables 4,5,6 and 7. To show the improvement in agility gained by

making the above modifications, the Agility Ratings for the ARH are presented with those for the B and T configurations in Table 8.

Intuitively, the T configuration should be less agile than the other two helicopters. This is confirmed by the results in Table 8. The most noticeable point about these results is the large gap between the Agility Ratings for the T and those for the B and the ARH configurations. The size of the difference, due to the different types of rotor, the rigid rotors of the B and the ARH supplying a much larger moment for a given control displacement. There is however only a very small difference between the ratings of the B and ARH vehicles. This suggests a "law of diminishing return". The completely different rotor system of the T configuration produces totally different values of Agility Rating, whilst the similar rotors of the B and ARH give similar results - the modified rotor of the ARH making it slightly more agile (slightly lower Agility Ratings).

As only small improvements were observed by making the above modifications to the rotor, it can be concluded that the extra complexity of the rotor outweighs the gains in agility.

4.4 Conclusions

The above studies were intended to illustrate how calculating Agility Ratings for a helicopter can help to identify possible benefits to be gained by making changes to its basic configuration. The examples chosen, although relatively simple in nature, (the changes are considered to be made without any increase in weight, inertias or c.g. position etc.), show that useful quantitative results can be obtained - as against contemporary qualitative assessments - as to how agility is influenced by configuration.

CHAPTER 5

CONCLUSIONS

The importance of agility in helicopter NOE flight has been recognised for many years. Despite this, a general method of quantifying agility analytically has not previously been developed. Other authors have limited their approach to either small scale kinematic modelling or flight testing. This document describes a successful attempt to produce a general analytic method of quantifying helicopter inherent agility, (inherent agility being defined as the agility of a helicopter without pilot influences) and gives examples of its use.

The method is based on an algorithm which provides inverse solutions of the helicopter equations of motion. This allows time histories of state and control variables to be calculated for a particular helicopter configuration flying a given manoeuvre. The inherent agility of the helicopter flying this single manoeuvre is measured by an Agility Performance Index - the integral, over the manoeuvre time, of a weighted quadratic cost function of the state and control time histories (calculated by the inverse procedure). An Agility Rating is awarded for the helicopter's performance over a series of similar manoeuvres of varying severity. The Agility Rating is a measure of the helicopter's agility flying that single type of manoeuvre. In order to give a complete

measure of the helicopter's agility, ratings are calculated for its performance over a series of different types of manoeuvre, the choice of manoeuvres being dependent on the helicopter's role.

The two studies in Chapter 4 show how this method can be applied successfully at both the design stage and during development. The first study, the influence of tailplane area on agility, is an example of the use of the method to investigate changes to an existing configuration, perhaps at the development stage. The second study, the design of an "Advanced Rotor Helicopter", is an example of using the method at the design stage of a project. The method can be used to calculate Agility Ratings for any single main and tail rotor helicopter (other layouts would require a different mathematical model) provided sufficient information on its configurational parameters is available.

The success of this method depends largely on the performance of the inverse algorithm. Its full potential will not be realised until the inverse algorithm can provide solutions for a wide range of manoeuvres, from the most gentle to the most severe. At present, as discussed in Chapter 2, the inverse algorithm has limitations, some numerically based and some inherent in the mathematical model. Both of these areas require improving if this method of calculating agility is to be completely general.

There are obvious benefits to be gained from being able to quantify a value for the agility of a helicopter, particularly at the design stage. Using the method described in this dissertation, other benefits may also be found at the operational stage. Since inverse solutions are

used, the starting point is the definition of standard manoeuvres. It should then be possible to find the most suitable manoeuvre to perform a particular task, by testing the agility of a helicopter flying a series of possible manoeuvres and finding the optimum solution. In general, this method could be applied to any area of helicopter operations where manoeuvres can be precisely defined. The examples given in this document refer only to battlefield NOE operations but there are other areas where helicopters have to manoeuvre, with precision, close to obstacles. For example, operations from offshore platforms (ships and oil rigs) where the helicopter has to take off and land close to the super-structure of the platform or ship : helicopters in "commando" type operations also have to take off and land rapidly within a confined area. The method of evaluating agility described in this document could prove helpful in studies of helicopter performance in all of these areas.

APPENDIX 1 : HELICOPTER EQUATIONS OF MOTION

Equations of Translational Motion

$$\left. \begin{aligned} m\dot{u} &= -m(wq - vr) + X - mg \sin\theta \\ m\dot{v} &= -m(ur - wp) + Y + mg \cos\theta \sin\phi \\ m\dot{w} &= -m(vp - uq) + Z + mg \cos\theta \cos\phi \end{aligned} \right\} \dots\dots\dots (A1.1)$$

Equations of Rotational Motion

$$\left. \begin{aligned} I_{xx} \dot{p} &= (I_{yy} - I_{zz}) qr + I_{xz} (\dot{r} + pq) + L \\ I_{yy} \dot{q} &= (I_{zz} - I_{xx}) rp + I_{xz} (r^2 - p^2) + M \\ I_{zz} \dot{r} &= (I_{xx} - I_{yy}) pq + I_{xz} (\dot{p} - qr) + N \end{aligned} \right\} \dots (A1.2)$$

Euler Angle Rates

$$\left. \begin{aligned} \dot{\phi} &= p + q \sin\phi \tan\theta + r \cos\phi \tan\theta \\ \dot{\theta} &= q \cos\phi - r \sin\phi \\ \dot{\psi} &= q \sin\phi \sec\theta + r \cos\phi \sec\theta \end{aligned} \right\} \dots\dots\dots (A1.3)$$

APPENDIX 2 : TRANSFORMATION BETWEEN AXES SYSTEMS

1. Definition of Axes Systems.

Both axes systems used are orthogonal right-handed triads.

a) *Earth axes* are used for the definition of flight paths. This inertial reference frame assumes a flat non-rotating earth. The origin is located arbitrarily with the x-axis pointing northward, the y-axis eastward and the z-axis 'down' towards the earth's centre.

b) *Body axes* are used when deriving the aircraft equations of motion since they ensure that the moments and products of inertia are constant. This system has its origin at the aircraft's centre of gravity with the x-axis pointing forward, the y-axis to starboard and the z-axis 'down' (Fig. A1).

2. Helicopter Attitude.

An aircraft's attitude is given by the orientation of its body axes with respect to the earth axes. This orientation is given by three consecutive rotations through the *attitude* or *Euler angles* (see Ref. 20). The sequence of rotations is given as follows (see Fig. A2) :

- i) a rotation of γ about Oz_e to give $(0, x_1, y_1, z_e)$;
- ii) a rotation of θ about Oy_1 to give $(0, x_2, y_1, z_2)$;
- iii) a rotation of ϕ about Ox_2 to give $(0, x_b, y_b, z_b)$.

3. Transformation from Earth to Body Frames of Reference.

Transformation from earth to body axes (or vice versa) is achieved by use of the direction cosine matrix (Ref. 20). Thus body axes velocities are found from earth axes velocities by :

$$\begin{bmatrix} u \\ v \\ w \end{bmatrix} = \begin{bmatrix} l_1 & l_2 & l_3 \\ m_1 & m_2 & m_3 \\ n_1 & n_2 & n_3 \end{bmatrix} \begin{bmatrix} \dot{x} \\ \dot{y} \\ \dot{z} \end{bmatrix} \quad \dots(A2.1)$$

where :

$$l_1 = \cos\theta \cos\psi$$

$$l_2 = \cos\theta \sin\psi$$

$$l_3 = -\sin\theta$$

$$m_1 = \sin\phi \sin\theta \cos\psi - \cos\phi \sin\psi$$

$$m_2 = \sin\phi \sin\theta \sin\psi + \cos\phi \cos\psi$$

$$m_3 = \sin\phi \cos\theta$$

$$n_1 = \cos\phi \sin\theta \cos\psi + \sin\phi \sin\psi$$

$$n_2 = \cos\phi \sin\theta \sin\psi - \sin\phi \cos\psi$$

$$n_3 = \cos\phi \cos\theta$$

The accelerations can be found by differentiating equation A2.1 :

$$\begin{bmatrix} \dot{u} \\ \dot{v} \\ \dot{w} \end{bmatrix} = \begin{bmatrix} l_1 & l_2 & l_3 \\ m_1 & m_2 & m_3 \\ n_1 & n_2 & n_3 \end{bmatrix} \begin{bmatrix} \ddot{x} \\ \ddot{y} \\ \ddot{z} \end{bmatrix} + \begin{bmatrix} \dot{l}_1 & \dot{l}_2 & \dot{l}_3 \\ \dot{m}_1 & \dot{m}_2 & \dot{m}_3 \\ \dot{n}_1 & \dot{n}_2 & \dot{n}_3 \end{bmatrix} \begin{bmatrix} \dot{x} \\ \dot{y} \\ \dot{z} \end{bmatrix} \dots(A2.2)$$

where (with manipulation) :

$$\dot{l}_1 = \dot{\theta} l_3 \cos\psi - \dot{\psi} l_2$$

$$\dot{l}_2 = \dot{\theta} l_3 \sin\psi + \dot{\psi} l_1$$

$$\dot{l}_3 = -\dot{\theta} \cos\theta$$

$$\dot{m}_1 = \dot{\phi} n_1 + \dot{\theta} m_3 \cos\psi - \dot{\psi} m_2$$

$$\dot{m}_2 = \dot{\phi} n_2 + \dot{\theta} m_3 \sin\psi + \dot{\psi} m_1$$

$$\dot{m}_3 = \dot{\phi} n_3 + \dot{\theta} l_3 \sin\theta$$

$$\dot{n}_1 = -\dot{\phi} m_1 + \dot{\theta} n_3 \cos\psi - \dot{\psi} n_2$$

$$\dot{n}_2 = -\dot{\phi} m_2 + \dot{\theta} n_3 \sin\psi + \dot{\psi} n_1$$

$$\dot{n}_3 = -\dot{\phi} m_3 + \dot{\theta} l_3 \cos\theta$$

In order to transform from body to earth axes the transpose of the direction cosine matrix of equation (A2.1) is used.

APPENDIX 3 : CALCULATION OF TURN RATE FROM FLIGHT PATH GEOMETRY

When the flight path is specified by cartesian co-ordinates the track angle x , is found from :

$$x = \tan^{-1} \frac{dy}{dx} \dots (A3.1)$$

The turn rate is calculated by differentiating equation (A3.1) as follows :

$$\dot{x} = \frac{dx}{dx} \frac{dx}{dt} \dots (A3.2)$$

and from (A3.1) :

$$\frac{dx}{dx} = \frac{d^2y}{dx^2} \left[\frac{1}{1 + (dy/dx)^2} \right] \dots (A3.3)$$

also :

$$\frac{dx}{dt} = V \cos x$$

but from (A3.1) :

$$\tan x = \frac{dy}{dx} ,$$

$$\cos x = \frac{dx}{\sqrt{(dx)^2 + (dy)^2}} = \frac{1}{\sqrt{1 + (dy/dx)^2}} \dots (A3.4)$$

Substitution of (A3.4) and (A3.3) into (A3.2) gives :

$$\dot{x} = \frac{V (d^2y/dx^2)}{(1 + (dy/dx)^2)^{3/2}}$$

i.e $\dot{x} = V/R_c \dots (A3.5)$

where R_c = radius of curvature of the track.

APPENDIX 4 : HELICOPTER MATHEMATICAL MODEL

The following appendix outlines the expressions for the external forces and moments on a single rotor helicopter used in the computer package HELISTAB. This package is used to study the flight mechanics of single main and tail rotor helicopters. The section of HELISTAB used in the inverse algorithm is the TRIM routine. In its standard form this routine calculates the fuselage attitude angles and the rotor conditions for a general steady flight condition. For use in an inverse algorithm the TRIM routine has been extended to include unsteady terms. In both versions, the TRIM routine is used to solve six nonlinear equations of motion (eqns. A1-1, A1-2), the rotor speed being assumed constant. The external forces and moments for the equations of motion are considered as a sum of the contributions from the main rotor (suffix R), the aerodynamics of the fuselage and empennage (suffix A), and the tail rotor (suffix TR). Hence

$$\left. \begin{aligned} X &= X_A + X_R \\ Y &= Y_A + Y_R + Y_{TR} \\ Z &= Z_A + Z_R \\ L &= L_A + L_R + L_{TR} \\ M &= M_A + M_R \\ N &= N_A + N_R + N_{TR} \end{aligned} \right\} \dots\dots (A4-1)$$

Expressions for these components are derived by Padfield (Ref. 18) and are discussed in the following sections. The symbols used are given in the Nomenclature and in Figure A3.

1. Aerodynamic Forces and Moments of Fuselage and Empennage

Since it is not possible to obtain analytic expressions for the aerodynamic properties of the fuselage (due to the complex flow pattern around it), empirical wind tunnel data has been used to formulate relationships (in the form of polynomials) between aerodynamic coefficients and angles of attack and sideslip. The coefficients of fuselage drag, sideforce and pitching moment are given by :

$$\left. \begin{aligned} C_{Xf} &= a_1 + a_2\alpha + a_3\alpha^2 + a_4\alpha^3 \\ C_{Yf} &= b_1 + b_2\beta + b_3\beta^2 + b_4\beta^3 \\ C_{Mf} &= c_1 + c_2\alpha + c_3\alpha^2 + c_4\alpha^3 + c_5\alpha\beta \end{aligned} \right\} \quad (A4-2)$$

where $\alpha = \tan^{-1} (w/u)$,
 $\beta = \sin^{-1} (v/V)$,

and the polynomial coefficients a_{1-4} , b_{1-4} , c_{1-5} are found from the wind tunnel data.

Coefficients for the tailplane and fin, C_{Ztp} and C_{Yfin} , are based on 2-d steady incompressible aerodynamics (i.e. the coefficients are functions of aerofoil lift curve slope and local angle of attack). For example, if a_{otp} is the lift curve slope of the tailplane section and α_{otp} is the fixed incidence of the tailplane, then the force coefficient of the tailplane is given by :

$$C_{Ztp} = a_{otp} \alpha_{tp}$$

where $\alpha_{tp} = \alpha + \alpha_{otp}$

The effect of main rotor downwash at the tailplane is ignored. Provision

is also made for the inclusion of a wing and longitudinal auxiliary thrust. The components of the external forces and moments due to the aerodynamic properties of the fuselage and empennage are given by the following expressions. The force and moment coefficients of the fuselage are referred to rotor disc area and rotor radius, whilst those of the fin and tailplane are referred to their respective areas, S_{tp} , and S_{fin} , and their distances to the centre of gravity. These dimensions are given by adding the distances from the tail and fin centres of pressure, l_{tp} and l_{fin} , to the distance between the centre of gravity and the fuselage reference point (directly below the rotor hub), x_{cg} . The aerodynamic forces and moments are :

$$\begin{aligned}
 X_A &= \rho(\Omega R)^2 \pi R^2 C_{Xf} \\
 Y_A &= \rho(\Omega R)^2 [(\pi R^2) C_{Yf} + S_{fin} C_{Yfin}] \\
 Z_A &= \rho(\Omega R)^2 [(\pi R^2) C_{Zf} + S_{tp} C_{Ztp}] \\
 L_A &= \rho(\Omega R)^2 h_{fin} S_{fin} C_{Yfin} \\
 M_A &= \rho(\Omega R)^2 [\pi R^2 (R C_{Mf} + x_{cg} C_{Zf}) + (l_{tp} + x_{cg}) S_{tp} C_{Ztp}] \\
 N_A &= \rho(\Omega R)^2 [\pi R^2 (R C_{Nf} - x_{cg} C_{Yf}) - (l_{fin} + x_{cg}) S_{fin} C_{Yfin}]
 \end{aligned}
 \tag{A4-3}$$

2. Rotor Forces and Moments

The main rotor consists of rigid, constant chord blades hinged with stiffness in flap at the centre of the rotor. Coupling effects between flapping and lagging are ignored. In modelling the kinematics of the rotor, flapping angles are assumed to be small allowing a certain amount of linearisation (calculation of the x,y,z components of rotor thrust, for example). Yaw and sideslip rates are also assumed to be small in

comparison with the rotational speed of the main rotor. Rotor forces are expressed in shaft-hub axes then converted to the body axes system.

Quasi-steady flapping and coning is assumed in the derivation of reaction forces and moments from the rotor on the fuselage, the interaction of disc tilt modes with fuselage modes is neglected.

Blade flapping is simulated by using a centre spring equivalent rotor with flapping stiffness spring constant K_B . The value of the spring constant for equivalent rotor is chosen to give the same rotating and non-rotating flapping frequencies as those of the true blade (Ref. 19). The aerodynamic properties of the main rotor blades are based on 2-d aerodynamic theory with the blade assumed to be of constant chord, c , and section (although the option of having linearly varying twist, θ_{tw} , is included). The local airflow is assumed to be steady and incompressible. The lift of a blade is found by assuming a constant lift curve slope, a_0 , and its profile drag, δ , is found from a quadratic function of rotor thrust coefficient (see eqns. A4-5). Stall and reverse flow effects are ignored.

The above assumptions allow closed form analytic expressions for the rotor forces and moments to be found in terms of the thrust coefficient and the flapping angles. These are now stated for a rotor rotating in the anticlockwise direction when viewed from above. The forward tilt of the shaft, γ_g , is assumed to be small, allowing small angle simplifications to be made.

$$\begin{aligned}
X_R &= \rho(\Omega R)^2 \pi R^2 [C_T(\beta_{1c} + \gamma_s) - \delta s \mu_x / 4] \\
Y_R &= \rho(\Omega R)^2 \pi R^2 [-C_T \beta_{1s} - \delta s \mu_y / 4] \\
Z_R &= \rho(\Omega R)^2 \pi R^2 (-C_T) \\
L_R &= -b/2 K_B \beta_{1s} + h_R Y_R \\
M_R &= -b/2 K_B \beta_{1c} - [h_R X_R + x_{cg} Z_R] \\
N_R &= \rho(\Omega R)^2 \pi R^3 (C_Q) + \gamma_s L_R
\end{aligned}
\tag{A4-4}$$

where, if

- s = rotor solidity,
- b = number of blades,
- h_R = height of rotor above reference point,
- μ = the normalised hub velocity,
- μ_x, μ_y, μ_z = normalised components of hub velocity,
- λ_0 = normalised uniform downwash component,
- β_{1cw} = longitudinal flapping angle in wind axes,
- C_Q = rotor torque coefficient,

then

$$\delta = \delta_0 + \delta_2 C_T^2 \tag{A4-5}$$

$$s = bc/\pi R \tag{A4-6}$$

$$\begin{aligned}
\mu_x &= [(u - qh_R) \cos \gamma_s + (w + qx_{cg}) \sin \gamma_s] / (\Omega R) \\
\mu_y &= (v + ph_R) / (\Omega R) \\
\mu_z &= [(w + qx_{cg}) \cos \gamma_s - (u - qh_R) \sin \gamma_s] / (\Omega R) \\
\mu &= \sqrt{ \mu_x^2 + \mu_y^2 } = V / \Omega R
\end{aligned}
\tag{A4-7}$$

$$C_Q = -C_T [(\mu_z - \lambda_0) - \mu \beta_{1cw}] + \delta s (1 + \mu^2) / 8 \tag{A4-8}$$

$$\beta_{1cw} = \beta_{1c} (\mu_x / \mu) - \beta_{1s} (\mu_y / \mu) \tag{A4-9}$$

The induced flow through the rotor is approximated by a simple uniform distribution with a longitudinal variation produced by the rotor wake.

The vortex ring state is not modelled. The uniform component, normal to the rotor disc is given, from momentum theory, by the expression :

$$\lambda_0 = \frac{C_T}{2\sqrt{[\mu^2 + (\mu_z - \lambda_0)^2]}} \quad (A4-10)$$

which is solved for λ_0 by an iterative process.

3. Tail Rotor Forces and Moments

The tail rotor thrust is calculated in a similar fashion to that of the main rotor, but without flapping terms. The induced velocity at the tail rotor due to the wake from the main rotor is taken to be the uniform induced velocity, λ_0 , multiplied by a set factor. A fin blockage factor is also included. The thrust of the tail rotor is small in comparison with that of the main rotor. The drag and sideforce from the tail rotor blades can therefore be neglected. The contributions to the external forces and moments from the tail rotor can be expressed as follows.

$$\left. \begin{aligned} Y_{TR} &= \rho (\Omega_{tr} R_{tr})^2 \pi R_{tr}^2 C_{Ttr} \\ L_{TR} &= h_{tr} Y_{TR} \\ N_{TR} &= - (l_{tr} + x_{cg}) Y_{TR} \end{aligned} \right\} \quad (A4-11)$$

where

Ω_{tr} = rotational velocity of tail rotor,

R_{tr} = tail rotor radius

h_{tr}, l_{tr} = height and distance of tail rotor from
from fuselage reference point.

4. Determination of Control Angles

The inverse solution is used to calculate the helicopter attitude angles θ and ϕ , the rotor parameters $C_T, \beta_{1S}, \beta_{1C}$, and the tail rotor thrust coefficient C_{Ttr} , directly from the equations of motion, using the expressions of the external forces and moments given above. The method of calculating the control angles from these parameters is now discussed. The forces, control and flapping angles, and velocities are expressed in hub-wind axes (suffix w).

4.1 Main Rotor Control Angles

The force component normal to the rotor, f_z , per unit length, on an element of length, dr_b , of a single blade, is given by the expression :

$$f_z = -l \cos\phi - d \sin\phi$$

where, referring to figure A4

ϕ = the incidence of the blade element,

l = lift of blade element,

d = drag of blade element.

If it is assumed that ϕ is small, then

$$f_z = -l - d\phi \quad (A4.12)$$

Hence, the force in the z-direction, exerted by b blades, on the rotor hub, is given by

$$Z_{Hw} = \sum_{i=1}^b \int_0^R (f_z - m a_{zb} + m a_{xb} \beta)_i dr_b$$

where m = mass distribution of element,

β = flapping angle,

a_{xb}, a_{zb} = acceleration components of blade element.

When the flapping angle is expanded in harmonics of the rotor speed, Ω , the inertial terms cancel. Hence, the rotor thrust, T , is given by

$$Z_{Hw} = -T = \sum_{i=1}^b \int_0^R f_{zi} dr_b \quad (A4.13)$$

The lift and drag of the element, as functions of azimuth and radial position (ψ, r_b) , are given by

$$\left. \begin{aligned} l(\psi, r_b) &= \frac{1}{2} \rho (U_T^2 + U_P^2) c a_0 \left[\theta + \frac{U_P}{U_T} \right] \\ d(\psi, r_b) &= \frac{1}{2} \rho (U_T^2 + U_P^2) c \delta \end{aligned} \right\} \quad (A4.14)$$

where $-U_T$ and U_P are the velocity components along the y_b and z_b axes (see Figure A4). Making the assumption that $U_T^2 \gg U_P^2$ (i.e. $U_T^2 + U_P^2 \approx U_T^2$), substituting equations A4.14 into equation A4.12 and then A4.13, and normalising, gives the equation

$$\frac{Z_{Hw}}{1/2 \rho (\Omega R)^2 \pi R^2 s a_0} = - \frac{2 C_T}{a_0 s} = - \frac{1}{b} \sum_{i=1}^b \int_0^1 (U_T^2 \theta_i + U_P U_T) dr_b \quad (A4.15)$$

The normalised velocity components are given by the expressions

$$\left. \begin{aligned} \bar{U}_T &= r_b (1 + \omega_x \beta) + \mu \sin \nu \\ \bar{U}_P &= (\mu_z - \lambda_0 - \mu \beta \cos \nu) + r_b (\omega_y - \beta' - \lambda_1) \end{aligned} \right\} \quad (\text{A4.16})$$

where $r_b = \frac{r_b}{R}$ and $\beta' = \frac{d\beta}{d\nu}$

The normalised angular velocities in rotating axes, ω_x, ω_y , are

$$\omega_x = p_w \cos \nu - q_w \sin \nu \quad \text{and} \quad \omega_y = p_w \sin \nu + q_w \cos \nu$$

where the normalised rotational velocities in wind-axes, p_w and q_w are found from

$$p_w = [p \cos \nu_w + q \sin \nu_w] / \Omega \quad \text{and} \quad q_w = [q \cos \nu_w - p \sin \nu_w] / \Omega,$$

the rotor sideslip angle, ν_w , being

$$\cos \nu_w = \frac{\mu_x}{\mu} \quad \text{and} \quad \sin \nu_w = \frac{\mu_y}{\mu}$$

The induced flow through the rotor is modelled by the expression

$$\lambda = \lambda_0 + \lambda_1 r_b,$$

λ_0 being the uniform component normal to the flow. The harmonic component, λ_1 , is expressed as

$$\lambda_1 = \lambda_{1cw} \cos \nu + \lambda_{1sw} \sin \nu$$

where, if $x = \tan^{-1} \left[\frac{\mu}{\lambda_0 - \mu_z} \right]$, then

$$\lambda_{1cw} = \lambda_0 \tan(x/2) \quad \text{and} \quad \lambda_{1sw} = 0$$

All of the above equations are substituted into equations A4.15. This gives expressions for the normalised component velocities as functions of the radial and azimuth position of the blade element. Taking into account

only the first harmonic, the flapping of the blade can be written as :

$$\beta = \beta_0 + \beta_{1cw} \cos\psi + \beta_{1sw} \sin\psi \quad (\text{A4.17})$$

where β_0 is the coning angle, and the longitudinal and lateral flapping angles in hub-wind axes are given by

$$\beta_{1cw} = \beta_{1c} \cos\psi_w - \beta_{1s} \sin\psi_w \quad \text{and} \quad \beta_{1sw} = \beta_{1s} \cos\psi_w + \beta_{1c} \sin\psi_w.$$

The pitch angle of the blade, again only taking account first harmonics, with linear twist θ_{tw} , is expressed as

$$\theta = \theta_0 + \theta_{1sw} \sin\psi + \theta_{1cw} \cos\psi + r_b \theta_{tw} \quad (\text{A4.18})$$

Substitution of equations A4.18, A4.17, and the modified A4.16, allows equation A4.15 to be integrated for each blade, and then summed for the whole rotor. The resulting expression is

$$\frac{2C_T}{a_0^2} = \theta_0 \left[\frac{1}{3} + \frac{\mu^2}{2} \right] + \frac{\mu}{2} \left[\theta_{1sw} + \frac{\bar{P}_w}{2} \right] + \frac{1}{2} (\mu_z - \lambda_0) + \frac{1}{4} (1 + \mu^2) \theta_{tw} \quad (\text{A4.19})$$

Expressions relating the cyclic angles to the flapping angles are found by studying the blade flapping motion. Flapping motion is described by equating to zero the sum of the aerodynamic, inertial and elastic moments. For the "i th" blade :

$$\int_0^R r_b [f_z(r_b) - m a_{zb}] dr_b + K_\beta \beta_i = 0 \quad (\text{A4.20})$$

where a_{zb} , the component of blade acceleration in the z-direction is given by

$$a_{zb} = r_b [2\Omega\omega_x + (\dot{q}_w \cos\psi + \dot{p}_w \sin\psi) - r_w\omega_x - (\Omega \cdot r_w)^2 \beta - \ddot{\beta}] \quad (A4.21)$$

and

$$\left. \begin{aligned} \dot{q}_w &= - (\dot{p} + \dot{v}_w q) \sin\psi_w + (\dot{q} - \dot{v}_w p) \cos\psi_w \\ \dot{p}_w &= (\dot{p} + \dot{v}_w q) \cos\psi_w + (\dot{q} - \dot{v}_w p) \sin\psi_w \\ \dot{v}_w &= \frac{\dot{\mu}}{\mu} y \cos\psi_w - \frac{\dot{\mu}}{\mu} x \sin\psi_w \\ r_w &= r + \dot{v}_w \end{aligned} \right\} \quad (A4.22)$$

The aerodynamic force, f_z , is given by equations A4.12 and A4.14. By substitution of these equations into A4.20, with the acceleration, a_{zb} , (A4.21) expanded using equations A4.22, allows the flapping motion of the i th blade to be expressed, in normalised form, as

$$\begin{aligned} \beta_i'' + \lambda_\beta^2 \beta_i' &= 2 \left[(\overline{p}_w + \frac{\overline{q}_w'}{2}) \cos\psi_i - (\overline{q}_w - \frac{\overline{p}_w'}{2}) \sin\psi_i \right] \\ &+ 4n_\beta \int_0^1 [\overline{U}_T^2 \theta + \overline{U}_T \overline{U}_p] r_b dr_b \end{aligned} \quad (A4.23)$$

The normalised rotating flapping frequency, λ_β^2 , is given by

$$\lambda_\beta^2 = 1 + \frac{K_\beta}{I_\beta \Omega^2},$$

the blade flapping moment of inertia, I_β , by

$$I_\beta = \int_0^R m r_b^2 dr_b$$

and n_β , the blade inertia number by

$$n_\beta = \frac{\rho c a_0 R^4}{8 I_\beta}.$$

The expansion of equation A4.23 is completed by substitution of the normalised component velocities, given by equations A4.16, then evaluation of the integral component. The resulting differential equation can be used to define individual blade motions. The version implemented in HELISTAB, however, defines flapping motion using multi-blade co-ordinates. Making the appropriate transformations, and expanding equation A4.23 gives the flapping equation

$$\dot{E}_m'' + C_{mo} \dot{E}_m' + D_{mo} E_m = h_{mo} \quad (A4.24)$$

Since it has been assumed that blade flapping dynamics have negligible effect on the overall dynamics of the aircraft, the quasi-steady form of equation A4.24 has been used to define flapping motion i.e.

$$D_{mo} E_m = h_{mo} \quad (A4.25)$$

where

$$E_m = [\beta_o, \beta_d, \beta_{1cw}, \beta_{1sw}]^T$$

$$D_{mo} = \begin{bmatrix} \lambda_\beta^2 & 0 & 0 & 0 \\ 0 & \lambda_\beta^2 & 0 & 0 \\ \frac{4}{3} \mu n_\beta & 0 & \lambda_\beta^2 - 1 & n_\beta \left[1 + \frac{\mu^2}{2} \right] \\ 0 & 0 & -n_\beta \left[1 + \frac{\mu^2}{2} \right] & \lambda_\beta^2 - 1 \end{bmatrix}$$

$$h_{mo} = \begin{bmatrix} n_{\beta} \left\{ \theta_0(1+\mu^2) + 4\theta_{tw} \left[\frac{1}{5} + \frac{\mu^2}{6} \right] + \frac{4}{3} \mu\theta_{1sw} + \frac{4}{3} (\mu_z - \lambda_0) + \frac{2}{3} \mu(\bar{p}_w - \lambda_{1sw}) \right\} \\ 0 \\ 2 \left[\bar{p}_w + \frac{q_w'}{2} \right] + n_{\beta} \left\{ \theta_{1cw} \left[1 + \frac{\mu^2}{2} \right] + (q_w - \lambda_{1cw}) \right\} \\ -2 \left[q_w - \frac{p_w'}{2} \right] + n_{\beta} \left[\frac{8}{3} \mu\theta_0 + 2\mu\theta_{tw} + \theta_{1sw} \left(1 + \frac{2}{3} \mu^2 \right) + 2\mu(\mu_z - \lambda_0) + (\bar{p}_w - \lambda_{1sw}) \right] \end{bmatrix}$$

On expansion, neglecting the differential coning angle, β_d , equation A4.25 gives three expressions in terms of the flapping angles, β_{1cw} , β_{1sw} , the coning angle, β_0 , the control angles θ_0 , θ_{1sw} , θ_{1cw} and various known rotor parameters (C_T , λ_0 , μ_z etc.). These three equations, along with equation A4.19, can be solved for the control angles and the coning angle. The resulting expressions, neglecting the normalised roll and pitch accelerations, are

$$\theta_0 = \frac{3}{2} \mu \frac{k_1}{k_4} \beta_{1cw} - \frac{1}{2} \mu s_{\beta} \beta_{1sw} + \frac{2k_2}{a_0 s} C_T + \frac{\mu k_3}{4} \bar{p}_w - \frac{\mu}{n_{\beta}} q_w - \frac{1}{2} k_1 (\mu_z - \lambda_0) - \frac{1}{4} \left[1 - \frac{3}{2} \mu^2 (1 - \mu^2) \right] \theta_{tw}$$

$$\theta_{1sw} = \frac{3}{k_4} \left[-\frac{1}{3} k_1 k_2 \beta_{1cw} + \frac{1}{3} s_{\beta} k_2 \beta_{1sw} - \frac{16}{9 a_0 s} C_T - \frac{1}{3} k_1 \bar{p}_w + \frac{2k_2}{3 n_{\beta}} q_w + \frac{2}{3} \mu k_3 (\mu_z - \lambda_0) - \frac{1}{3} \mu^3 \theta_{tw} \right]$$

$$\beta_0 = \frac{n_{\beta}}{\lambda_{\beta}^2 - 1} \left[(1 + \mu^2) \theta_0 + \frac{4}{3} \mu (\theta_{1sw} + \frac{1}{2} \bar{p}_w) + \frac{4}{3} (\mu_z - \lambda_0) + 4 \left(\frac{1}{5} + \frac{1}{6} \mu^2 \right) \theta_{tw} \right]$$

$$\theta_{1cw} = \frac{-1}{(1 + 1/2 \mu^2)} \left[-\frac{4}{3} \mu \beta_0 - s_\beta \beta_{1cw} - (1 + \frac{1}{2} \mu^2) \beta_{1sw} + \frac{2}{n_\beta} p_w + q_w \right]$$

where

$$k_1 = 1 - \frac{1}{2} \mu^2, \quad k_2 = 1 + \frac{3}{2} \mu^2$$

$$k_3 = 1 - \frac{3}{2} \mu^2, \quad k_4 = 1 - \mu^2 + \frac{4}{3} \mu^4$$

and the stiffness number, s_β is defined as

$$s_\beta = \frac{\lambda_\beta^2 - 1}{n_\beta}$$

4.2 Tail Rotor Collective Pitch

The tail rotor collective pitch angle is found using equation A4.19, with the flapping and blade twist terms neglected. This gives

$$\theta_{otr} = \frac{3}{1 + 1.5 \mu_{tr}^2} \left[\frac{2 C_{Ttr}}{s_{otr} s_{tr}} - \frac{1}{2} (\mu_{ztr} - \lambda_{otr}) \right]$$

where

$$\mu_{tr} = \sqrt{[u^2 + (w + q (l_{tr} + x_{cg}))^2]} / (\Omega_{tr} R_{tr})$$

$$\mu_{ztr} = [-v + r (l_{tr} + x_{cg}) - h_{tr} p] / (\Omega_{tr} R_{tr})$$

$$s_{tr} = (b_{tr} c_{tr}) / (\pi R_{tr})$$

The normalised tail rotor downwash velocity, λ_{otr} is found by a Newton-Raphson iterative solution of

$$\lambda_{otr} = \frac{C_{Ttr}}{2 \sqrt{(\mu_{tr})^2 + (\mu_{ztr} - \lambda_{otr})^2}}$$

APPENDIX 5 : CALCULATION OF ψ AND $\dot{\psi}$ IN SIDESLIP CONSTRAINED FLIGHT.

The azimuth angle ψ is calculated from the sideslip velocity, i.e. from eqn. (A2.1)

$$v = m_1 \dot{x} + m_2 \dot{y} + m_3 \dot{z} \quad \dots (A5.1)$$

The coefficients m_1, m_2, m_3 are given in Appendix 2 and v by equation 2.40. Equation A5.1, with rearrangement, becomes

$$a \cos \psi + b \sin \psi + c = 0 \quad \dots (A5.2)$$

where

$$\left. \begin{aligned} a &= \dot{x} \sin \phi \sin \theta + \dot{y} \cos \phi \\ b &= -\dot{x} \cos \phi + \dot{y} \sin \phi \sin \theta \\ c &= \dot{z} \sin \phi \cos \theta - v \end{aligned} \right\} \dots (A5.3)$$

Since an iterative calculation is being used, and two of the unknown variables are ϕ and θ , at any point in the numerical process ϕ and θ have known values (albeit updated estimates). Hence the corresponding value of ψ may be found simply by the solution of equation (A5.2). This equation is easily solved numerically by a Newton-Raphson method (Ref. 21). With ψ calculated it is possible then to find its rate from eqn. (A2.2) and equation 2.41

$$\dot{\psi} = m_1 \dot{x} + m_2 \dot{y} + m_3 \dot{z} + \dot{m}_1 \dot{x} + \dot{m}_2 \dot{y} + \dot{m}_3 \dot{z} \quad \dots (A5.4)$$

Expanding and rearranging gives

$$\dot{\psi} = - \frac{a_1 \cos \psi + b_1 \sin \psi + e_1}{c_1 \sin \psi + d_1 \cos \psi} \quad \dots (A5.5)$$

where

$$a_1 = \dot{x} [\dot{\phi} \cos\phi \sin\theta + \dot{\theta} \sin\phi \cos\theta] - \dot{y} \dot{\phi} \sin\phi + \ddot{x} \sin\phi \sin\theta + \ddot{y} \cos\phi$$

$$b_1 = \dot{x} \dot{\phi} \sin\phi + \dot{y} [\dot{\phi} \cos\phi \sin\theta + \dot{\theta} \sin\phi \cos\theta] - \ddot{x} \cos\phi + \ddot{y} \sin\phi \sin\theta$$

$$c_1 = - [\dot{x} \sin\phi \sin\theta + \dot{y} \cos\phi]$$

$$d_1 = \dot{y} \sin\phi \sin\theta - \dot{x} \cos\phi$$

$$e_1 = \dot{z} [\dot{\phi} \cos\phi \cos\theta - \dot{\theta} \sin\phi \sin\theta] + \ddot{z} \sin\phi \cos\theta - \dot{v}$$

APPENDIX 6 : NUMERICAL DIFFERENTIATION

Two types of numerical differentiation are used in the inverse algorithm. Both are described in this Appendix.

1. Backward Differences

Referring to figure A4, the derivative with respect to t of x at point i is given by the series

$$\frac{dx_i}{dt} = (\nabla x_i + \frac{1}{2} \nabla^2 x_i + \frac{1}{3} \nabla^3 x_i + \frac{1}{4} \nabla^4 x_i + \dots) / \delta t$$

where

$$\nabla x_i = x_i - x_{i-1}$$

$$\begin{aligned} \nabla^2 x_i &= (x_i - x_{i-1}) - (x_{i-1} - x_{i-2}) \\ &= x_i - 2x_{i-1} + x_{i-2} \end{aligned}$$

$$\nabla^3 x_i = x_i - 3x_{i-1} + 3x_{i-2} - x_{i-3}$$

$$\nabla^4 x_i = x_i - 4x_{i-1} + 6x_{i-2} - 4x_{i-3} + x_{i-4}$$

etc.

2. Central Differences

Referring to Figure A4, the derivative of x with respect to t , at point $i-3$ is given by the series

$$\frac{dx_{i-3}}{dt} = [(\delta x_{1/2} + \delta x_{-1/2})/2 - (\delta^3 x_{1/2} + \delta^3 x_{-1/2})/12 + \dots] / \delta t \quad (\text{A6.1})$$

where

$$\delta x_{1/2} = x_{i-4} - x_{i-3} \quad , \quad \delta x_{-1/2} = x_{i-3} - x_{i-2} \quad (\text{A6.2})$$

$$\begin{aligned} \delta^3 x_{1/2} &= [(x_{i-5} - x_{i-4}) - (x_{i-4} - x_{i-3})] - [(x_{i-4} - x_{i-3}) - (x_{i-3} - x_{i-2})] \\ &= x_{i-5} - 3x_{i-4} + 3x_{i-3} - x_{i-2} \quad (\text{A6.3}) \end{aligned}$$

$$\begin{aligned} \delta^3 x_{-1/2} &= [(x_{i-4} - x_{i-3}) - (x_{i-3} - x_{i-2})] - [(x_{i-3} - x_{i-2}) - (x_{i-2} - x_{i-1})] \\ &= x_{i-4} - 3x_{i-3} + 3x_{i-2} - x_{i-1} \quad (\text{A6.4}) \end{aligned}$$

Hence A6.1 - A6.4

$$\frac{dx_{i-3}}{dt} = [2 (x_{i-4} - x_{i-3}) - \frac{1}{4} (x_{i-5} - x_{i-1})] / 3\delta t$$

APPENDIX 7 : ROTATIONAL VELOCITIES AND ACCELERATIONS

The kinematic expressions for attitude rates (equation (A1.3)) in terms of rotational velocities can be rearranged to give rotational velocities in terms of attitude rates. These expressions are given below.

$$\left. \begin{aligned} p &= \dot{\phi} - \dot{\gamma} \sin\theta \\ q &= \dot{\theta} \cos\phi + \dot{\gamma} \sin\phi \cos\theta \\ r &= \dot{\gamma} \cos\theta \cos\phi - \dot{\theta} \sin\phi \end{aligned} \right\} \dots (A7.1)$$

The rotational accelerations are then found by differentiation of these equations i.e.

$$\left. \begin{aligned} \dot{p} &= \ddot{\phi} - \ddot{\gamma} \sin\theta - \dot{\gamma} \dot{\theta} \cos\theta \\ \dot{q} &= \ddot{\theta} \cos\phi - \dot{\phi} \dot{\theta} \sin\phi - \dot{\gamma} (\dot{\theta} \sin\phi \sin\theta - \dot{\phi} \cos\phi \cos\theta) + \ddot{\gamma} \sin\phi \cos\theta \\ \dot{r} &= \ddot{\gamma} \cos\theta \cos\phi - \dot{\gamma} (\dot{\theta} \sin\theta \cos\phi + \dot{\phi} \cos\theta \sin\phi) - \ddot{\theta} \sin\phi - \dot{\theta} \dot{\phi} \cos\phi \end{aligned} \right\} \dots (A7.2)$$

APPENDIX 8 : LINEARISED APPROACH TO INVERSE PROBLEM

1. Linearising the Equations of Motion

The first step in the linearisation process is to define the reference trim state. Since all of the manoeuvres used in the HELINV program begin and end in a rectilinear flight state, (possibly with a non-zero value of sideslip) this state has been chosen for the following linearisation. This gives, using the subscript "o" to denote the reference state

$$p_o = q_o = r_o = 0.$$

The nonlinear equations of motion A1.1, A1.2 and A1.3 are linearised using the following process

i) Total values are replaced by reference plus perturbed values denoted by the superscript " ' ", i.e.

$$u = u_o + u' , \quad X = X_o + X' , \quad \psi = \psi_o + \psi' \quad \text{etc.}$$

ii) The equations are expanded and products of perturbations, assumed to be small, are neglected.

iii) Small angle assumptions are made (i.e. for a general angle, ξ , $\cos \xi \approx 1$, $\sin \xi \approx \xi$).

iv) The external forces and moments are expressed as a Taylor series, for example :

$$X = \frac{\partial X}{\partial u} u + \frac{\partial X}{\partial v} v + \dots + \frac{\partial X}{\partial \psi} \psi + \frac{\partial X}{\partial \theta_o} \theta_o + \dots + \frac{\partial X}{\partial \theta_{otr}} \theta_{otr}$$

This is more commonly written in terms of aerodynamic derivatives as

$$X = X_u u + X_v v + \dots$$

The aerodynamic derivatives used in HELISTAB are calculated by numerical differentiation of equations A4.1, formulation of expressions for the derivatives would be time consuming and tedious. Use of numerical differentiation also has the advantage of simplifying the task of changing the mathematical model - only expressions for the forces and moments need be changed.

Dropping the " ' " notation for perturbation values, the linearised equations of motion are

$$\dot{u} = - (w_0 q - v_0 r) - g \theta \cos \theta_0 + \frac{X}{m}$$

$$\dot{v} = - (u_0 r - w_0 p) + g (\phi \cos \theta_0 \sin \phi_0 - \theta \sin \theta_0 \sin \phi_0) + \frac{Y}{m}$$

$$\dot{w} = - (v_0 p - u_0 q) - g (\theta \sin \theta_0 \cos \phi_0 + \phi \sin \phi_0 \cos \theta_0) + \frac{Z}{m}$$

$$I_{xx} \dot{p} = I_{xz} \dot{r} + L$$

$$I_{yy} \dot{q} = M$$

$$I_{zz} \dot{r} = I_{xz} \dot{p} + N$$

$$\dot{\phi} = p + q \sin \phi_0 \tan \theta_0 + r \cos \phi_0 \tan \theta_0$$

$$\dot{\theta} = q \cos \phi_0 - r \sin \phi_0$$

$$\dot{\psi} = q \sin \phi_0 + r \cos \phi_0$$

The linearised equations of motion can then be written in the form

$$\dot{\underline{x}} = \mathbf{A} \underline{x} + \mathbf{B} \underline{u} \quad (\text{A8.1})$$

where

$$\underline{x} = [u, v, w, p, q, r, \theta, \phi, \psi]^T,$$

$$\underline{u} = [\theta_0, \theta_{1S}, \theta_{1C}, \theta_{0tr}]^T,$$

\mathbf{A} = the system matrix,

\mathbf{B} = the control matrix.

The matrices, \mathbf{A} and \mathbf{B} , contain the aerodynamic derivatives and relevant gravitational and velocity terms and are given by

$$\mathbf{A} = \begin{bmatrix} X_u & X_v & X_w & X_p & X_{q-w_0} & X_{r+v_0} & X_{\theta-g\cos\theta_0} & X_\phi & X_\psi \\ Y_u & Y_v & Y_w & Y_{p+w_0} & Y_q & Y_{r-u_0} & Y_{\theta-g\sin\theta_0\sin\phi_0} & Y_{\phi+g\cos\theta_0\cos\phi_0} & Y_\psi \\ Z_u & Z_v & Z_w & Z_{p-v_0} & Z_{q+u_0} & Z_r & Z_{\theta-g\sin\theta_0\cos\phi_0} & Z_{\phi-g\cos\theta_0\sin\phi_0} & Z_\psi \\ L_u+iN_u & L_v+iN_v & L_w+iN_w & L_p+iN_p & L_q+iN_q & L_r+iN_r & L_\theta+iN_\theta & L_\phi+iN_\phi & L_\psi+iN_\psi \\ M_u & M_v & M_w & M_p & M_q & M_r & M_\theta & M_\phi & M_\psi \\ N_u+kL_u & N_v+kL_v & N_w+kL_w & N_p+kL_p & N_q+kL_q & N_r+kL_r & N_\theta+kL_\theta & N_\phi+kL_\phi & N_\psi+kL_\psi \\ 0 & 0 & 0 & 1 & \sin\phi_0\tan\theta_0 & \cos\phi_0\tan\theta_0 & 0 & 0 & 0 \\ 0 & 0 & 0 & 0 & \cos\phi_0 & \sin\phi_0 & 0 & 0 & 0 \\ 0 & 0 & 0 & 0 & \sin\phi_0 & \cos\phi_0 & 0 & 0 & 0 \end{bmatrix}$$

and

$$B = \begin{bmatrix} X_{\theta_0} & X_{\theta_{1s}} & X_{\theta_{1c}} & X_{\theta_{otr}} \\ Y_{\theta_0} & Y_{\theta_{1s}} & Y_{\theta_{1c}} & Y_{\theta_{otr}} \\ Z_{\theta_0} & Z_{\theta_{1s}} & Z_{\theta_{1c}} & Z_{\theta_{otr}} \\ L_{\theta_0} + iN_{\theta_0} & L_{\theta_{1s}} + iN_{\theta_{1s}} & L_{\theta_{1c}} + iN_{\theta_{1c}} & L_{\theta_{otr}} + iN_{\theta_{otr}} \\ M_{\theta_0} & M_{\theta_{1s}} & M_{\theta_{1c}} & M_{\theta_{otr}} \\ N_{\theta_0} + kL_{\theta_0} & N_{\theta_{1s}} + kL_{\theta_{1s}} & N_{\theta_{1c}} + kL_{\theta_{1c}} & N_{\theta_{otr}} + kL_{\theta_{otr}} \\ 0 & 0 & 0 & 0 \\ 0 & 0 & 0 & 0 \\ 0 & 0 & 0 & 0 \end{bmatrix}$$

where

$$i = \frac{I_{xz}}{I_{zz}} \quad \text{and} \quad k = \frac{I_{xz}}{I_{xx}}$$

Notes

a) All of the derivatives in the first three rows are divided by the helicopter mass, m (see linearised equations of motion above).

b) All entries in fourth column are multiplied by the factor

$$\frac{I_{zz}}{I_{zz}I_{xx} - I_{xz}^2}$$

c) All entries in the fifth column are divided by moment of inertia I_{yy} .

d) All entries in sixth column are multiplied by the factor

$$\frac{I_{xx}}{I_{zz}I_{xx} - I_{xz}^2}$$

2. Reduction from Full to Constrained System

The inverse solution of the nonlinear equations of motion is made unique by imposing four constraints on the helicopter's dynamics : the three accelerations in earth-axes, and sideslip velocity, are all given specified values. In effect, specifying the earth-axes accelerations, applies constraints to the body-axes accelerations. Specifying sideslip velocity leads, through yaw angle, ψ , to a constraint on yaw rate, r . The four constrained variables can be grouped together to form a sub-matrix x_1 . Hence, if

$$\underline{x}_1 = [u, v, w, r]^T \quad \text{and} \quad \underline{x}_2 = [p, q, \theta, \phi, \psi]^T,$$

then the system matrix of equation A8.1, when partitioned, becomes

$$\begin{bmatrix} \dot{\underline{x}}_1 \\ \dot{\underline{x}}_2 \end{bmatrix} = \begin{bmatrix} \mathbf{A}_{11} & \mathbf{A}_{12} \\ \mathbf{A}_{21} & \mathbf{A}_{22} \end{bmatrix} \begin{bmatrix} \underline{x}_1 \\ \underline{x}_2 \end{bmatrix} + \begin{bmatrix} \mathbf{B}_1 \\ \mathbf{B}_2 \end{bmatrix} \underline{u} \quad (\text{A8.2})$$

The vectors \underline{x}_1 and $\dot{\underline{x}}_1$ contain the specified values of the constraints and are therefore known at every point in the manoeuvre. The matrix equation A8.2 can be rewritten

$$\dot{\underline{x}}_1 = \mathbf{A}_{11} \underline{x}_1 + \mathbf{A}_{12} \underline{x}_2 + \mathbf{B}_1 \underline{u} \quad (\text{A8.3})$$

$$\dot{\underline{x}}_2 = \mathbf{A}_{21} \underline{x}_1 + \mathbf{A}_{22} \underline{x}_2 + \mathbf{B}_2 \underline{u} \quad (\text{A8.4})$$

From equation A8.3

$$\underline{u} = \mathbf{B}_1^{-1} [\dot{\underline{x}}_1 - \mathbf{A}_{11} \underline{x}_1 - \mathbf{A}_{12} \underline{x}_2].$$

Substituting this into equation A8.4 gives, with manipulation,

$$\dot{\underline{x}}_2 = [A_{22} - B_2 B_1^{-1} A_{12}] \underline{x}_2 + [(A_{21} - B_2 B_1^{-1} A_{11}) \dot{\underline{x}}_1 + (B_2 B_1^{-1}) \underline{x}_1] \quad (A8.5)$$

Hence, if

$$\left. \begin{aligned} A_C &= A_{22} - (B_2 B_1^{-1}) A_{12} \\ B_C &= [(A_{21} - (B_2 B_1^{-1}) A_{11}) \quad (B_2 B_1^{-1})] \\ \underline{u}_C &= \begin{bmatrix} \dot{\underline{x}}_1 \\ \underline{x}_1 \end{bmatrix} \end{aligned} \right\} \quad (A8.6)$$

then the constrained system is represented by

$$\dot{\underline{x}}_2 = A_C \underline{x}_2 + B_C \underline{u}_C \quad (A8.7)$$

A_C and B_C can be considered as the system and control matrices of the constrained helicopter. Since it contains the constraint vectors, \underline{u}_C is equivalent to a control vector in an inverse solution, the constraints, in effect, being the inputs to the system. The only limitation on the use of this analysis is that the matrix, B_1 , must be nonsingular.

3. Calculation of Constrained System and Control Matrices

In the following analysis the entries of the original system and control matrices are given the notation

$$A = \begin{bmatrix} a_{11} & \dots & a_{19} \\ \vdots & & \vdots \\ a_{91} & \dots & a_{99} \end{bmatrix} \quad \text{and} \quad B = \begin{bmatrix} b_{11} & \dots & b_{14} \\ \vdots & & \vdots \\ b_{91} & \dots & b_{94} \end{bmatrix}, \quad (\text{A8.8})$$

the order of the state and control variables being as in equation A8.1.

The first stage in the calculation of the new system and control matrices must be to replace the constrained variables (u,v,w,r) by their specifying functions.

3.1 Body-axes Velocities and Accelerations

The helicopter's body-axes velocities and accelerations are found using the transformations given in Appendix 2, the velocities and accelerations in the earth-axes system being specified as functions of time. By linearising equation A2.1, the perturbed body-axes velocities are given by

$$\begin{bmatrix} u \\ v \\ w \end{bmatrix} = \begin{bmatrix} l_{10} & l_{20} & l_{30} \\ m_{10} & m_{20} & m_{30} \\ n_{10} & n_{20} & n_{30} \end{bmatrix} \begin{bmatrix} \dot{x} \\ \dot{y} \\ \dot{z} \end{bmatrix} - \begin{bmatrix} u_0 \\ v_0 \\ w_0 \end{bmatrix} \quad (\text{A8.9})$$

where, by making small angle assumptions

$$l_{10} = \cos\theta_0 \cos\psi_0$$

$$l_{20} = \cos\theta_0 \sin\psi_0$$

etc.

The body-axes accelerations are given by the same transformation, viz

$$\begin{bmatrix} \dot{u} \\ \dot{v} \\ \dot{w} \end{bmatrix} = \begin{bmatrix} l_{10} & l_{20} & l_{30} \\ m_{10} & m_{20} & m_{30} \\ n_{10} & n_{20} & n_{30} \end{bmatrix} \begin{bmatrix} \ddot{x} \\ \ddot{y} \\ \ddot{z} \end{bmatrix} - \begin{bmatrix} w_0 q - v_0 r \\ u_0 r - w_0 p \\ v_0 p - u_0 r \end{bmatrix} \quad (\text{A8.10})$$

3.2 Yaw Rate and Acceleration

An expression relating yaw rate to the sideslip constraint can be developed from the second of equations A8.9

$$r = \frac{1}{u_0} (m_{10} \ddot{x} + m_{20} \ddot{y} + m_{30} \ddot{z} - \dot{v} + w_0 p) \quad (\text{A8.11})$$

and by differentiation

$$\dot{r} = \frac{1}{u_0} (m_{10} \dddot{x} + m_{20} \dddot{y} + m_{30} \dddot{z} - \ddot{v} + w_0 \dot{p}) \quad (\text{A8.11})$$

The fourth of the original equations of motion is used for \dot{p} , i.e.

$$\dot{p} = a_{41}u + a_{42}v + \dots + b_{44}\theta_{otr}$$

The value of \ddot{v} is found by differentiation of equation 2.43, i.e.

$$\ddot{v} = (\dot{V} - V\dot{\beta}^2) \sin\beta + (2V\dot{\beta} + \ddot{\beta}V) \cos\beta$$

3.3 The Reduced System and Control Matrices

Substitution of the expressions for $u, v, w, r, \dot{u}, \dot{v}, \dot{w}, \dot{r}$ (equations A8.9 - A8.12) into the original linearised equations of motion, expressed in the form given by equations A8.1 and A8.8, with some manipulation, gives the following :

$$\underline{\dot{x}}_2 = \begin{bmatrix} \dot{x} l_{10} + \dot{y} l_{20} + \dot{z} l_{30} \\ \dot{x} m_{10} + \dot{y} m_{20} + \dot{z} m_{30} \\ \dot{x} n_{10} + \dot{y} n_{20} + \dot{z} n_{30} \\ (\ddot{x} m_{10} + \ddot{y} m_{20} + \ddot{z} m_{30} - \dot{v})/u_0 \end{bmatrix}$$

$$\underline{\ddot{x}}_2 = \begin{bmatrix} \ddot{x} l_{10} + \ddot{y} l_{20} + \ddot{z} l_{30} \\ \ddot{x} m_{10} + \ddot{y} m_{20} + \ddot{z} m_{30} \\ \ddot{x} n_{10} + \ddot{y} n_{20} + \ddot{z} n_{30} \\ (\dddot{x} m_{10} + \dddot{y} m_{20} + \dddot{z} m_{30} - \ddot{v})/u_0 \end{bmatrix}$$

$$A_{11} = \begin{bmatrix} a_{11} & a_{12} & a_{13} & (a_{14} - v_0) \\ a_{21} & a_{22} & a_{23} & (a_{24} + u_0) \\ a_{31} & a_{32} & a_{33} & a_{34} \\ (a_{41} - ka_{51}) & (a_{42} - ka_{52}) & (a_{43} - ka_{53}) & (a_{44} - ka_{54}) \end{bmatrix}$$

$$A_{12} = \begin{bmatrix} a_{15} + (a_{14} - v_0)k & (a_{16} + w_0) & a_{17} & a_{18} & a_{19} \\ a_{25} + a_{24}k & a_{26} & a_{27} & a_{28} & a_{29} \\ a_{35} + v_0 + ka_{34} & (a_{36} - u_0) & a_{37} & a_{38} & a_{39} \\ k(a_{44} - a_{55} - ka_{54}) + a_{45} & (a_{46} - ka_{56}) & (a_{47} - ka_{57}) & (a_{48} - ka_{58}) & (a_{49} - ka_{59}) \end{bmatrix}$$

$$A_{21} = \begin{bmatrix} a_{51} & a_{52} & a_{53} & a_{54} \\ a_{61} & a_{62} & a_{63} & a_{64} \\ a_{71} & a_{72} & a_{73} & a_{74} \\ a_{81} & a_{82} & a_{83} & a_{84} \\ a_{91} & a_{92} & a_{93} & a_{94} \end{bmatrix}$$

$$A_{22} = \begin{bmatrix} (a_{55} + ka_{54}) & a_{56} & a_{57} & a_{58} & a_{59} \\ (a_{65} + ka_{64}) & a_{66} & a_{67} & a_{68} & a_{69} \\ (a_{75} + ka_{74}) & a_{76} & a_{77} & a_{78} & a_{79} \\ (a_{85} + ka_{84}) & a_{86} & a_{87} & a_{88} & a_{89} \\ (a_{95} + ka_{94}) & a_{96} & a_{97} & a_{98} & a_{99} \end{bmatrix}$$

$$B_1 = \begin{bmatrix} b_{11} & b_{12} & b_{13} & b_{14} \\ b_{21} & b_{22} & b_{23} & b_{24} \\ b_{31} & b_{32} & b_{33} & b_{34} \\ (b_{41} - kb_{51}) & (b_{42} - kb_{52}) & (b_{43} - kb_{53}) & (b_{44} - kb_{54}) \end{bmatrix}$$

$$B_2 = \begin{bmatrix} b_{51} & b_{52} & b_{53} & b_{54} \\ b_{61} & b_{62} & b_{63} & b_{64} \\ b_{71} & b_{72} & b_{73} & b_{74} \\ b_{81} & b_{82} & b_{83} & b_{84} \\ b_{91} & b_{92} & b_{93} & b_{94} \end{bmatrix}$$

where $k = \frac{w_0}{u_0}$.

In effect, equation A8.7 is the state space representation of a helicopter constrained to fly a manoeuvre with prescribed translational accelerations and sideslip angle. The linearised theory presented in this appendix is used in Chapter 2 to analyse results from the nonlinear HELINV inverse program.

APPENDIX 9 : CALCULATION OF THE VOLUME UNDER AN AGILITY SURFACE

An Agility Surface is constructed of a series of Agility Performance Indices (API) calculated at regular intervals on a rectangular grid. Each API value corresponds to a helicopter configuration flying a set flight path at a fixed velocity. Since the surface is not defined by a manageable analytic function (it is a function of time histories calculated by the inverse program HELINV) it is impossible to calculate the volume under it analytically. A numerical technique has been developed to perform this calculation. An Agility Surface (such as that in Figure 3.16), since it is based on a rectangular grid, can be considered as consisting of a series of pairs of right angled triangular prisms, each pair being joined along a common hypotenuse (see Figure A6). A good approximation of the volume under the Agility Surface can therefore be found by summing the volumes of the triangular prisms.

Figure A6 shows a typical element within an Agility Surface. The element is formed by joining four API values for manoeuvres at two velocities (denoted $y_{1,3}$ and $y_{2,4}$) and two distances (denoted $x_{1,2}$ and $x_{3,4}$). Consider triangular plane 123.

The equation of triangular plane 123 is

$$z = ax + by + c$$

The coefficients of this equation, a, b, and c can be found by substitution of the co-ordinates of the corner points : (x_1, y_1, z_1) etc. and solution of the resulting three linear simultaneous equations.

The volume under plane 123 is then

$$V_{123} = \int_{x_1}^{x_3} \int_{y_1}^{f(y)} (ax + by + c) \, dx \, dy$$

where $f(y)$ is the equation of the projection of the hypotenuse 2-3 on the xy plane. Thus

$$f(y) = mx + d,$$

$$\text{where } m = \frac{y_3 - y_2}{x_3 - x_2},$$

$$\text{and } d = y_3 - mx_3.$$

Hence, with manipulation

$$V_{123} = \frac{1}{3} k_1(x_3^3 - x_1^3) + \frac{1}{2} k_2(x_3^2 - x_1^2) + k_3(x_3 - x_1)$$

where

$$k_1 = am + \frac{1}{2} bm^2,$$

$$k_2 = cm + da + mdb - ay_1,$$

$$k_3 = dc + \frac{1}{2} bd^2 - cy_1 - \frac{1}{2} by_1^2.$$

The volume under plane 234 is found in a similar manner. The volume under the Agility Surface is then found by summation of the volumes of all of the triangular prisms.

REFERENCES

1. P. Brotherhood,
M.T. Charlton
An Assessment of Helicopter Turning Performance During Nap-of-Earth Flight. RAE TM FS(B) 534, Jan. 1984.
2. G.D. Padfield,
M.T. Charlton
Aspects of RAE Flight Research into Helicopter Agility and Pilot Control Strategy.
Handling Qualities Specification (Mil Spec 8501 Update), Specialists Meeting, Ames Research Center, June 1986.
3. B.N. Tomlinson,
G.D. Padfield
Piloted Simulation Studies of Helicopter Agility.
Vertica, Vol. 4, 1980.
4. R.M. Gerdes
A Pilot's Assessment of Helicopter Handling-Quality Factors Common to Both Agility and Instrument Flying Tasks. NASA TM 81217, July 1980.
5. R.L. Stewart,
F.L. Dominick,
R.B. Smith
Army Preliminary Evaluation YAH-1R Improved Cobra Agility and Maneuverability Helicopter.
USAAEFA 74-33, May 1975.
6. S. Houston,
A.E. Caldwell
A Computer Based Study of Helicopter Agility, Including the Influence of an Active Tailplane.
Paper No. 70, 10th European Rotorcraft Forum, The Hague, Sept. 1984.
7. Lt. P.J. Legge RN,
P.W. Fortescue,
P. Taylor
Preliminary Investigation into the Addition of Auxiliary Longitudinal Thrust on Helicopter Agility.
Paper No. 40, 7th European Rotorcraft Forum, Garmisch-Partenkirchen, Sept. 1981.
8. D.J. Merkley
An Analytical Investigation of the Effects of Increased Installed Horsepower on Helicopter Agility in the Nap-of-the-Earth Environment.
USAAMRDL-TN-21, Dec. 1975.

30. A.E. Caldwell,
S.S. Houston,
D.G. Thomson

A Review of the Applications of a
Horizontal Tailplane in the Single Main
and Tailrotor Helicopter.
Paper No. 84, 11th European Rotorcraft
Forum, London, Sept. 1985.

TABLES

Parameter	Helicopter Type		
	TRANSPORT	BATTLEFIELD	ARH
Mass (kg)	6000	4300	4300
Rotor Radius (m)	7.5	6.4	6.4
No. of Blades	4	4	5
Rotor Stiffness (kNm/rad)	48	166	300
Blade Flapping Inertia (kgm ²)	1300	680	800
Effective Hinge Offset	0.048	0.161	0.2284
Rotor Solidity	0.0906	0.0778	0.0973
Tailplane Area (m ²)	1.35	1.2	1.2

Table 1 : Configurational Data

Control	TRANSPORT	BATTLEFIELD / ARH
Main Rotor Collective	6 , 18	-5 , 20.3
Longitudinal Cyclic	-12.25 , 16.25	-15.7 , 7.5
Lateral Cyclic	3.5 , 6.5	-7.5 , 7.5
Tail Rotor Collective	-28 , 12	-8.5 , 33.5

Table 2 : Control Limits (in degrees)

State	Manoeuvre			
	Pop-up/Hurdle-hop	Level Turn	Accel/Decel	Climbing Turn
p (deg/s)	20	100	20	100
q (deg/s)	50	20	50	50
θ (deg)	20	10	20	20
ϕ (deg)	10	70	10	70

Table 3 : Maximum Allowable Values for States

Variable	Large Displacements Likely ?	Large Displacements Acceptable ?	Contribution Grading ($\epsilon = 16$)	Weighting Const.	
				Initial	Final
ϕ	N	N	1	0.0625	0.0200
θ	Y	Y	2	0.1250	0.1375
p	N	N	2	0.1250	0.1250
q	Y	Y	1	0.0625	0.0625
θ_o	Y	Y	1	0.0625	0.0175
θ_{1s}	Y	N	3	0.1875	0.2750
θ_{1c}	N	N	3	0.1875	0.2750
θ_{otr}	N	N	3	0.1875	0.2750

Table 4 : Weighting Constants for POP-UP and HURDLE-HOP Manoeuvres

Variable	Large Displacements Likely ?	Large Displacements Acceptable ?	Contribution Grading ($\Sigma = 16$)	Weighting Const.	
				Initial	Final
ϕ	N	N	1	0.0625	0.0625
θ	Y	N	1	0.0625	0.0075
p	N	N	1	0.0625	0.0625
q	Y	N	2	0.1250	0.1000
θ_0	Y	N	1	0.0625	0.0625
θ_{1s}	Y	Y	4	0.2500	0.2500
θ_{1c}	N	N	3	0.1875	0.2275
θ_{otr}	N	N	3	0.1875	0.2275

Table 5 : Weighting Constants for ACCELERATION / DECELERATION Manoeuvres

Variable	Large Displacements Likely ?	Large Displacements Acceptable ?	Contribution Grading ($\Sigma = 14$)	Weighting Const.	
				Initial	Final
ϕ	-----	-----	-----	0.0000	0.0000
θ	N	Y	1	0.0714	0.0714
p	Y	Y	1	0.0714	0.0928
q	N	N	1	0.0714	0.0200
θ_0	Y	N	3	0.2142	0.2242
θ_{1s}	Y	N	3	0.2142	0.2242
θ_{1c}	Y	Y	2	0.1428	0.1428
θ_{otr}	Y	N	3	0.2142	0.2242

Table 6 : Weighting Constants for LEVEL TURN Manoeuvre

Variable	Large Displacements Likely ?	Large Displacements Acceptable ?	Contribution Grading ($\Sigma = 14$)	Weighting Const.	
				Initial	Final
ϕ	-----	-----	-----	0.0000	0.0000
θ	N	N	2	0.1428	0.1828
p	Y	Y	1	0.0714	0.0714
q	N	N	2	0.1428	0.1428
θ_0	Y	Y	1	0.0714	0.0214
θ_{1s}	Y	N	3	0.2142	0.2242
θ_{1c}	Y	Y	1	0.0714	0.0714
θ_{otr}	Y	N	4	0.2856	0.2856

Table 7 : Weighting Constants for CLIMBING TURN Manoeuvre

Manoeuvre	Configuration		
	TRANSPORT	BATTLEFIELD	ARH
Pop-up	9.90	4.69	4.01
Hurdle-Hop	12.54	5.59	4.58
Level Turn	6.10	1.96	1.87
Acceleration	15.43	5.87	5.51
Deceleration	1.69	0.93	0.88
Climbing Turn	6.79	2.32	2.19

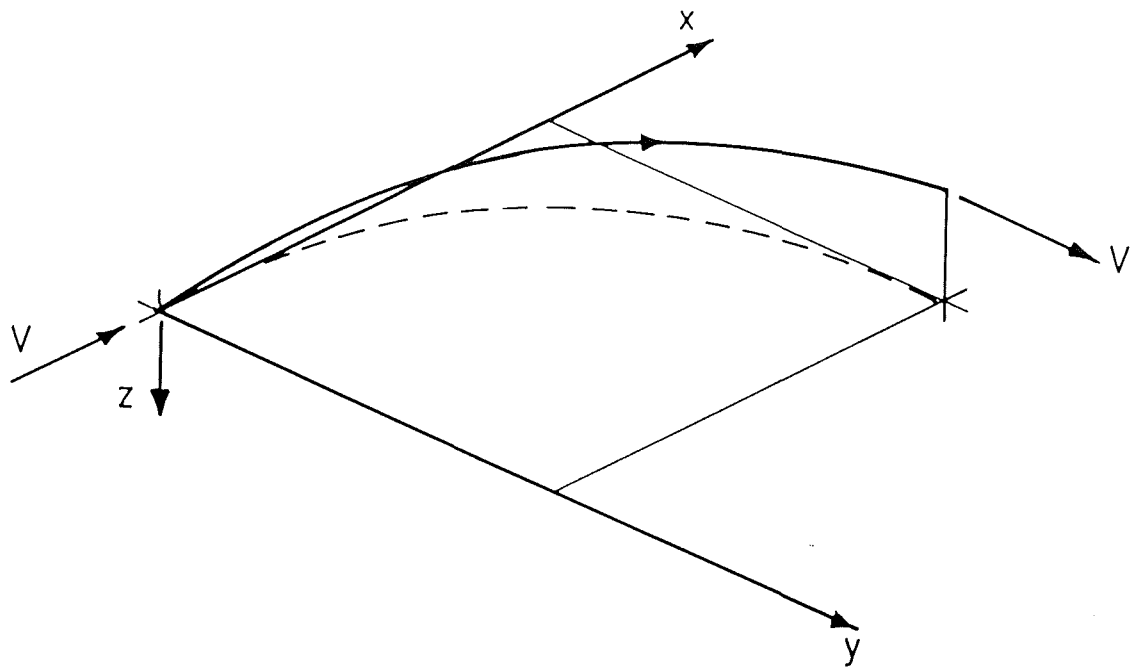
Table 8 : Agility Ratings for Complete Series of Manoeuvres

Tailplane Scale Area	BATTLEFIELD	TRANSPORT
-1.0	7.46	14.26
-0.5	5.53	11.55
0.0	4.64	9.96
0.5	4.39	9.46
1.0	4.69	9.90
1.5	5.37	10.97
2.0	6.31	12.36

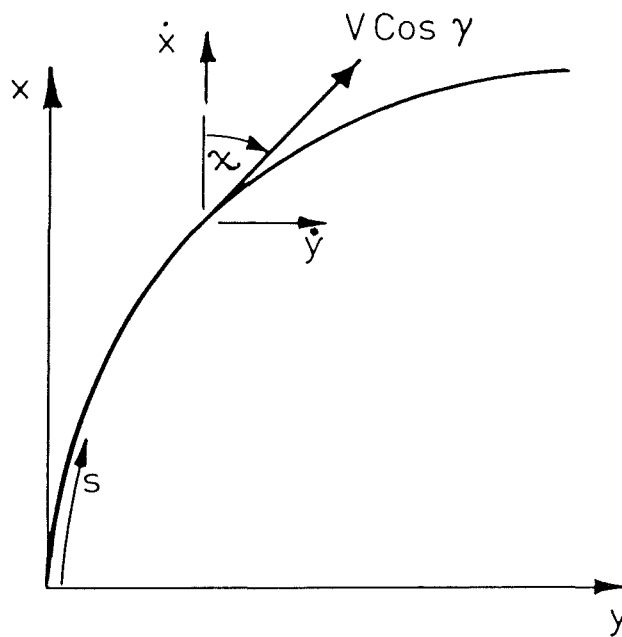
Table 9 : Agility Ratings for the POP-UP Manoeuvre

Tailplane Scale Area	BATTLEFIELD	TRANSPORT
-1.0	7.84	29.34
-0.5	5.89	18.16
0.0	5.07	13.00
0.5	5.04	11.79
1.0	5.59	12.54
1.5	6.56	14.15
2.0	7.82	16.17

Table 10 : Agility Rating for the HURDLE-HOP Manoeuvre

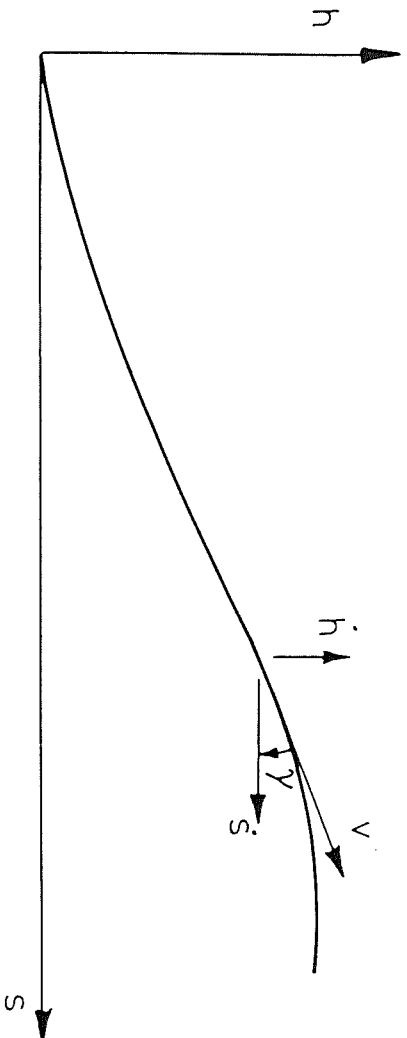


a) Flight Path



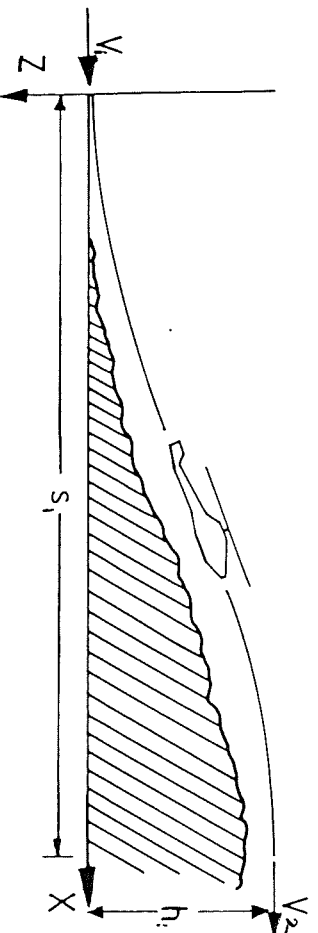
b) Track

FIGURE 2.1 : A General 3-Dimensional Manoeuvre

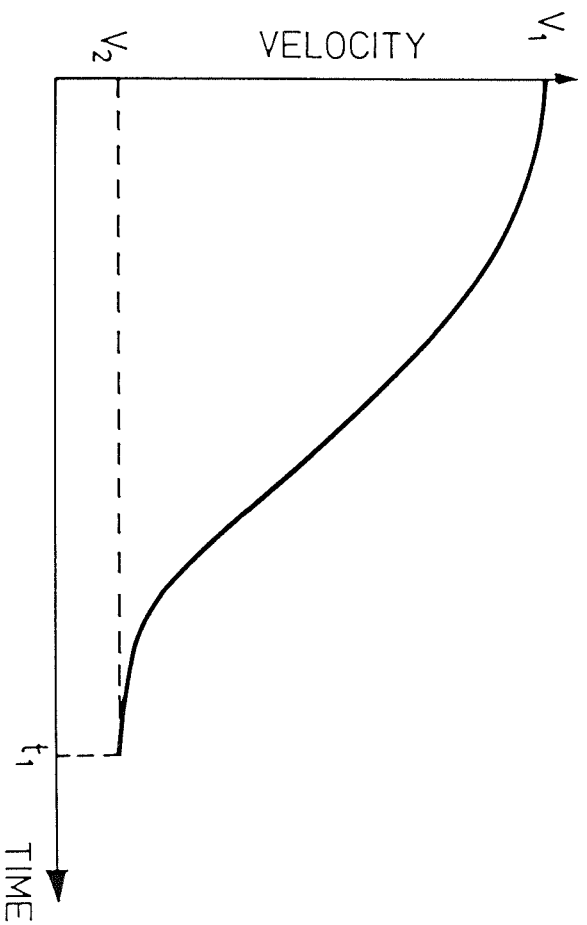


c) Altitude

FIGURE 2.1 Cont.

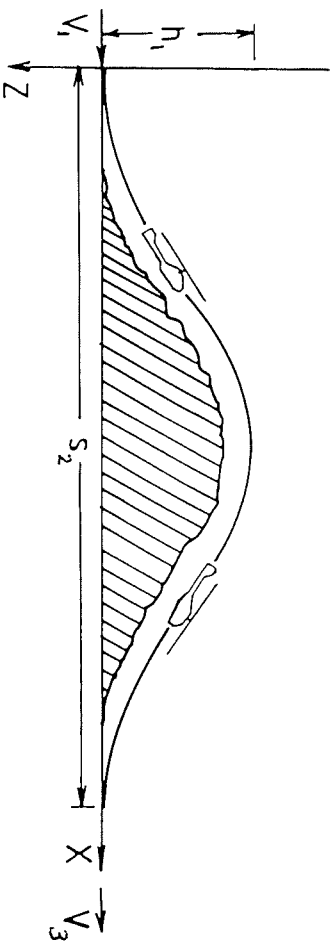


a) Flight Path

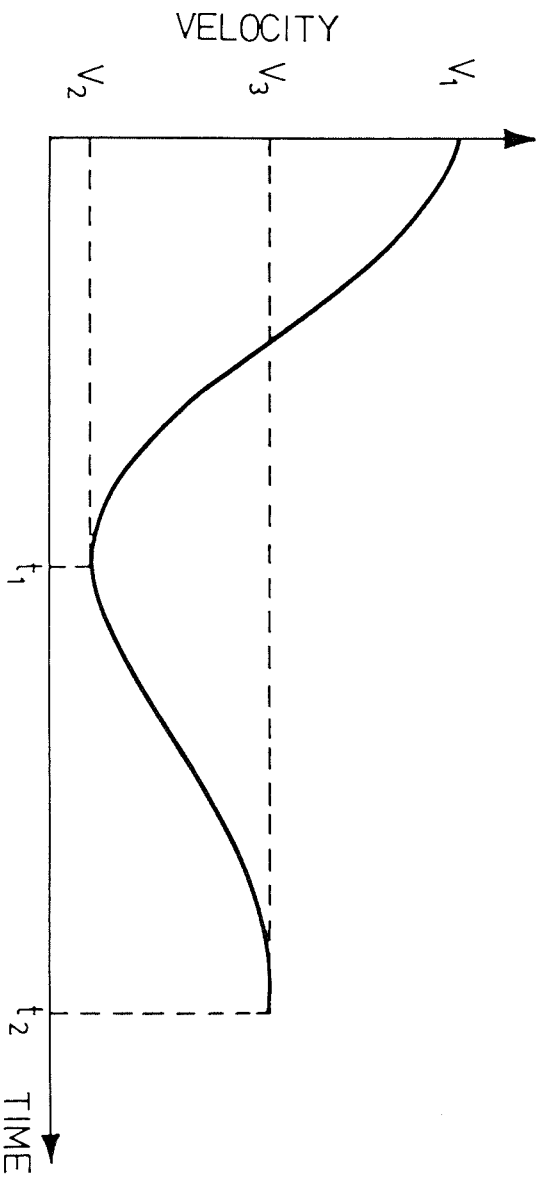


b) Velocity Change

FIGURE 2.2 : The Pop-up Manoeuvre



a) Flight Path



b) Velocity Change

FIGURE 2.3 : The Hurdle-Hop Manoeuvre

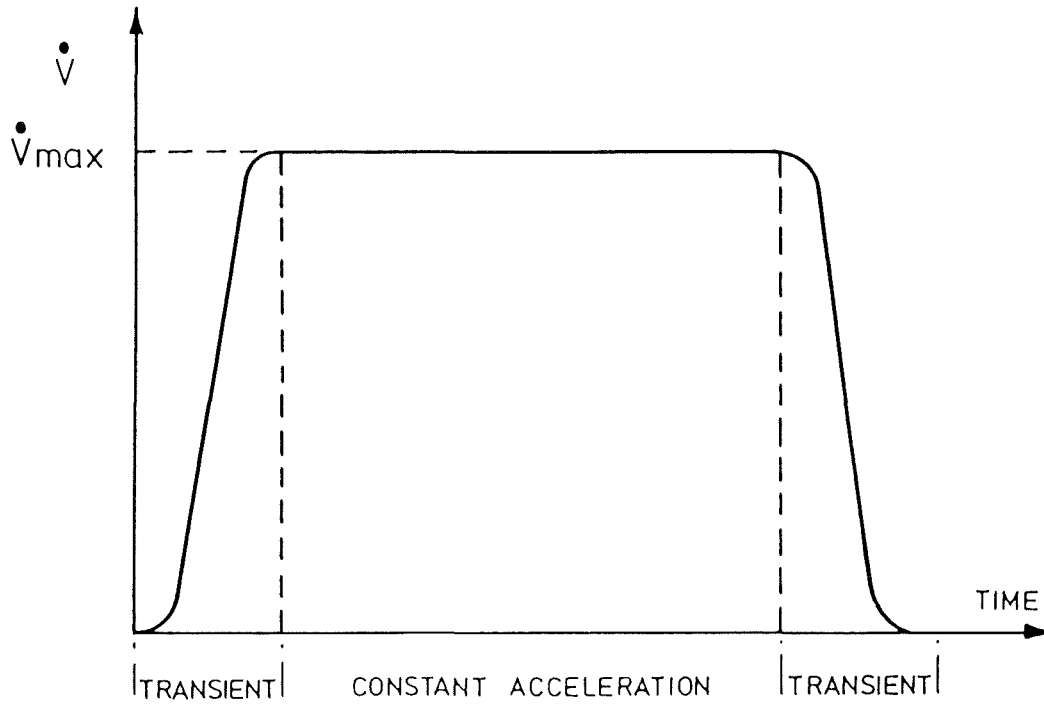
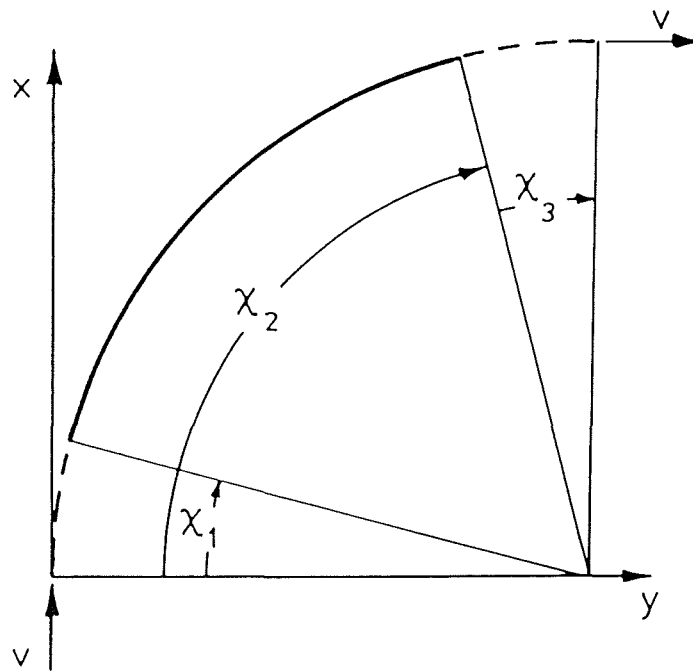
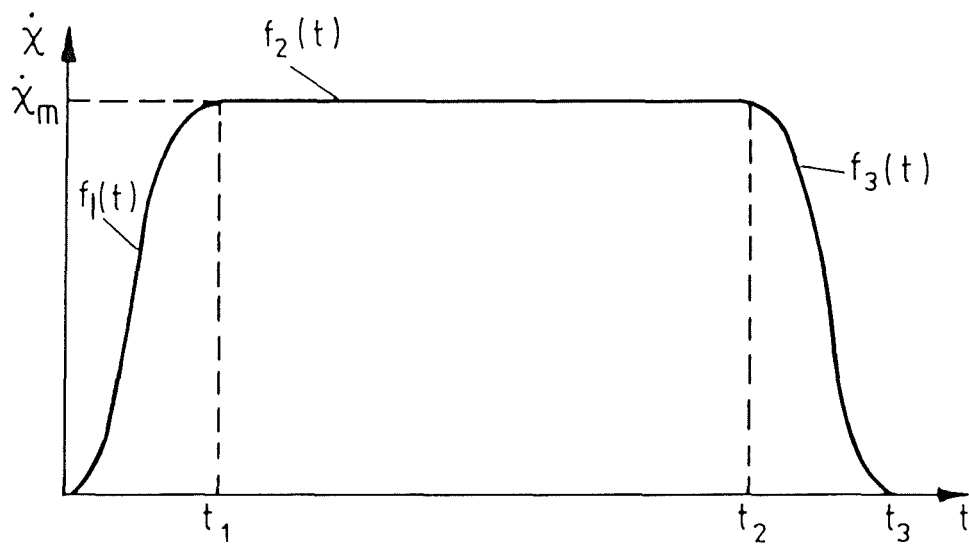


FIGURE 2.4 Constant Acceleration Speed Change

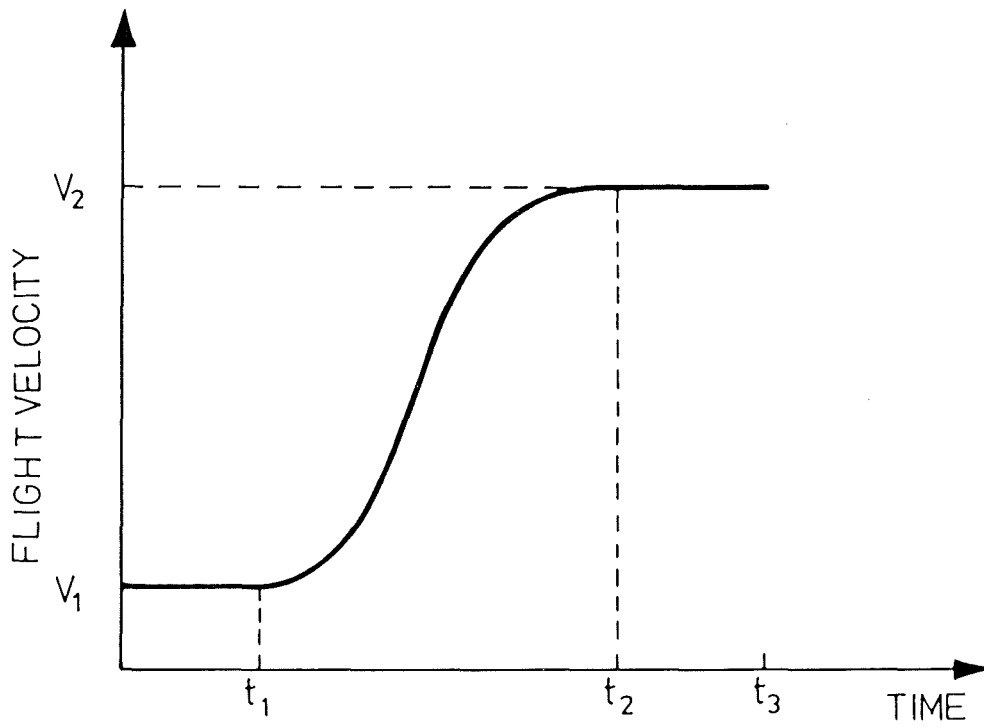


a) Track

FIGURE 2.5 : Level Turn Manoeuvre



b) Turn Rate



c) Velocity Change

FIGURE 2.5 : Cont.

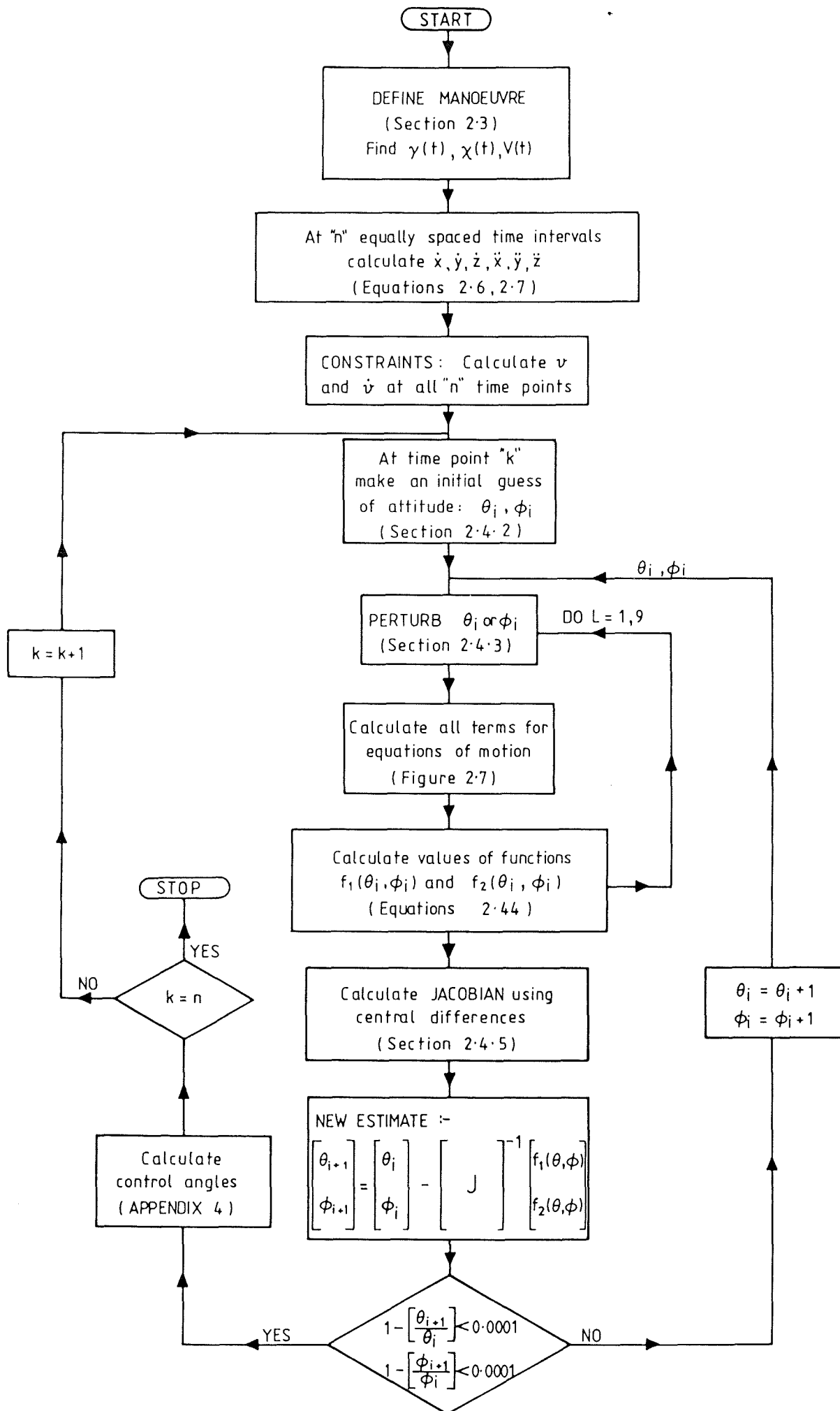


FIGURE 2.6 : Block Diagram of Inverse Algorithm

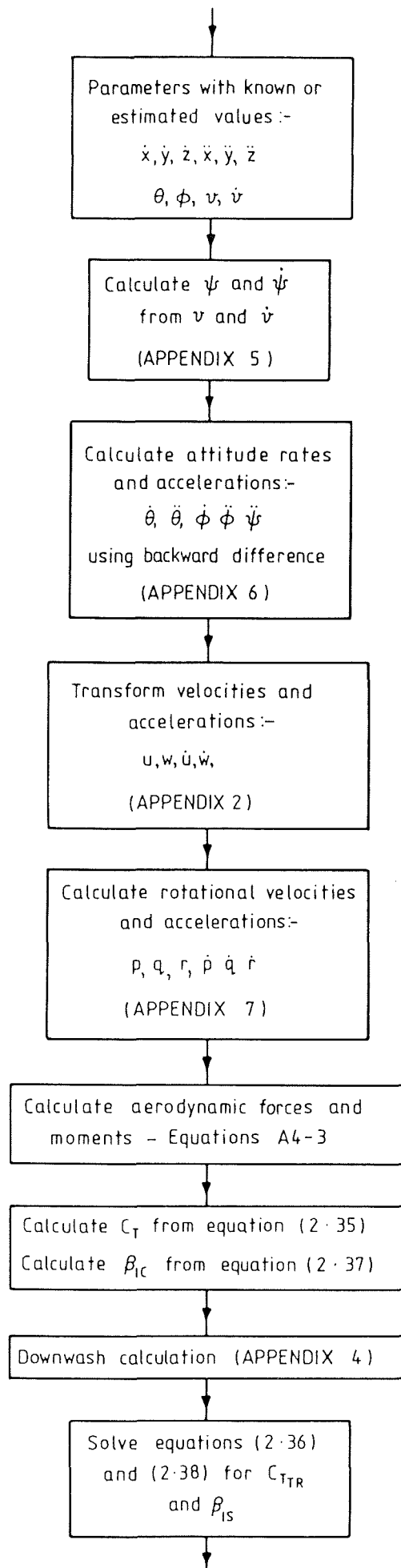


FIGURE 2.7 : Calculation of Functions

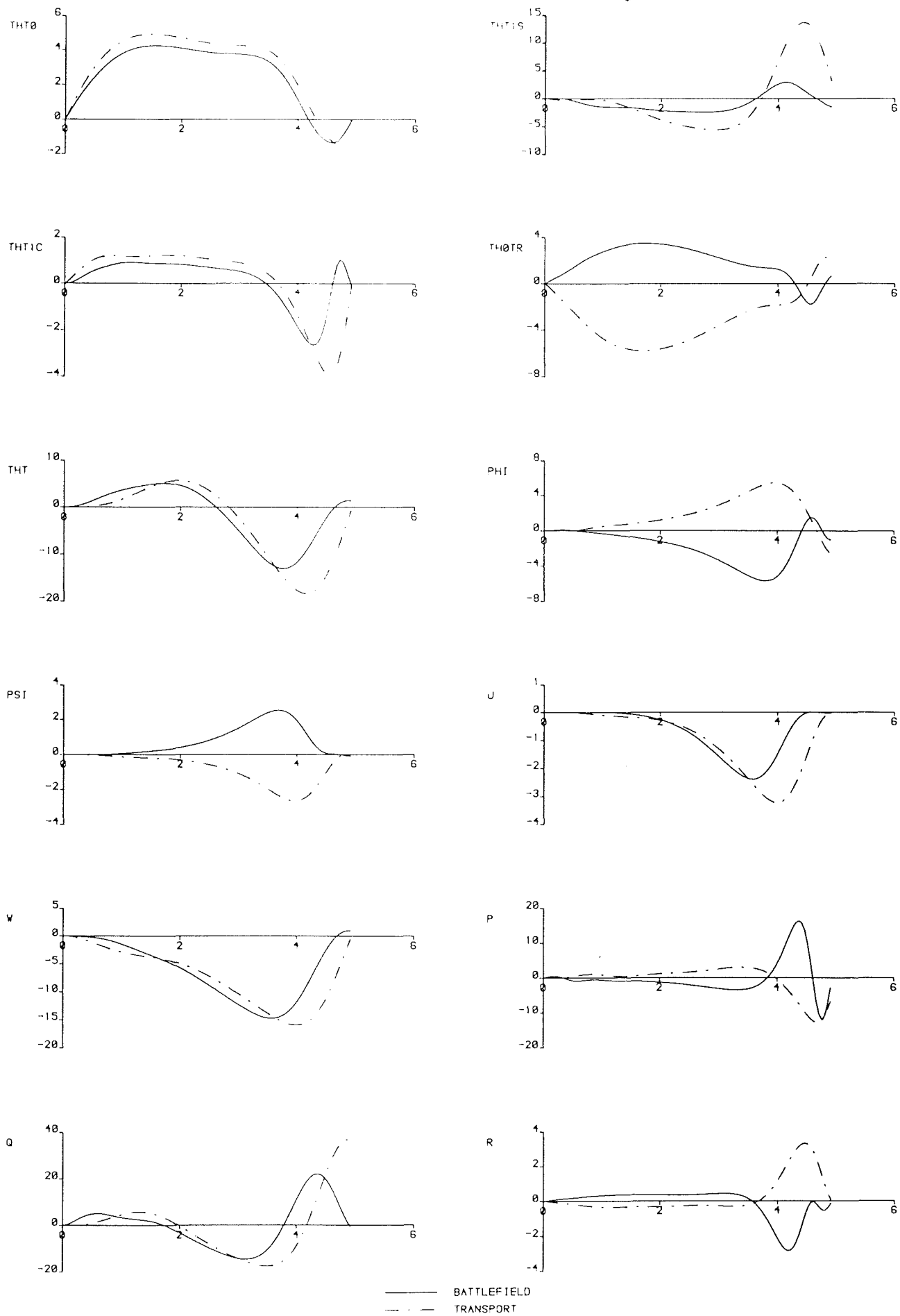


FIGURE 2.8 : Time Histories for Pop-up Manoeuvre

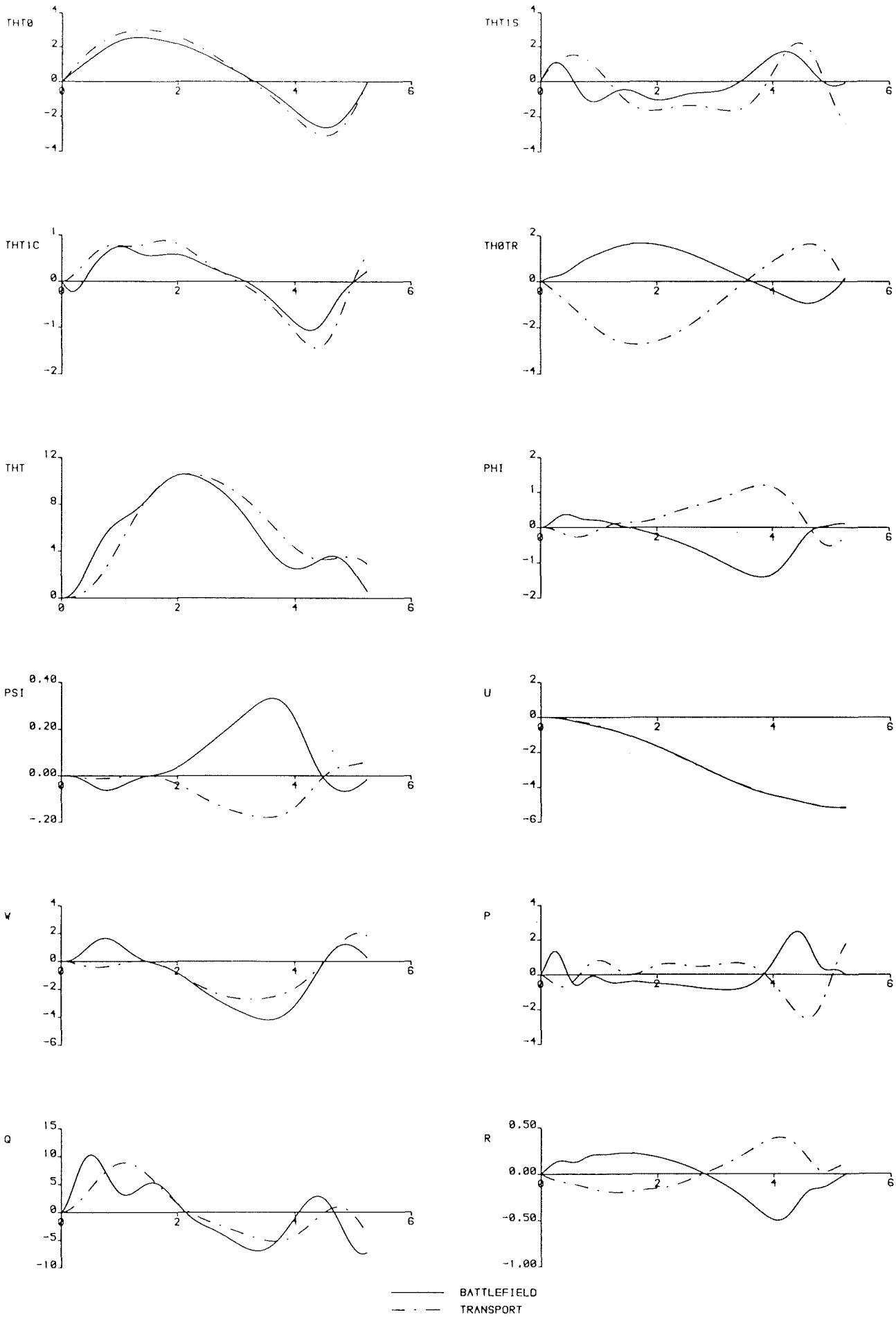


FIGURE 2.9 : Time Histories for Pop-up Manoeuvre with Speed Change

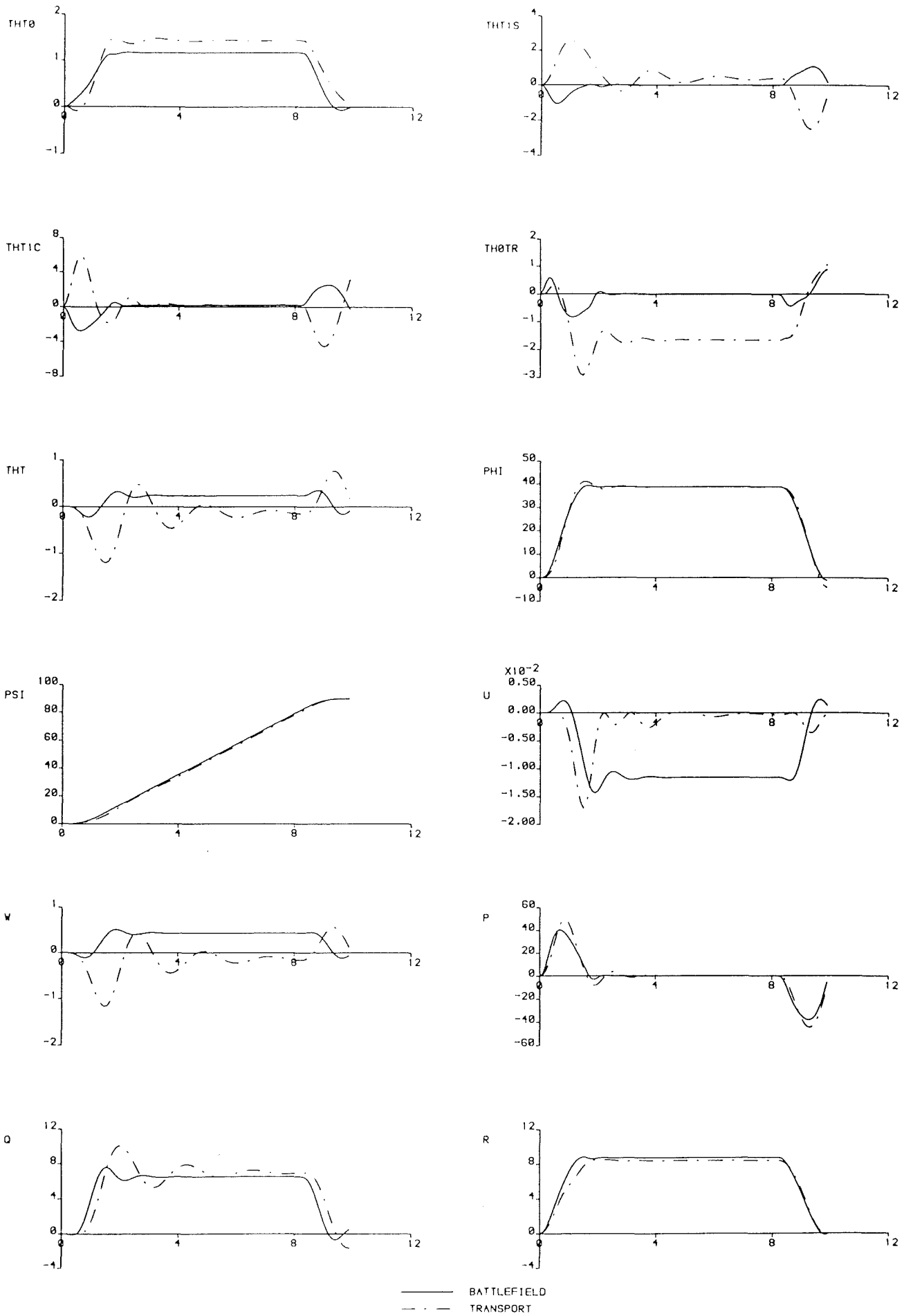


FIGURE 2.10 : Time Histories For Level Turn Manoeuvre

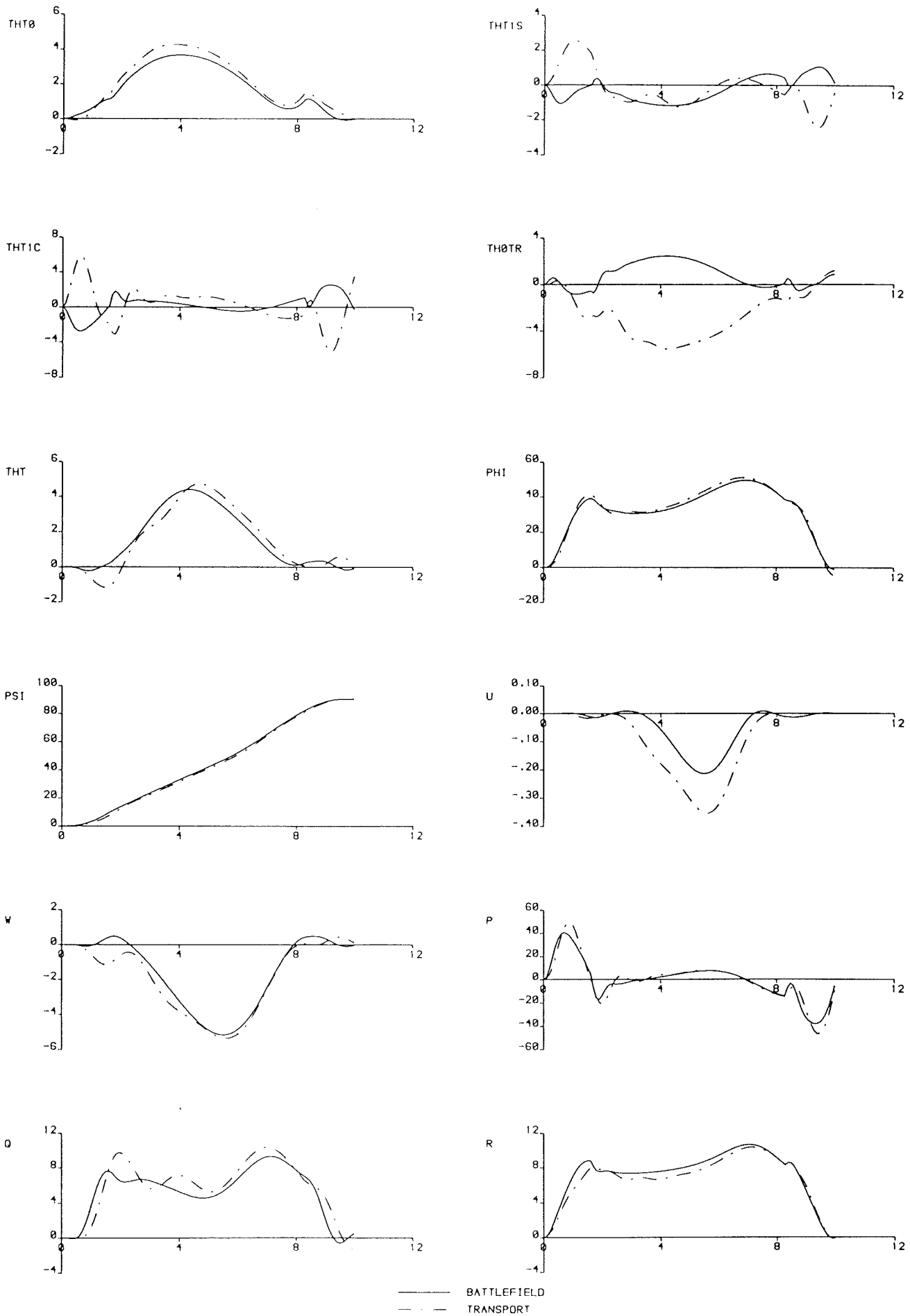
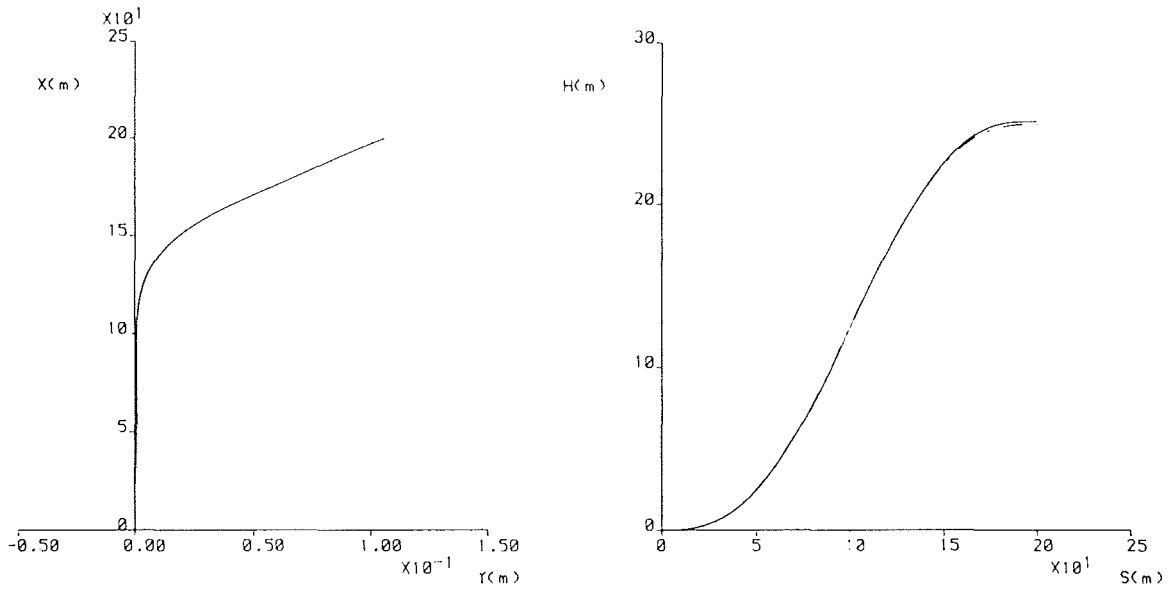
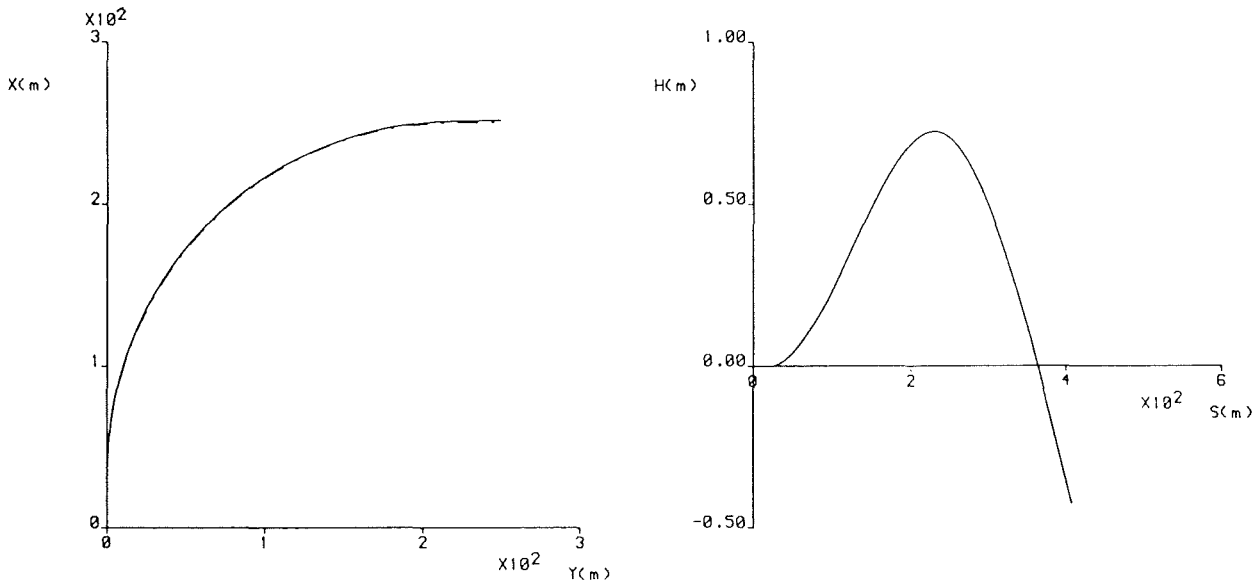


FIGURE 2.11 : Time Histories for Climbing Turn Manoeuvre



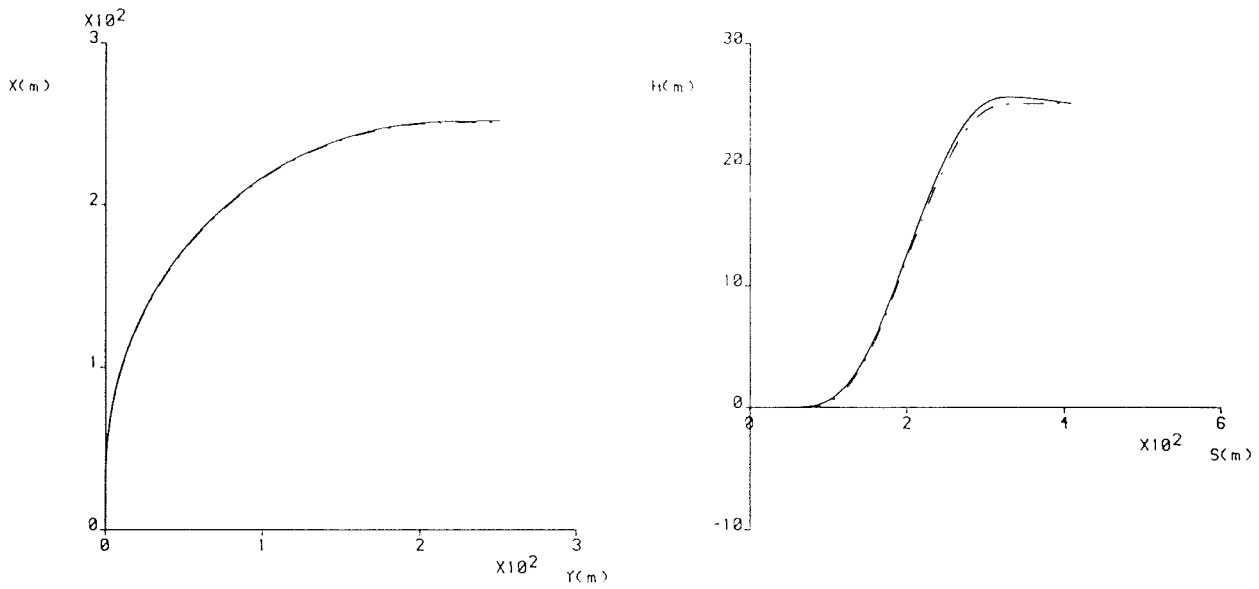
a) The Pop-up Manoeuvre



b) The Level Turn Manoeuvre

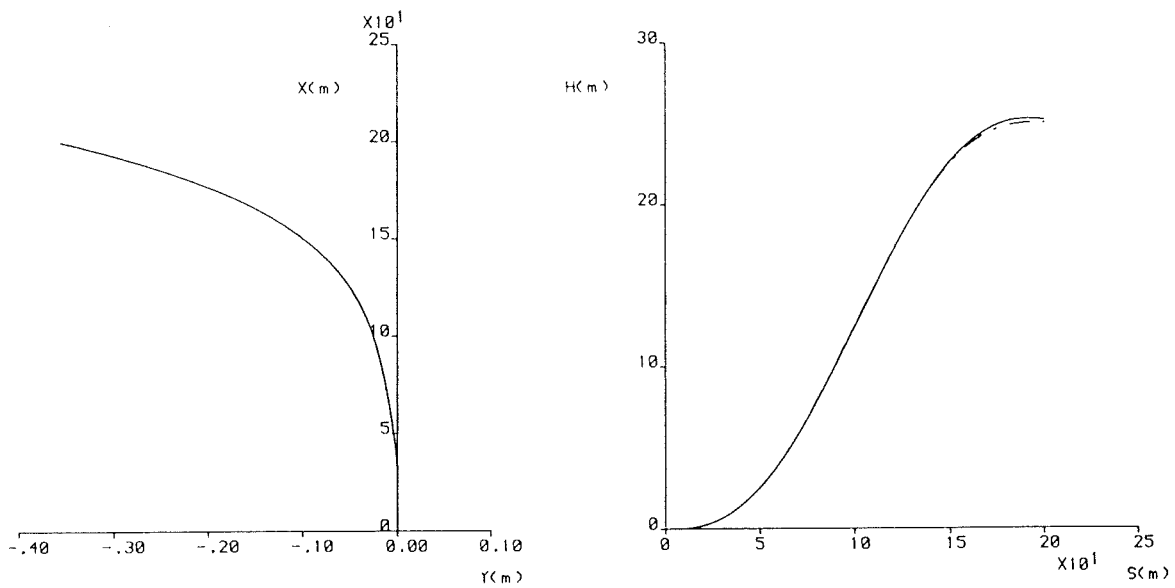
————— Time Response
 - - - - - Inverse

FIGURE 2.12 : Comparison of Flight Paths for BATTLEFIELD Helicopter



c) The Climbing Turn Manoeuvre

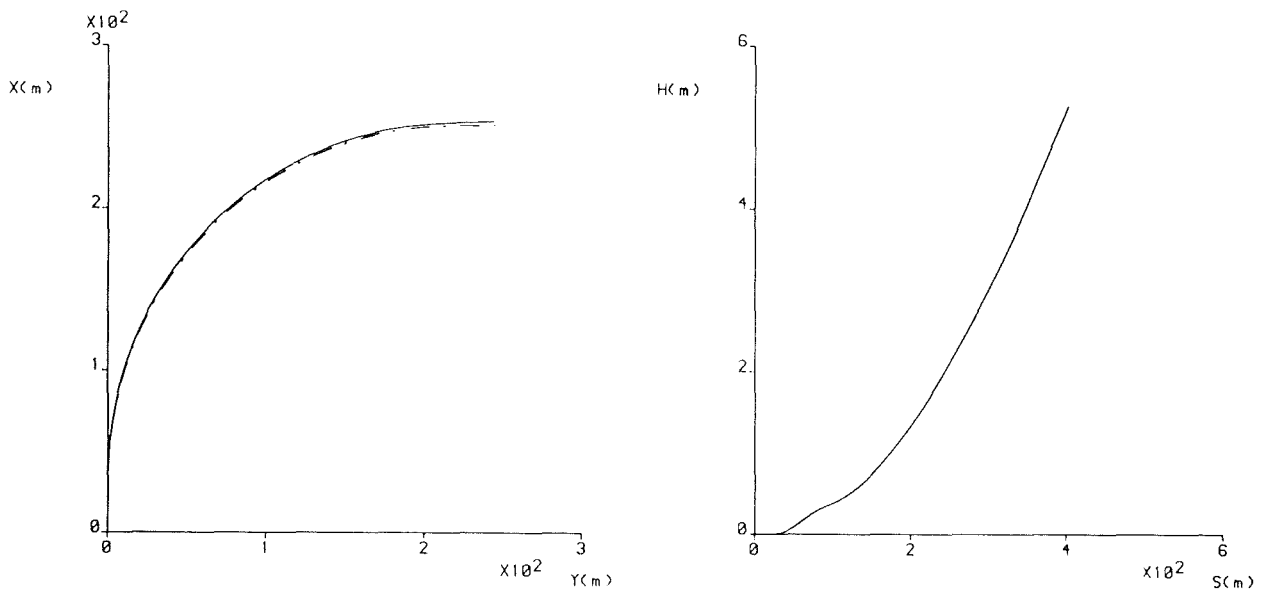
FIGURE 2.12 : Cont.



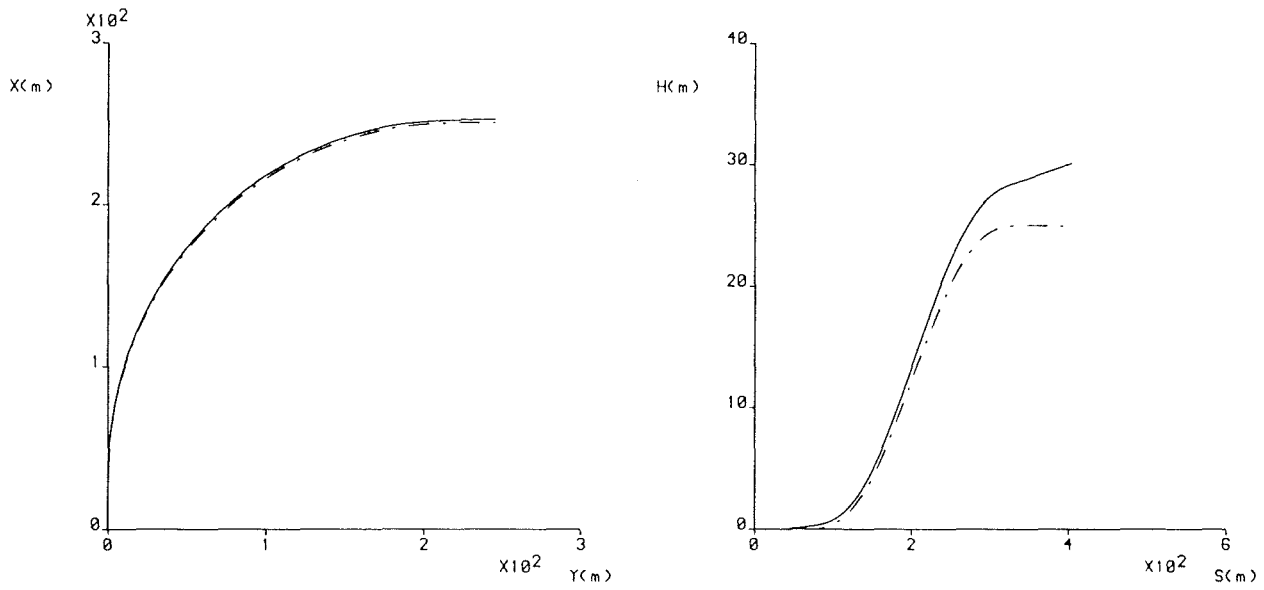
a) The Pop-up Manoeuvre

————— Time Response
 - - - - - Inverse

FIGURE 2.13 : Comparison of Flight Paths for TRANSPORT Helicopter



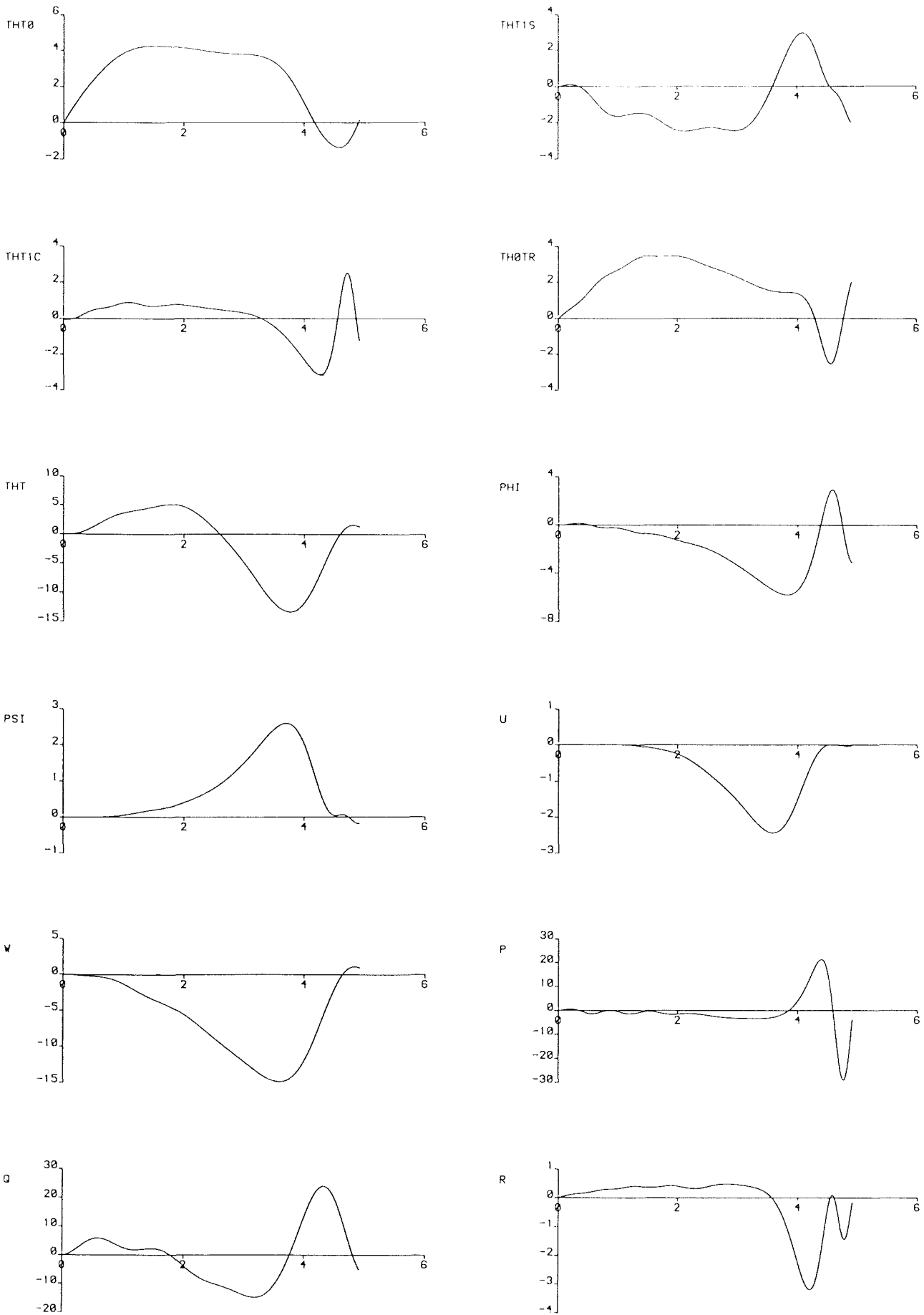
b) The Level Turn Manoeuvre



c) The Climbing Turn Manoeuvre

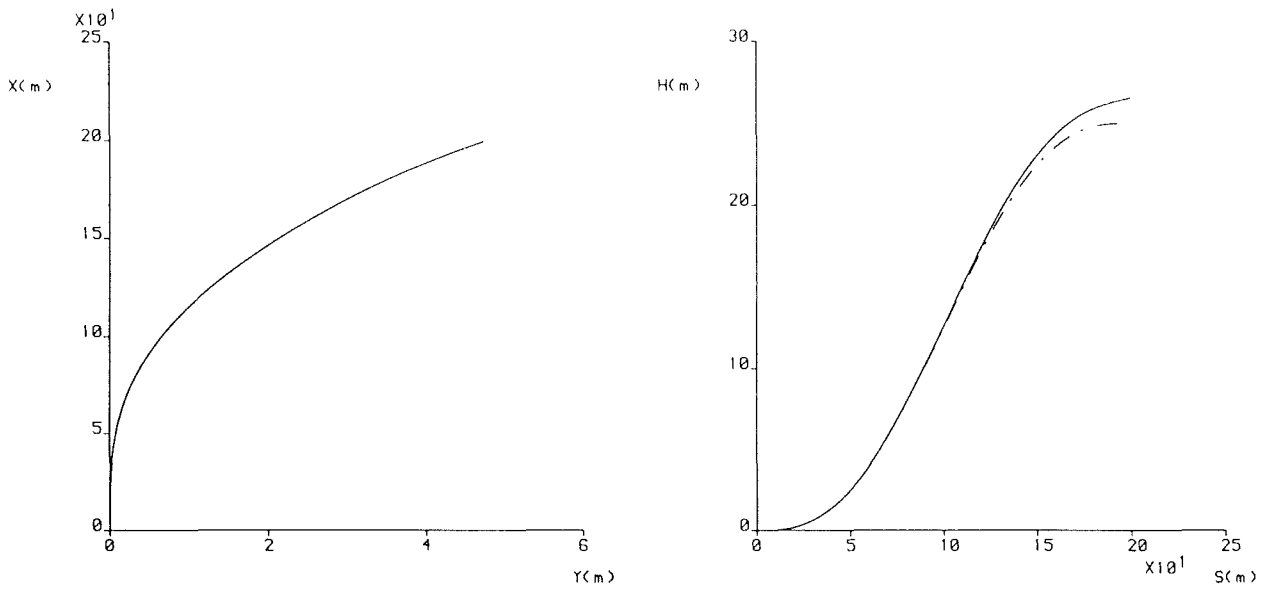
————— Time Response
 - - - - - Inverse

FIGURE 2.13 : Cont.

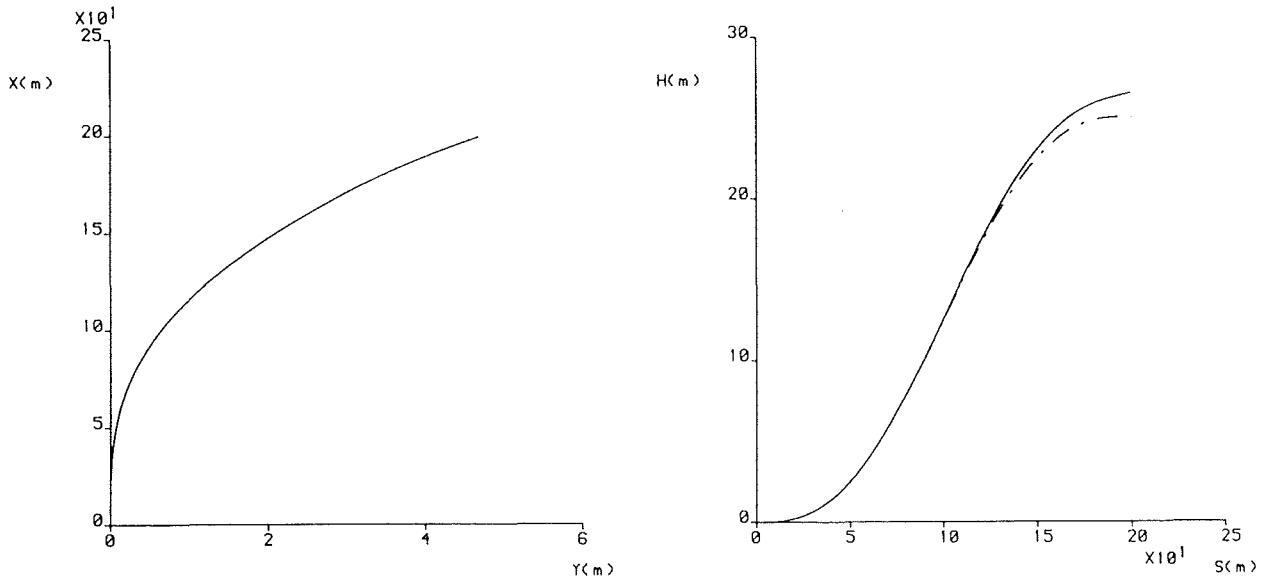


BATTLEFIELD Configuration

FIGURE 2.14 : Pop-up Manoeuvre with Time Step of 0.005 seconds.



a) Full Control Time History



b) Thinned Control Time History

——— Time Response
 - - - - - Inverse

FIGURE : 2.15 Comparison of Flight Paths for Pop-up Manoeuvre.

BATTLEFIELD Configuration

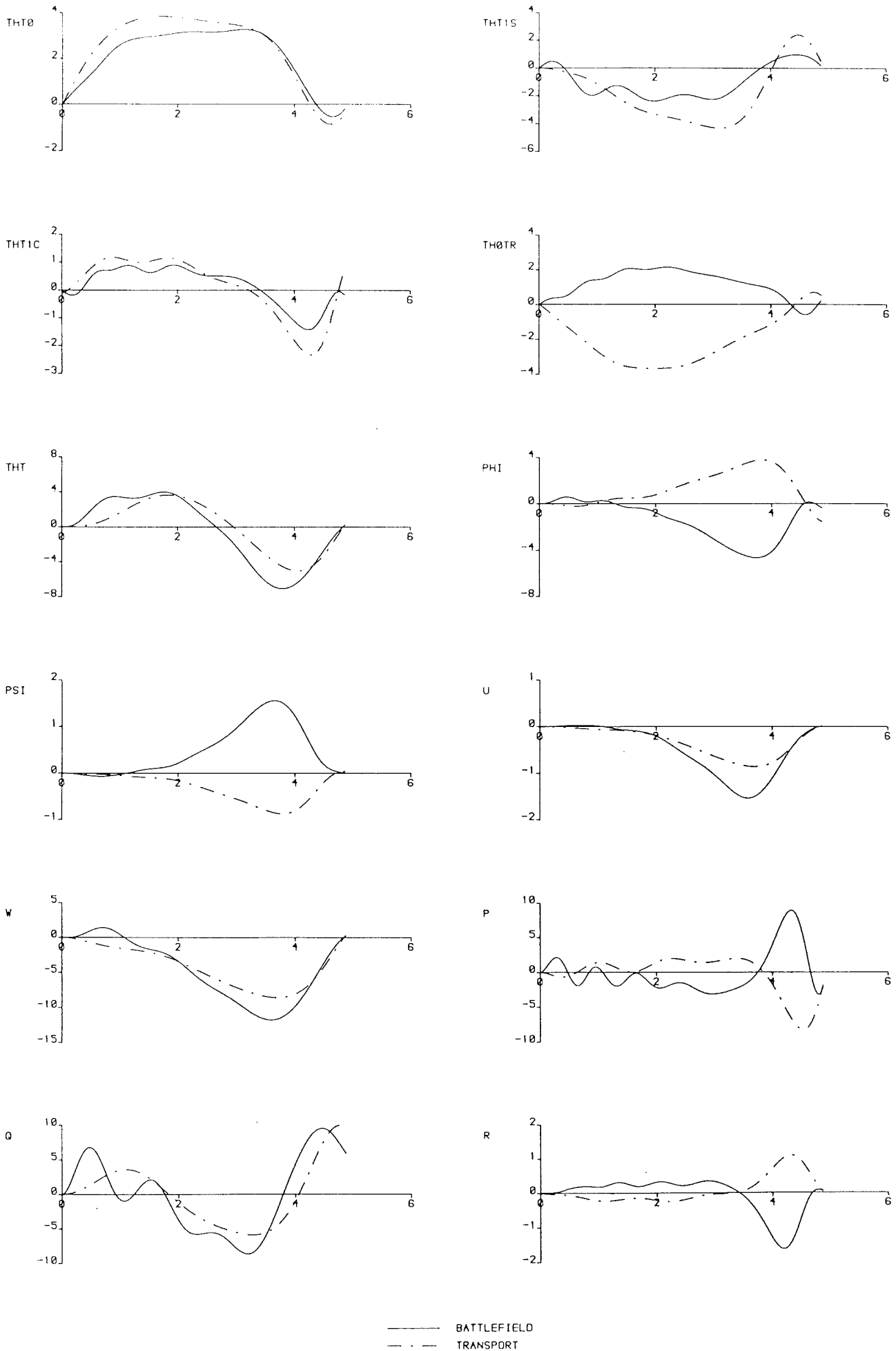
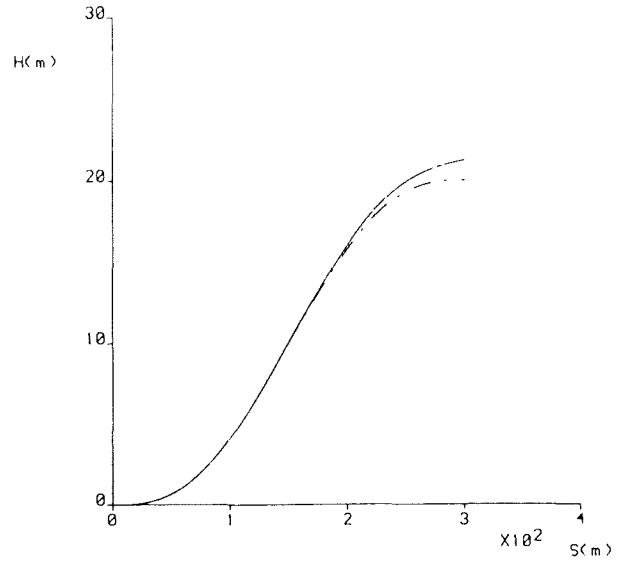
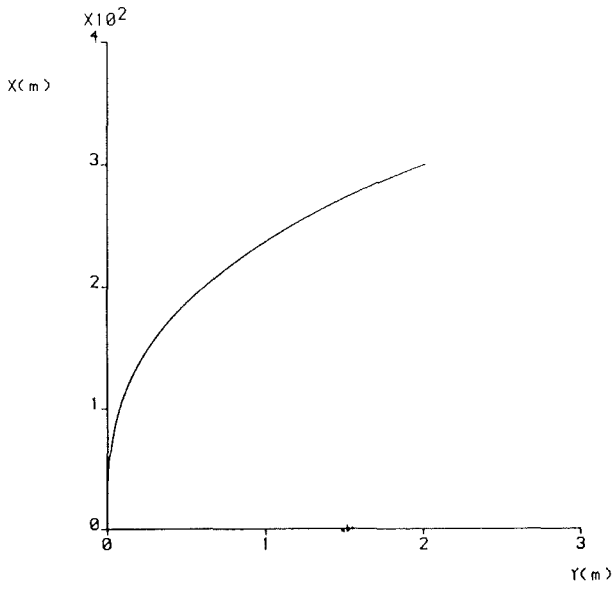
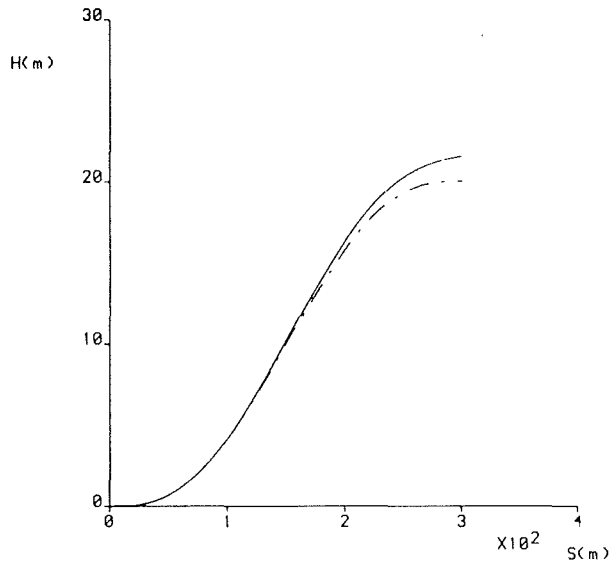
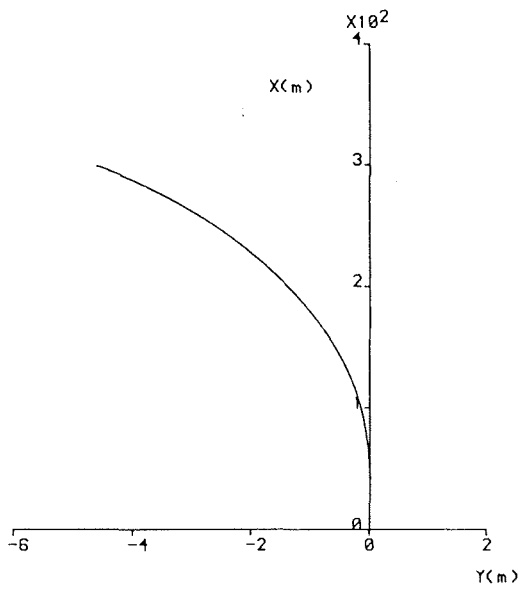


FIGURE 2.16 : Oscillatory Solution For Pop-up Manoeuvre with Small Time Step



BATTLEFIELD Configuration



TRANSPORT Configuration

——— Time Response
 - - - - - Inverse

FIGURE 2.17 : Comparison of Flight Paths for Small Step, Oscillatory Pop-up Manoeuvre

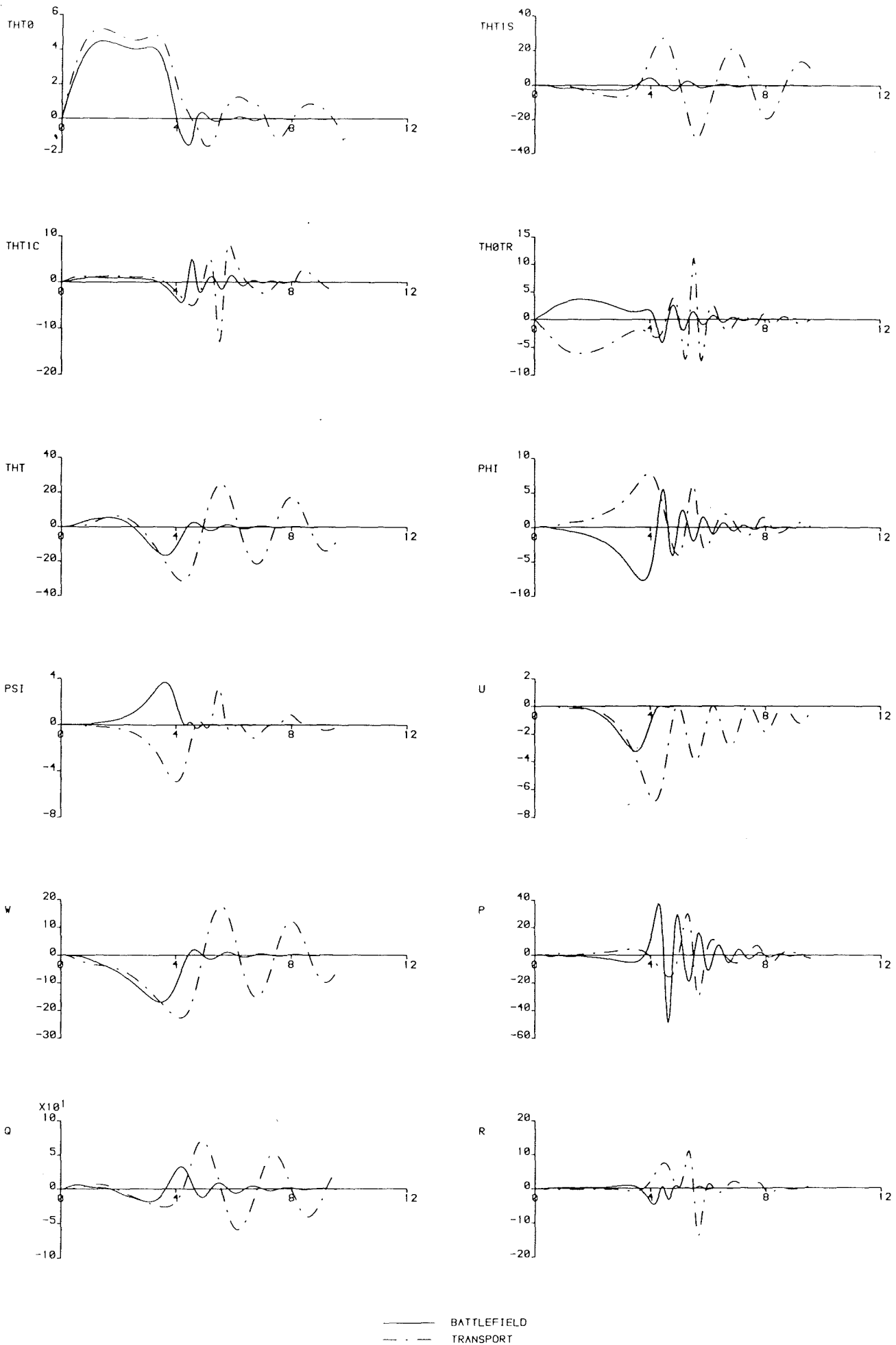
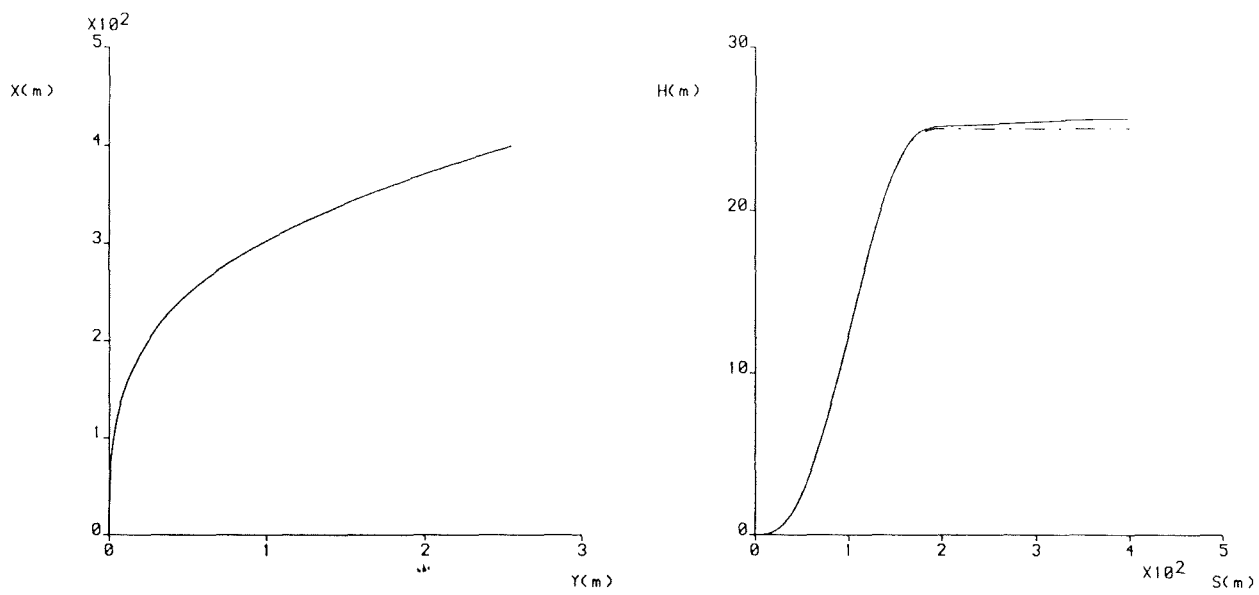
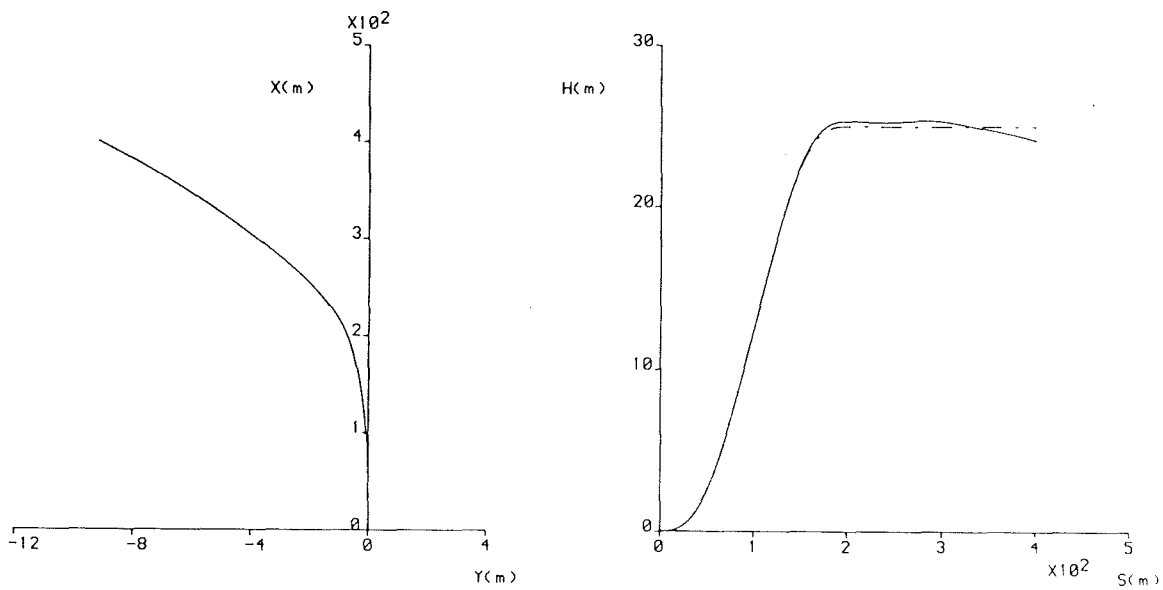


FIGURE 2.18 : Pop-up Manoeuvre with Straight and Level Section at Exit



BATTLEFIELD Configuration



TRANSPORT Configuration

— Time Response
 - - - Inverse

FIGURE 2.19 : Comparison of Flight Paths for Pop-up with

Straight/Level Section at Exit

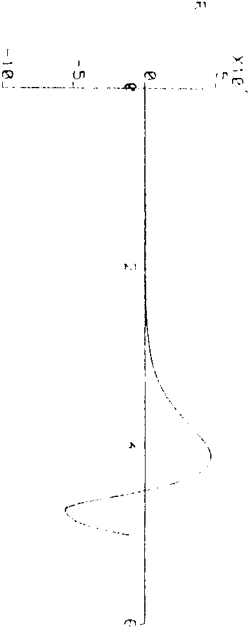
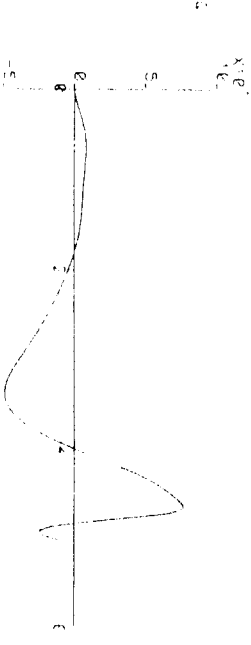
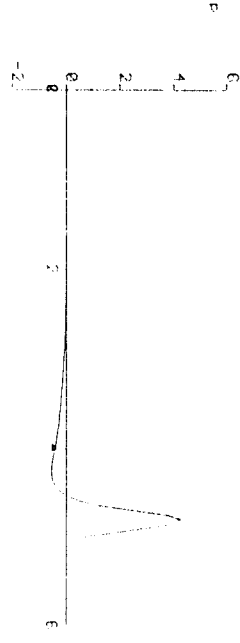
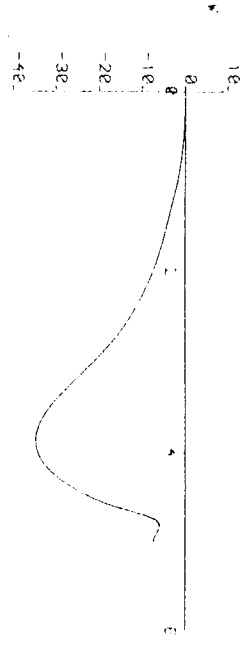
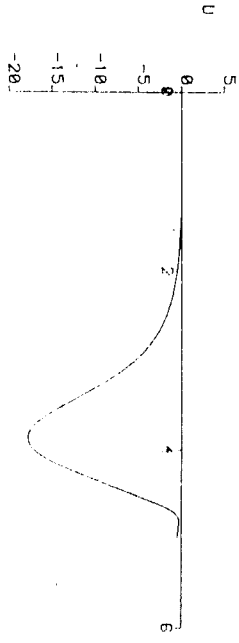
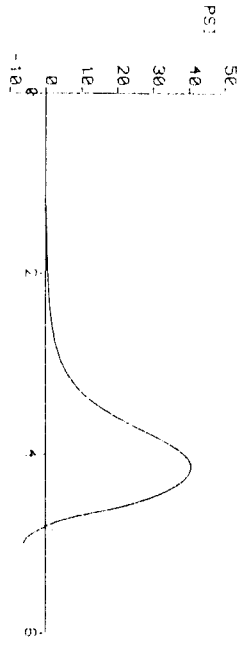
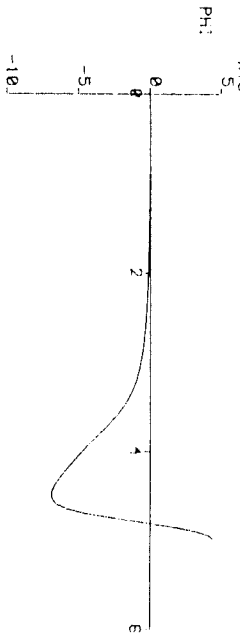
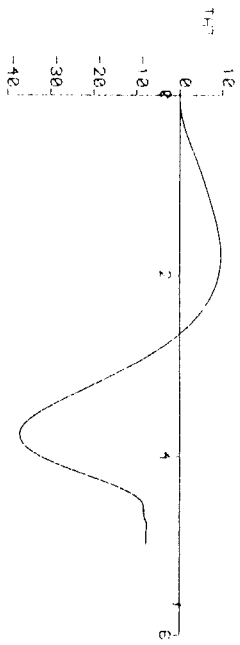
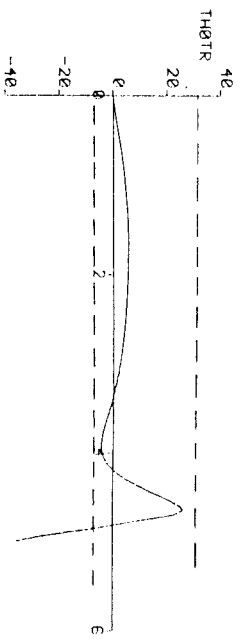
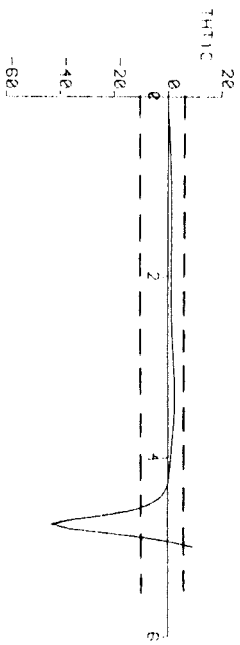
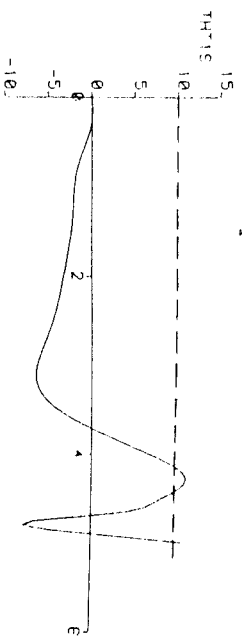
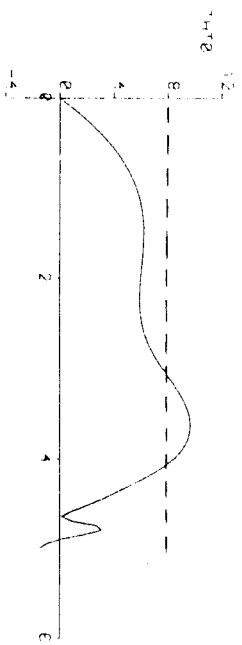


FIGURE 2.20 : Time Histories For BATTLEFIELD Configuration in Severe Pop-up Manoeuvre

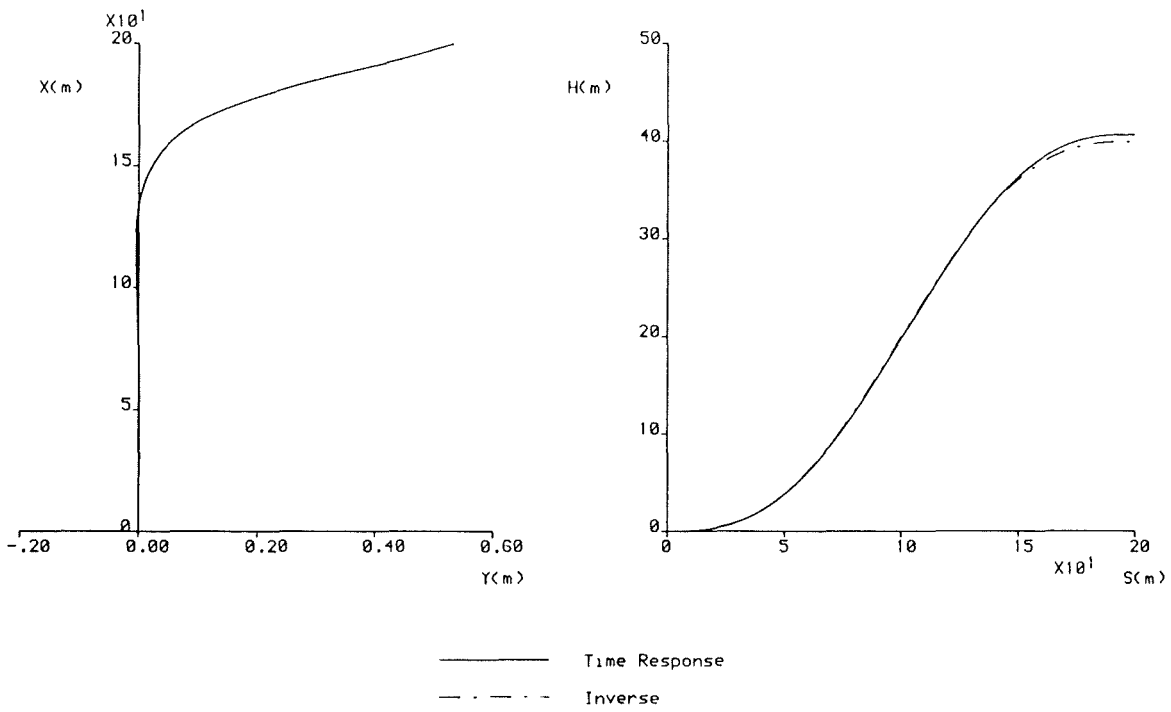


FIGURE 2.21 : Comparison of Flight Paths, BATTLEFIELD Configuration
in Severe Pop-up Manoeuvre

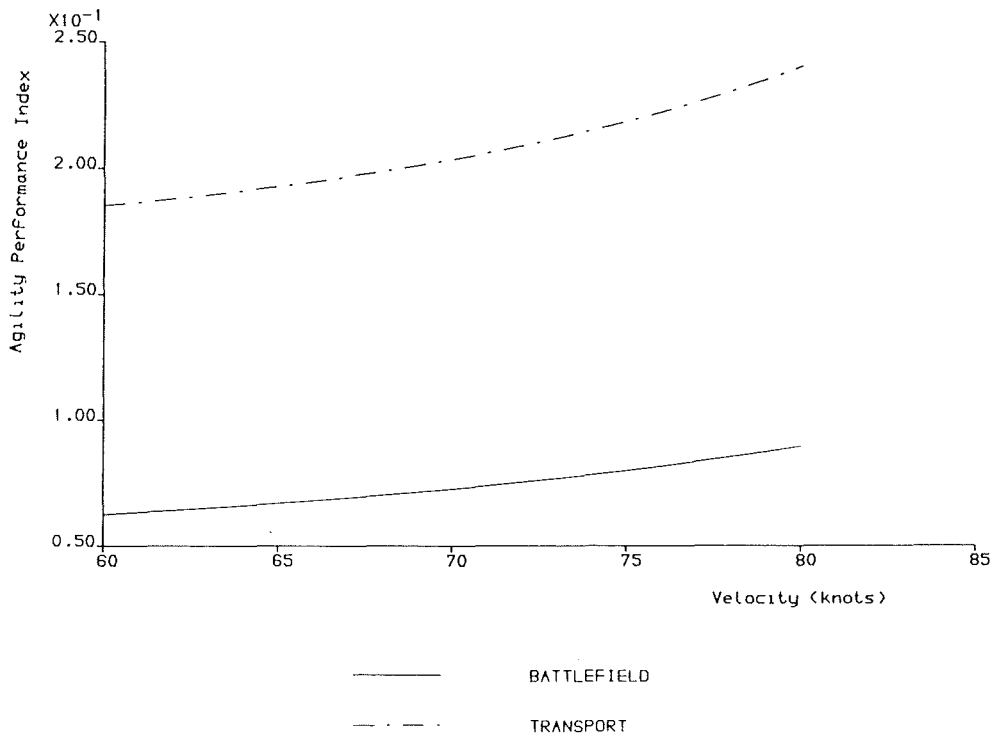
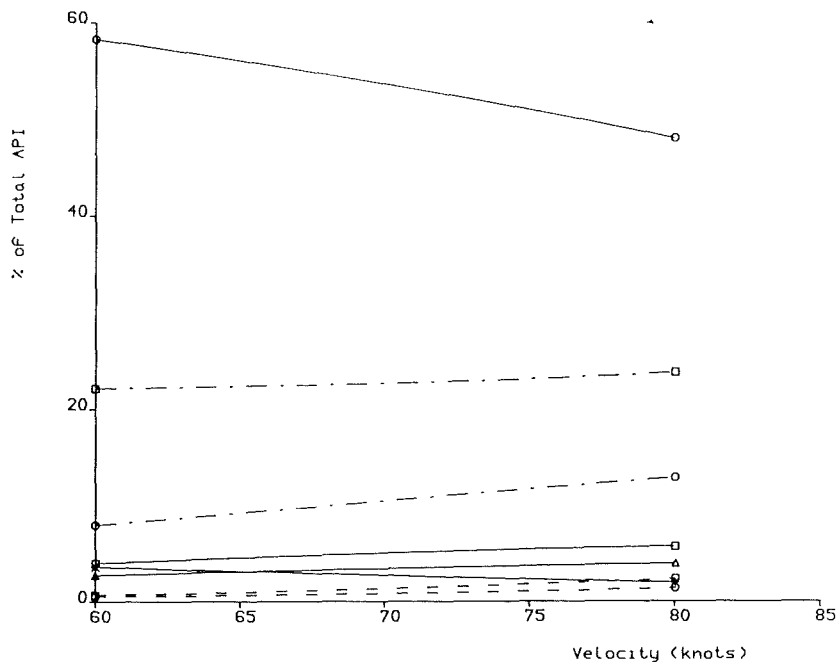
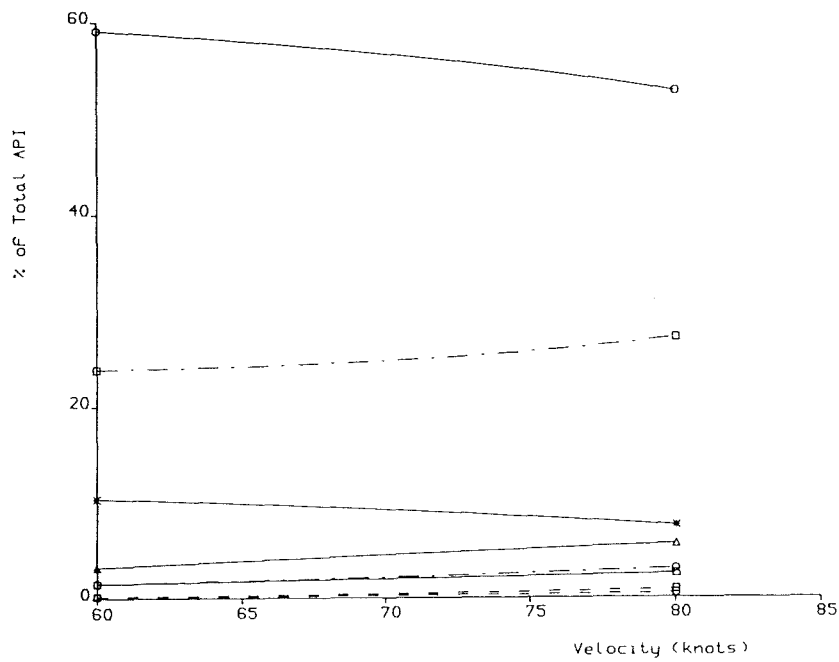


FIGURE 3.1 : API vs. Velocity For Pop-up Manoeuvre ($s = 250m$, $h = 25m$).
All Weighting Constants Equal.



BATTLEFIELD



TRANSPORT

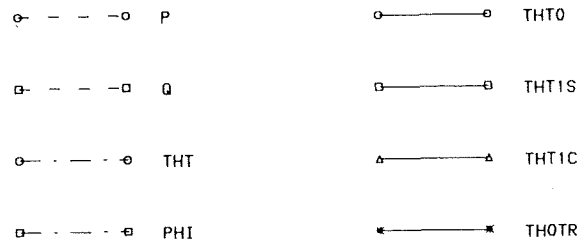


FIGURE 3.2 : Components of API for Pop-up Manoeuvre

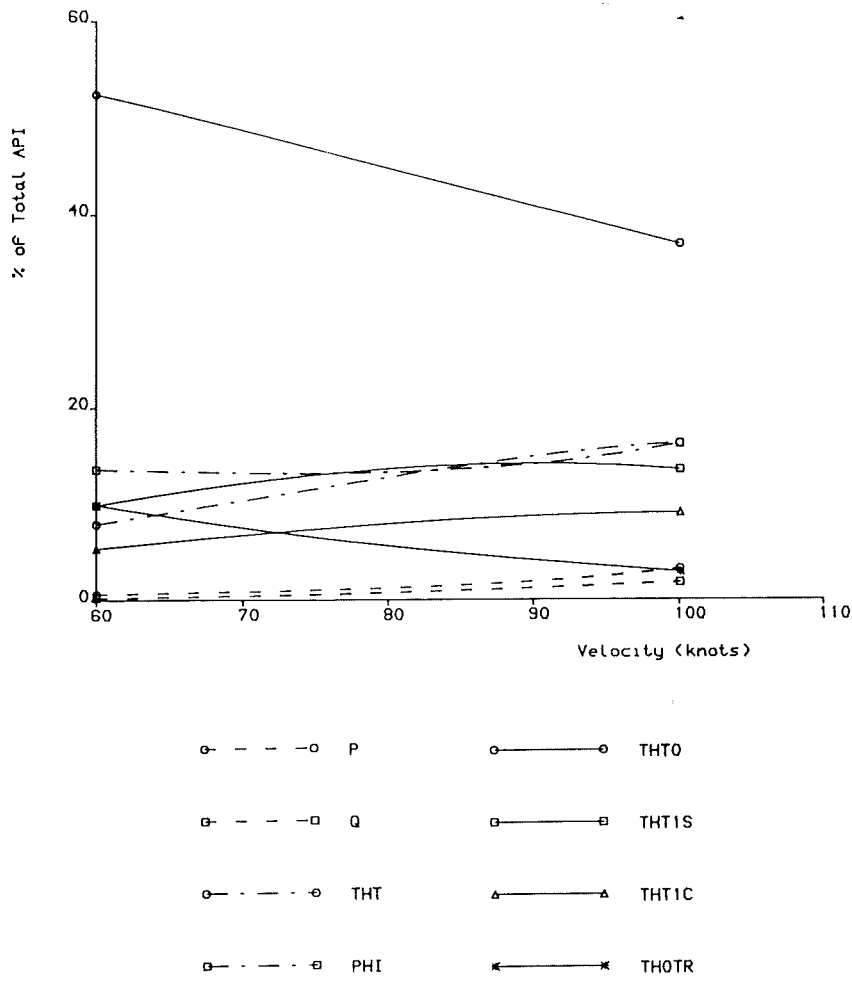
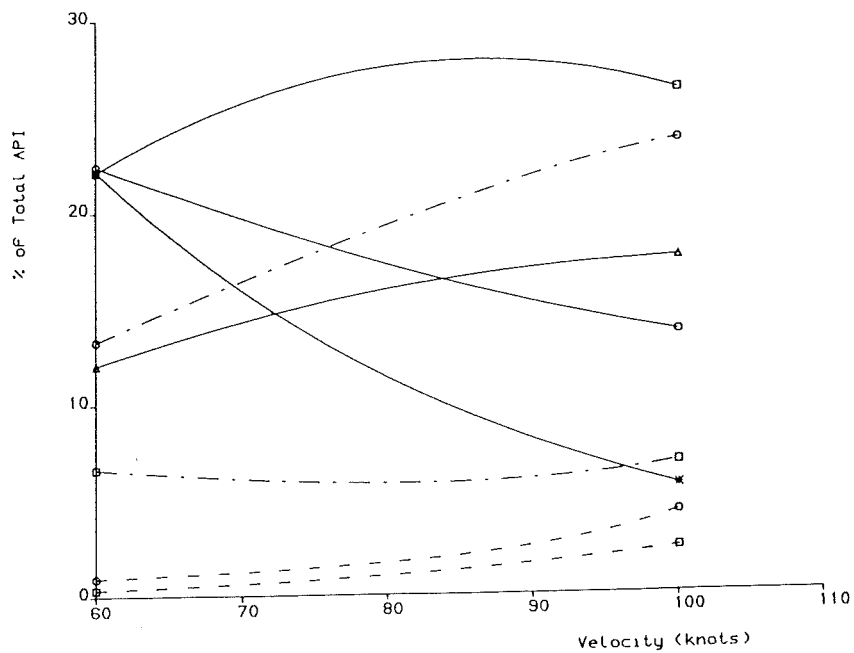
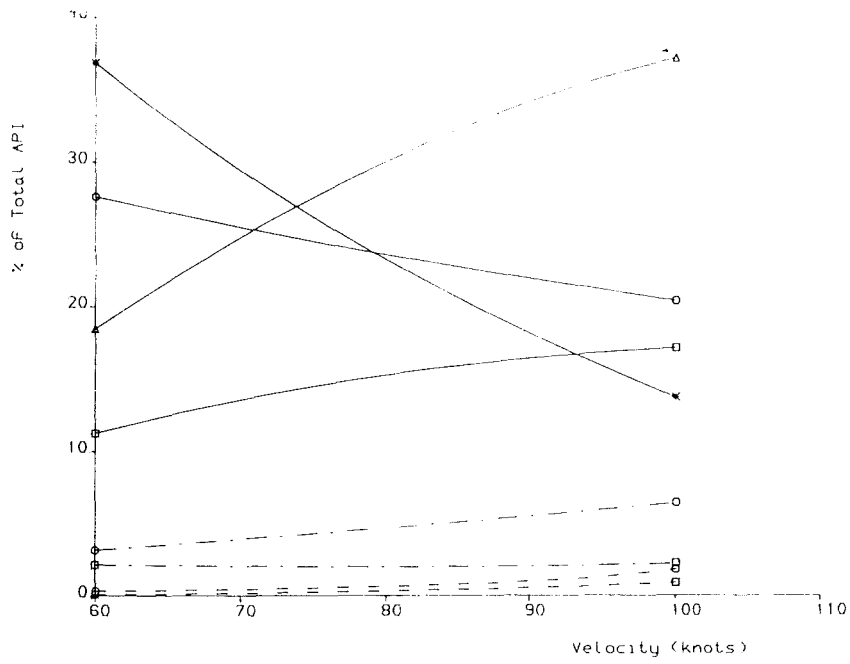


FIGURE 3.3 : Contributions to Total API For POP-UP and HURDLE-HOP Manoeuvres, BATTLEFIELD Configuration INITIAL Values of Weighting Constants



a) BATTLEFIELD Configuration

FIGURE 3.4 : Contributions to Total API For POP-UP and HURDLE-HOP Manoeuvres: FINAL Values of Weighting Constants



b) TRANSPORT Configuration

- - - - ○ P ○ ——— ○ THTO
- - - - □ Q □ ——— □ THTIS
- △ - - - △ THT △ ——— △ THTIC
- × - - - × PHI × ——— × THOTR

FIGURE 3.4 : Cont.

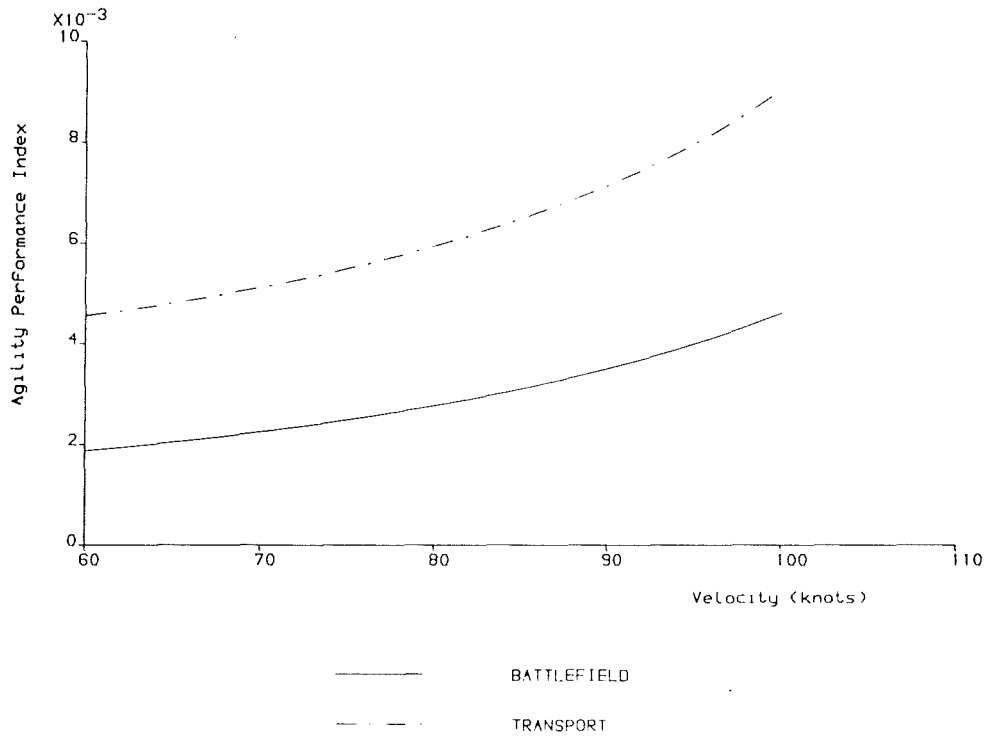


FIGURE 3.5 : API vs. Velocity for POP-UP Manoeuvre
(Distance = 300m , Height = 25m)

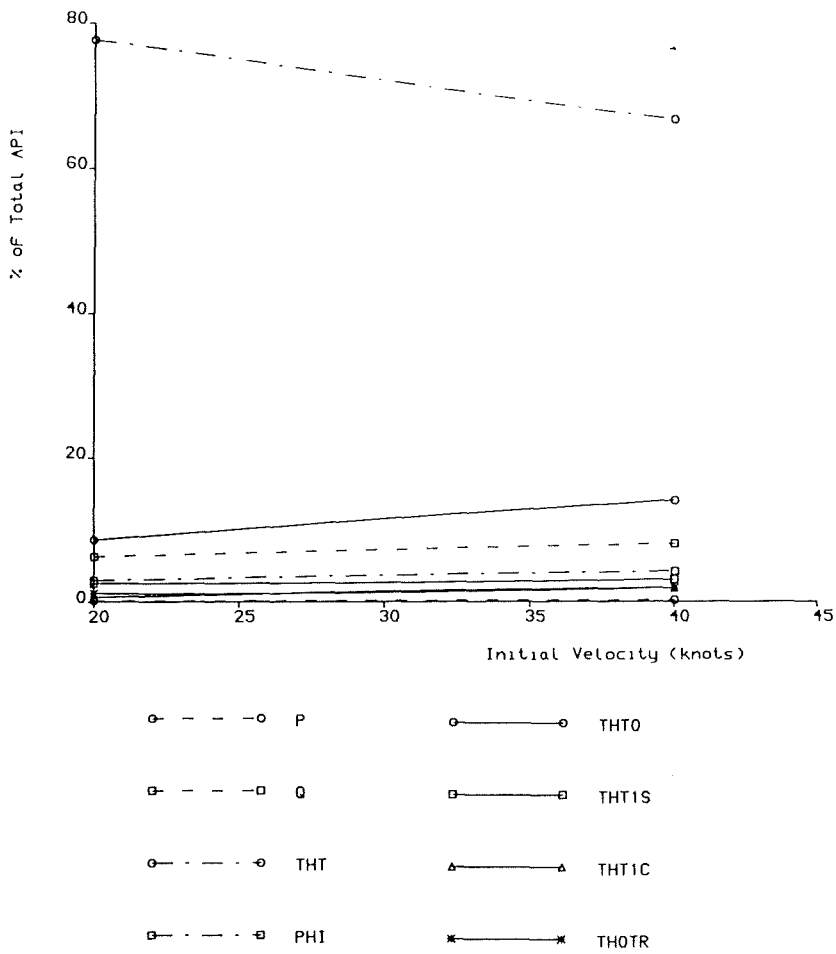
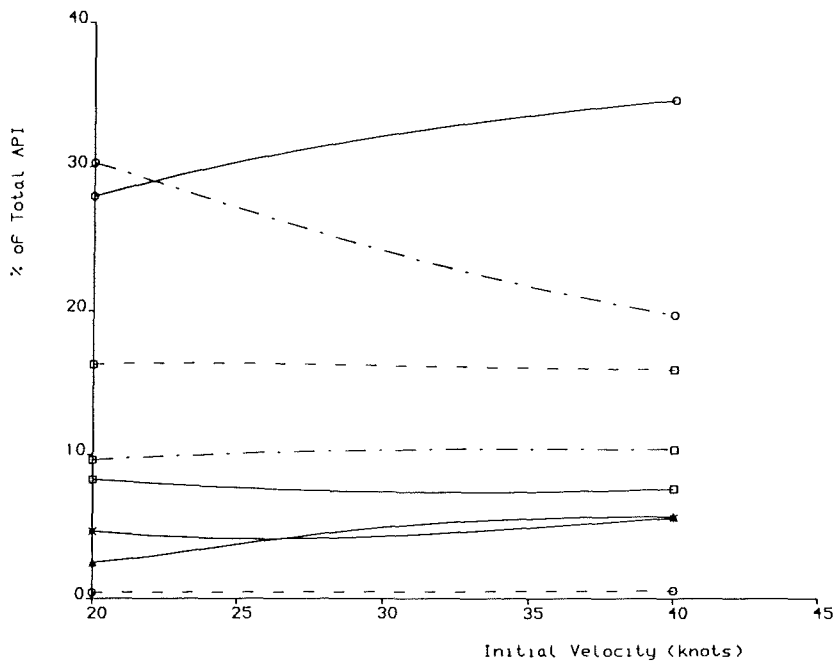
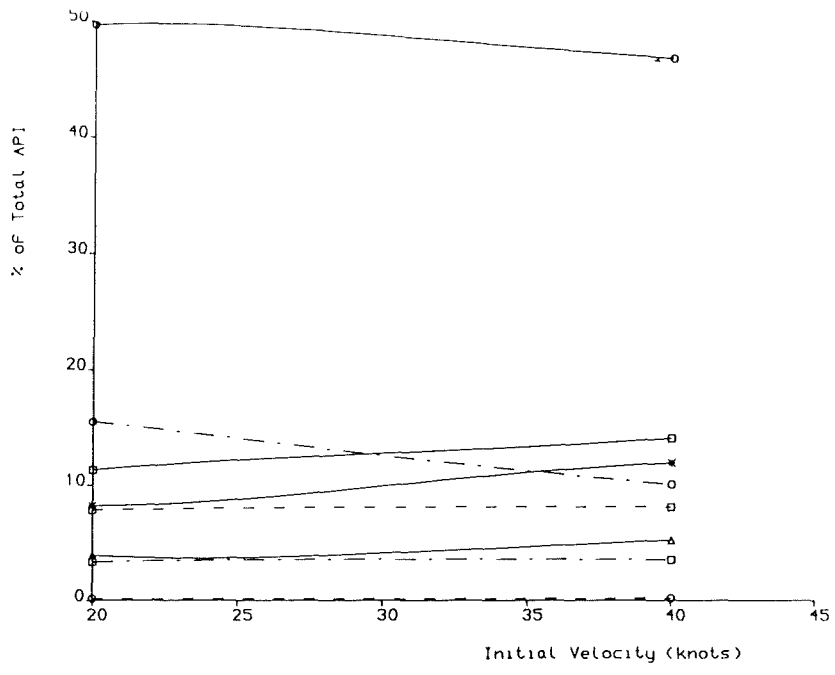


FIGURE 3.6 : Contributions to Total API For ACCELERATION and DECELERATION Manoeuvres
INITIAL Values of Weighting Constants BATTLEFIELD Configuration



a) BATTLEFIELD Configuration

FIGURE 3.7 : Contributions to Total API For ACCELERATION and DECELERATION Manoeuvres
FINAL Values of Weighting Constants



b) TRANSPORT Configuration

- - - - ○ P ○ ——— ○ THT0
- - - - □ Q □ ——— □ THT1S
- - - - ○ THT △ ——— △ THT1C
- - - - □ PHI ◀ ——— ▶ TH0TR

FIGURE 3.7 : Cont.

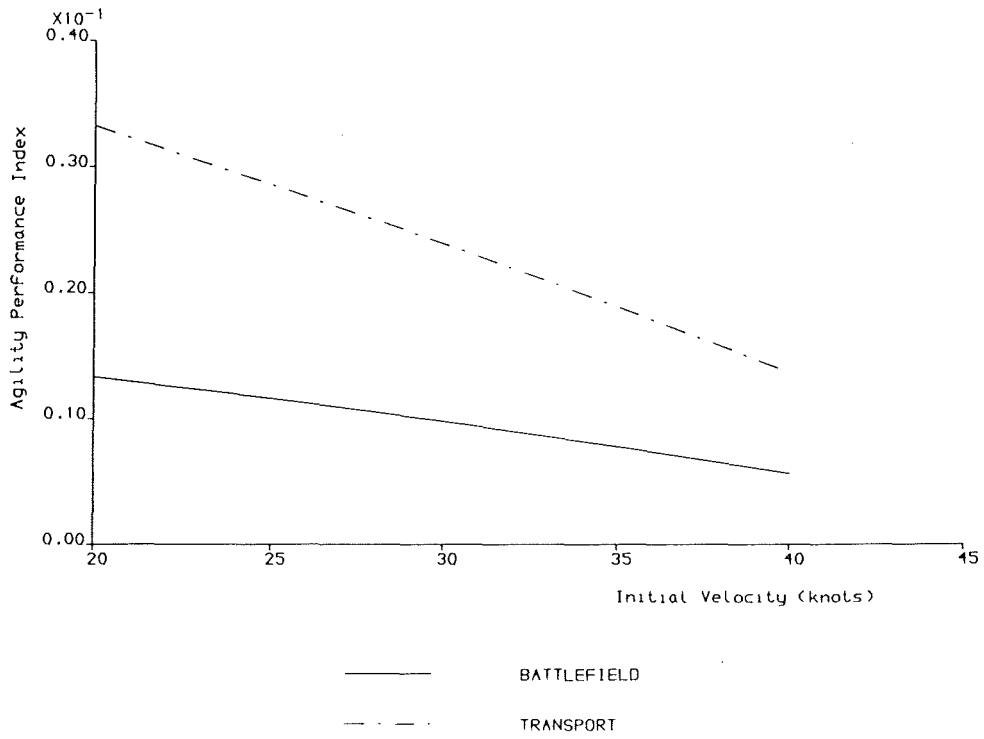


FIGURE 3.8 : API vs. Initial Velocity For an ACCELERATION to a Final Velocity of 60 knots over 150m

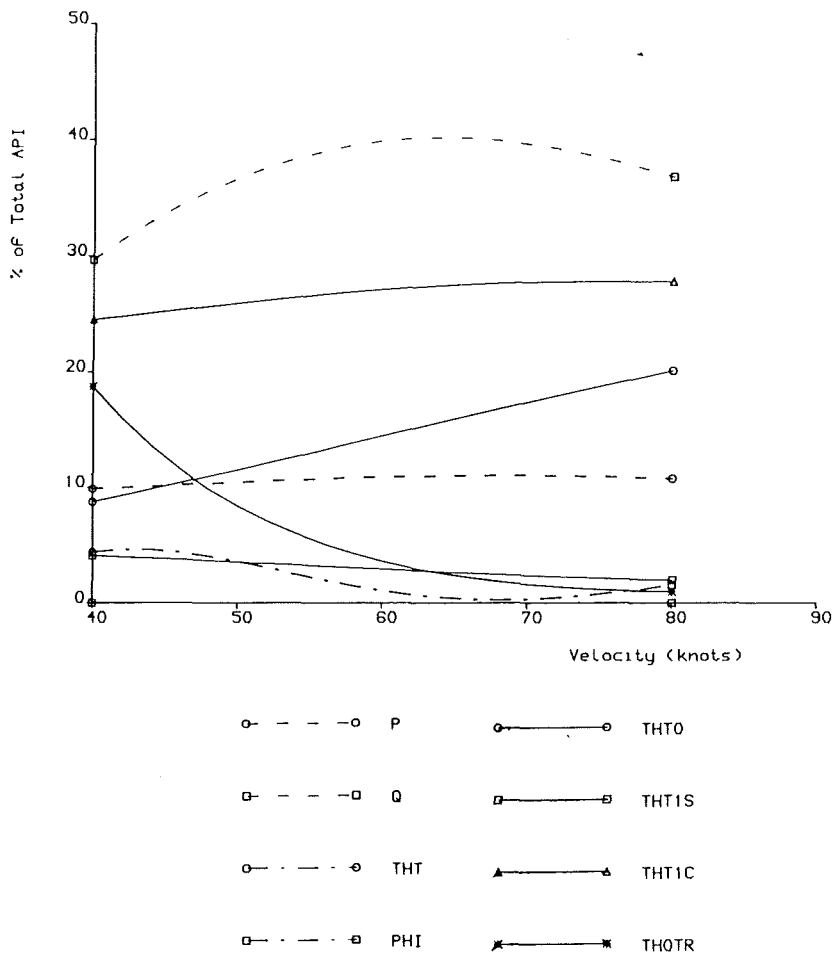
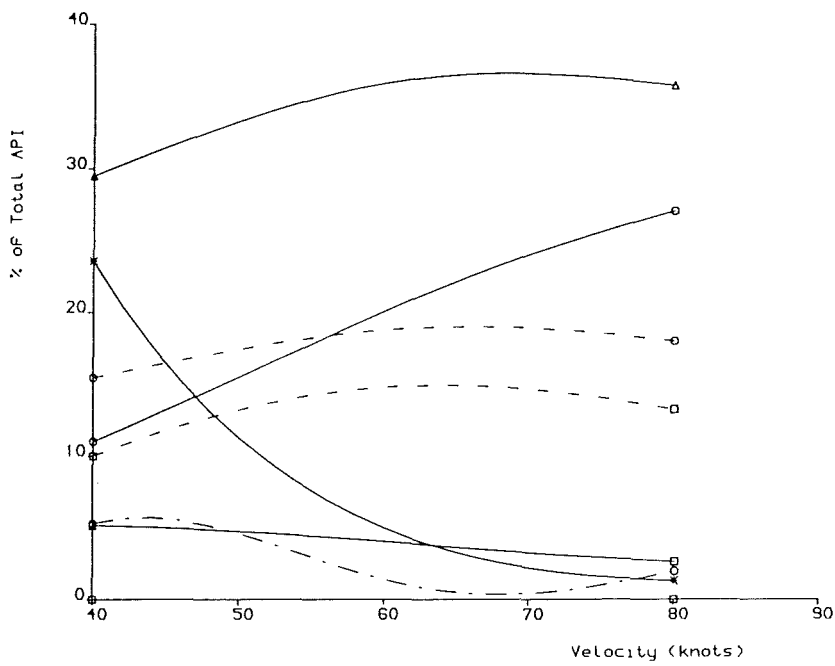
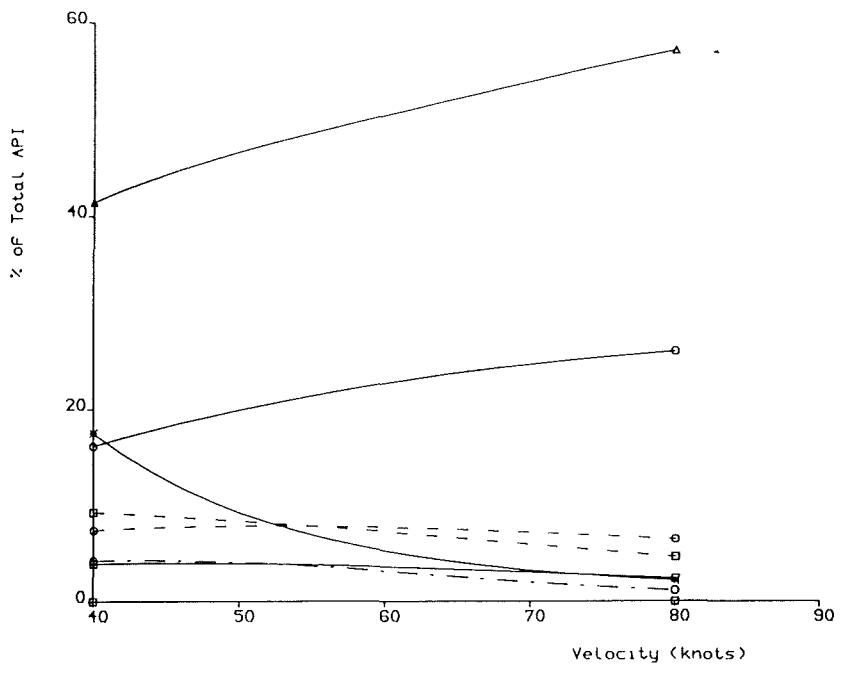


FIGURE 3.9 : Contributions to Total API For LEVEL TURN Manoeuvre
INITIAL Values of Weighting Constants
BATTLEFIELD Configuration



a) BATTLEFIELD Configuration

FIGURE 3.10 : Contributions to Total API For LEVEL TURN Manoeuvre
FINAL Values of Weighting Constants



b) TRANSPORT Configuration

- - - - ○ P
- - - - □ Q
- - . - . ○ THT
- - . - . □ PHI
- ——— ○ THT0
- ——— □ THT1S
- △ ——— △ THT1C
- * ——— * TH0TR

FIGURE 3.10 : Cont.

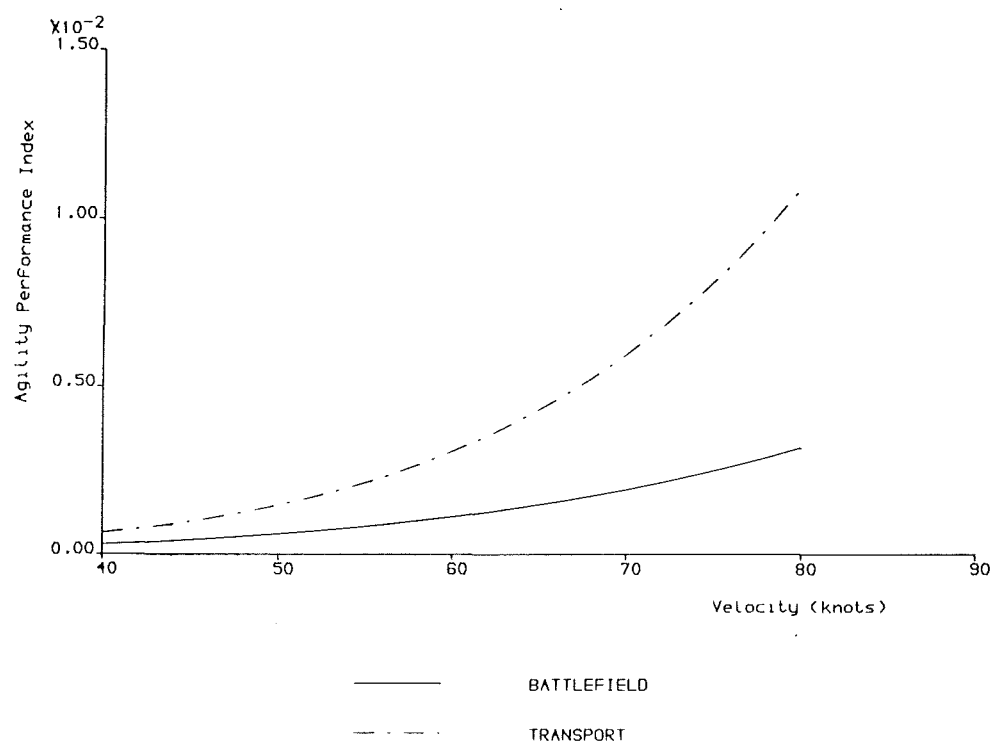


FIGURE 3.11 : API vs. Velocity For LEVEL TURN Manoeuvre of Radius 250m

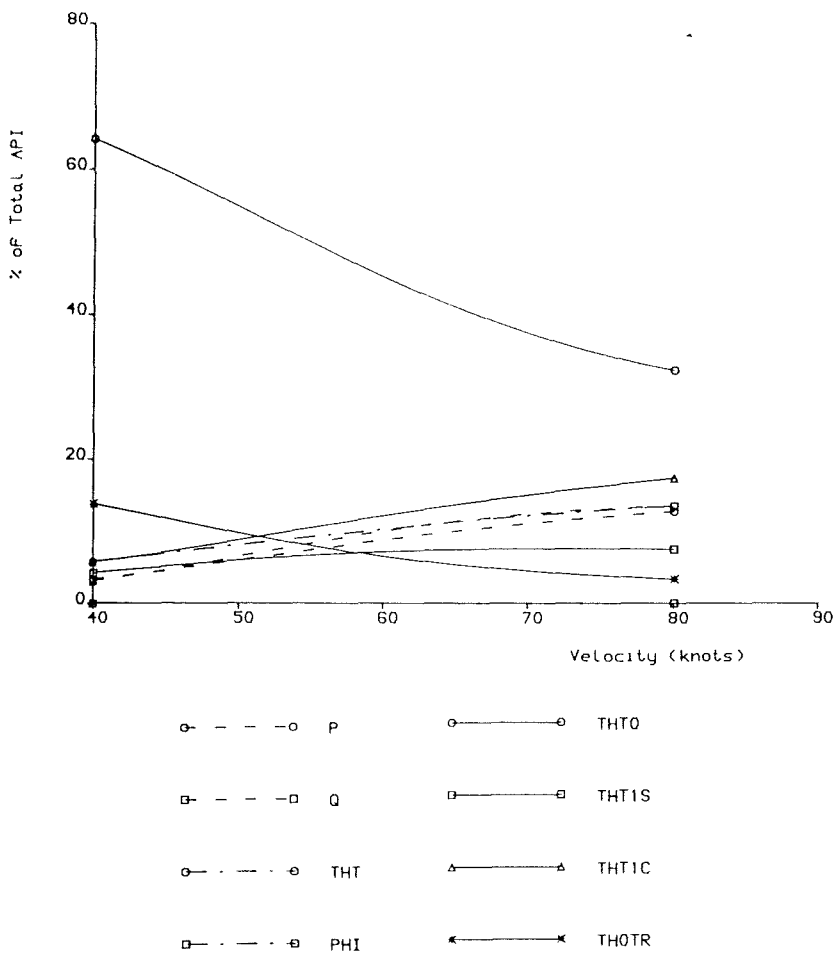
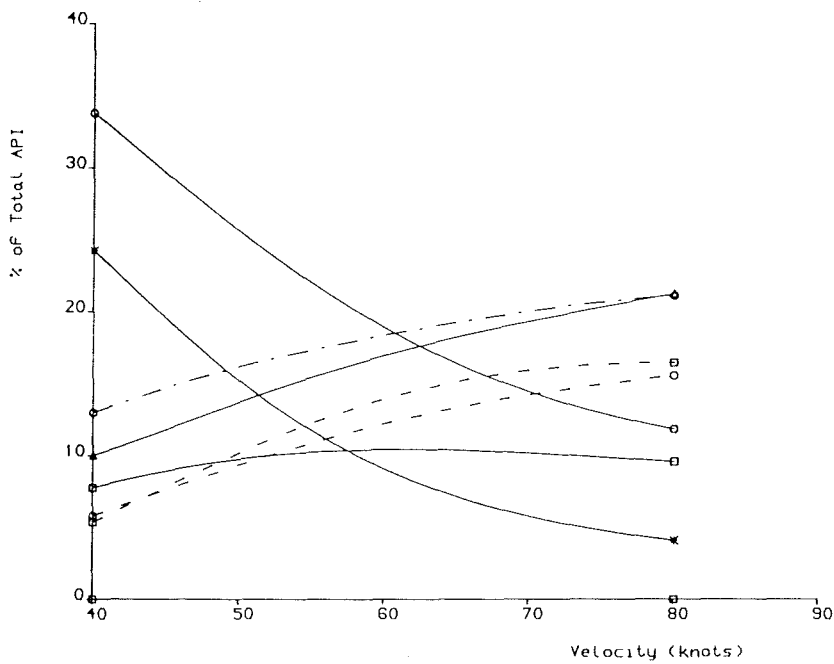
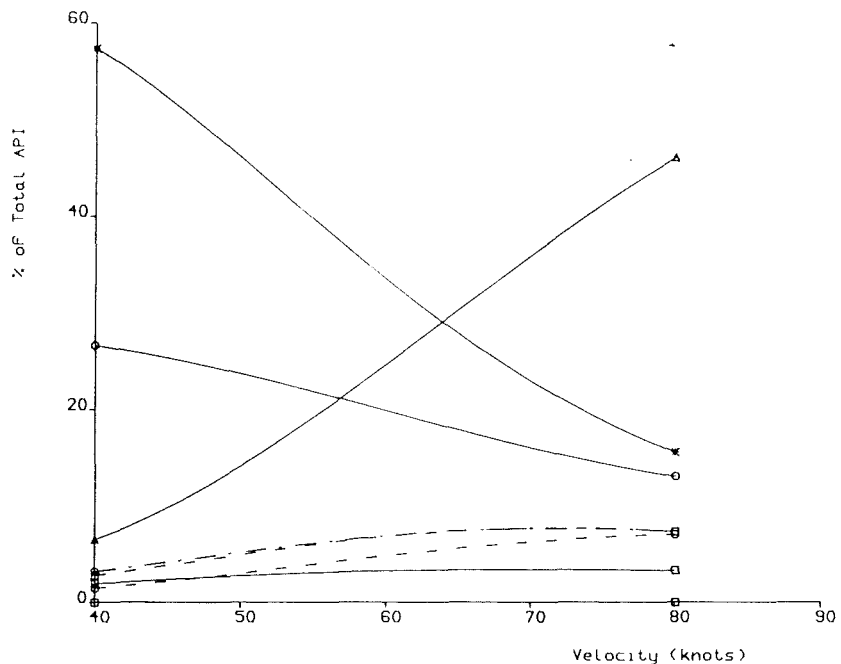


FIGURE 3.12 : Contributions to Total API For CLIMBING TURN Manoeuvre
INITIAL Values of Weighting Constants BATTLEFIELD Configuration



a) BATTLEFIELD Configuration

FIGURE 3.13 : Contributions to Total API For CLIMBING TURN Manoeuvre
FINAL Values of Weighting Constants



b) TRANSPORT Configuration

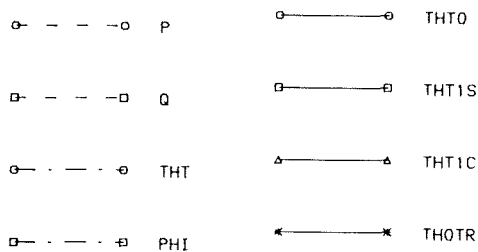


FIGURE 3.13 : Cont.

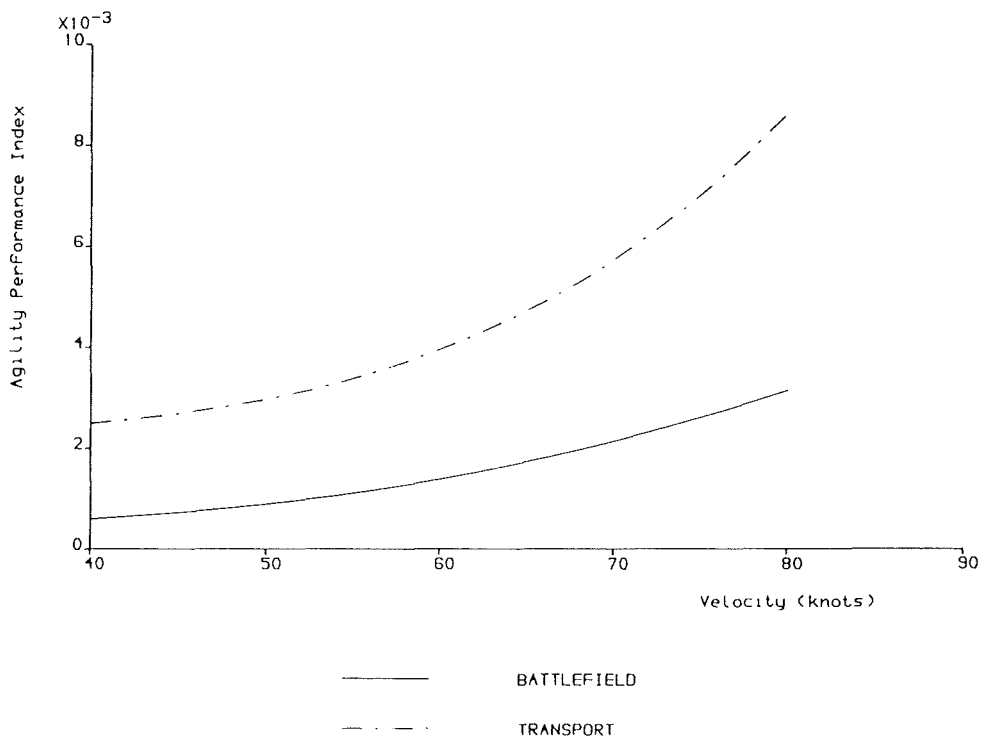


FIGURE 3.14 : API vs. Velocity for CLIMBING TURN Manoeuvre of Radius 250m to a Height of 25m

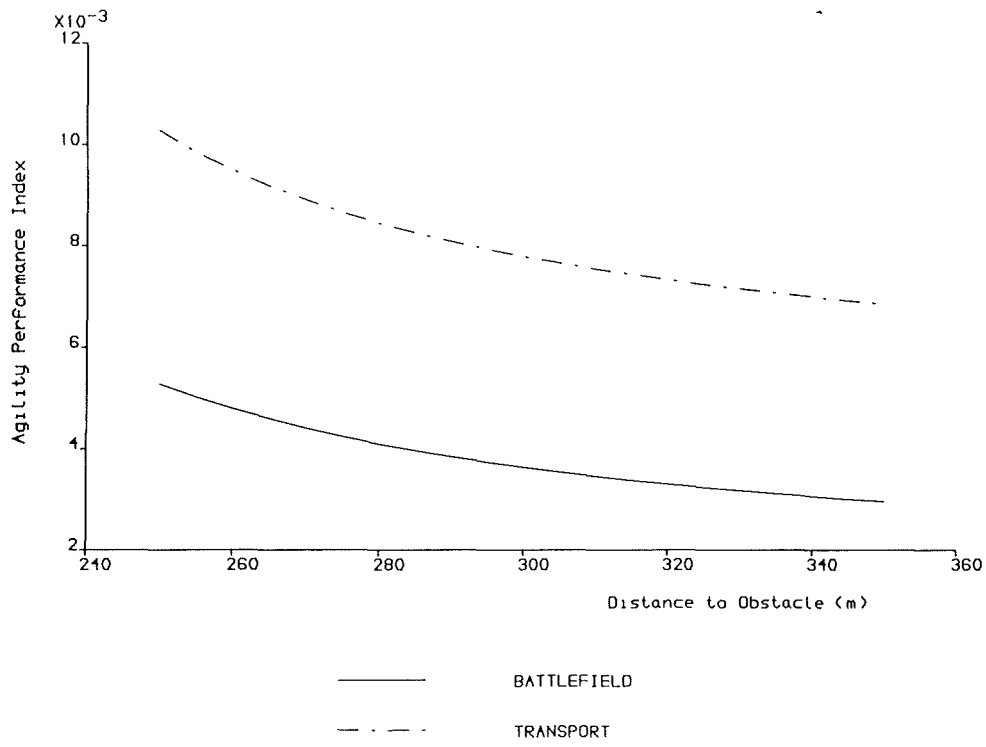


FIGURE 3.15 : API vs. Distance to Obstacle For POP-UP Manoeuvre at 80 knots.

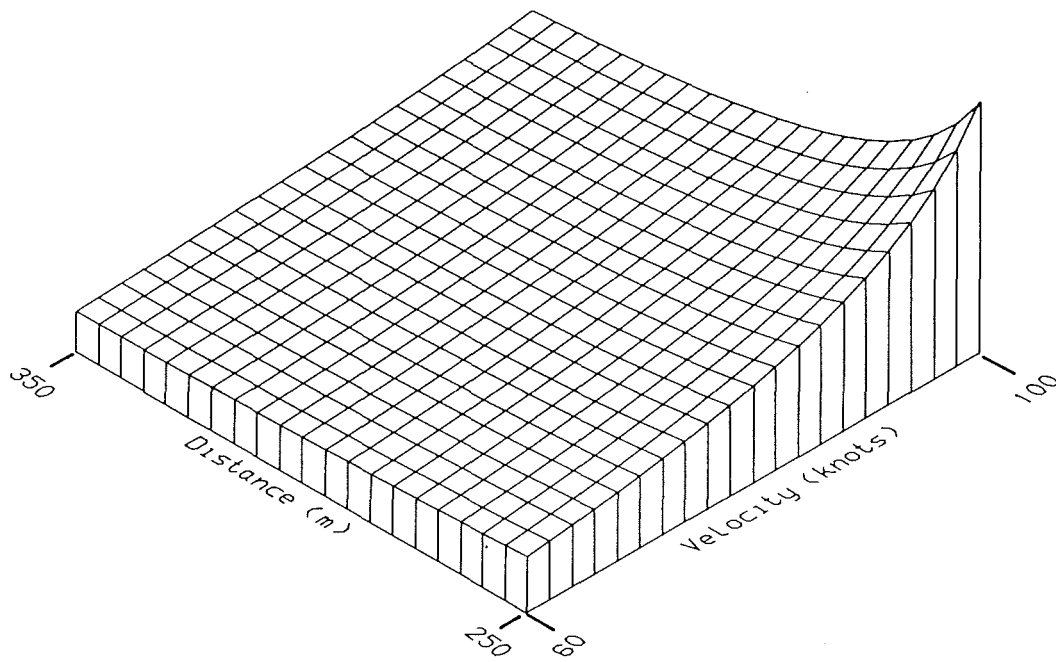
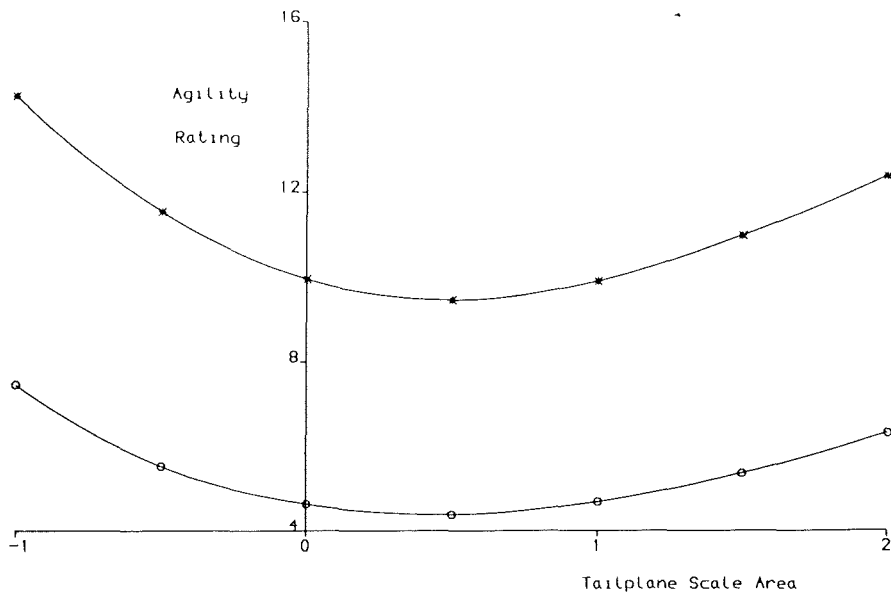
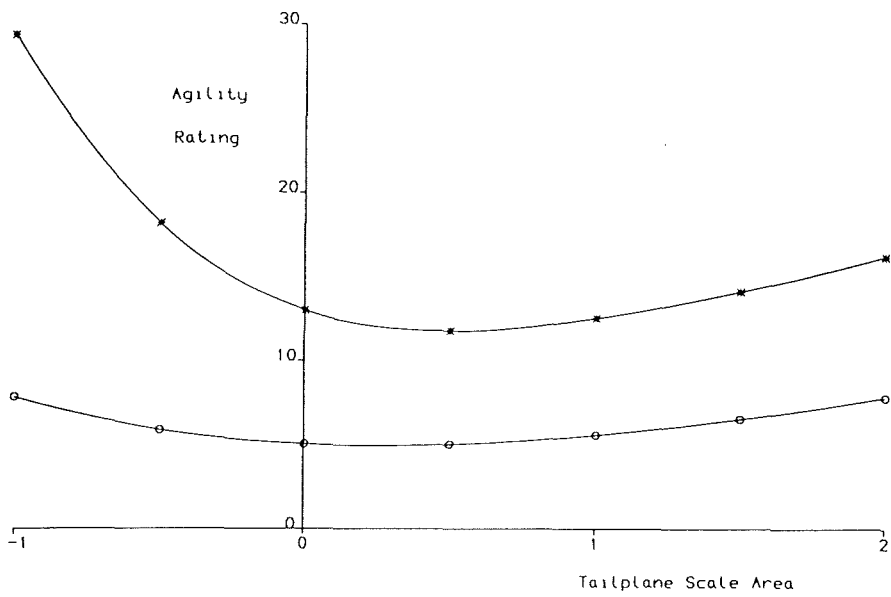


FIGURE 3.16 : Agility Surface For POP-UP Manoeuvre
BATTLEFIELD Configuration



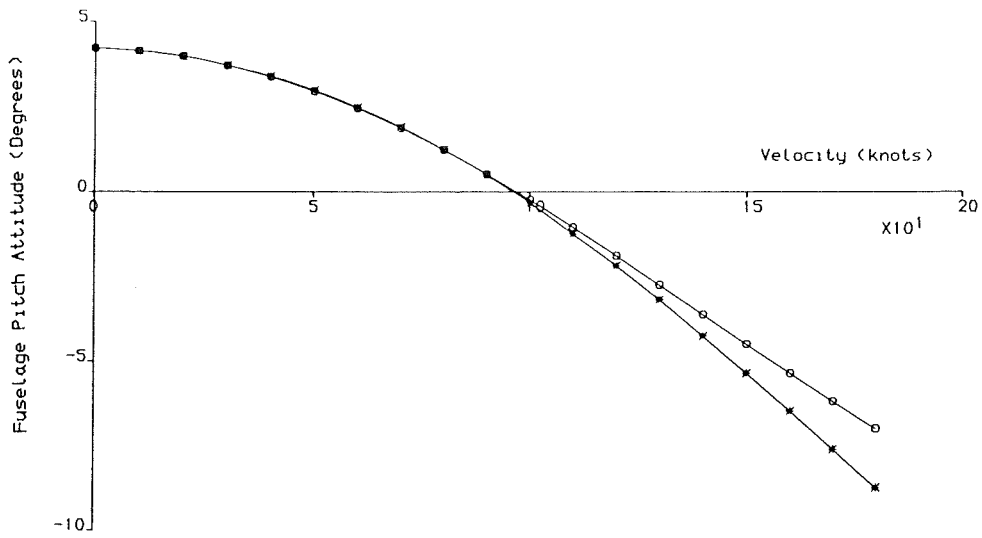
a) Results For POP-UP Manoeuvre



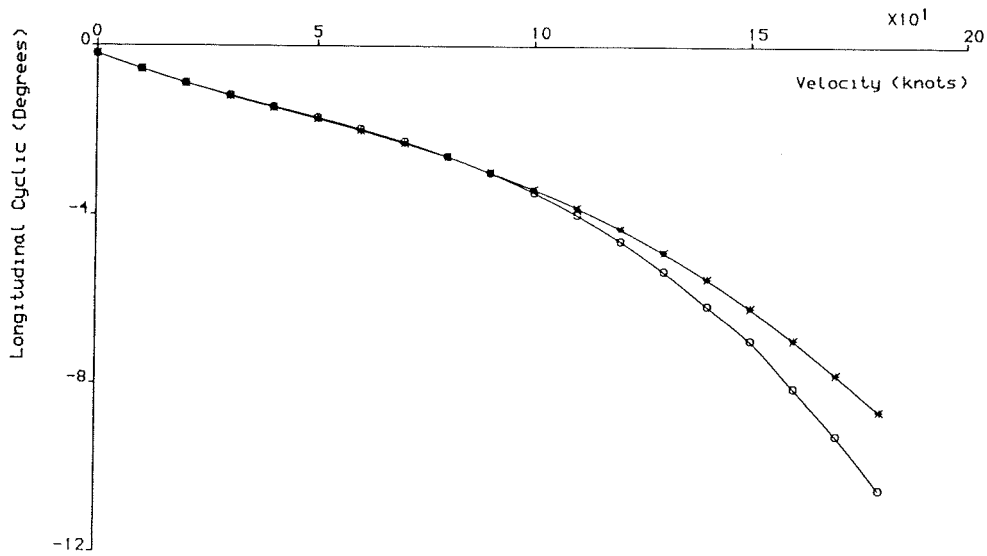
b) Results For HURDLE-HOP Manoeuvre

○ — ○ BATTLEFIELD
 * — * TRANSPORT

FIGURE 4.1 : Agility Rating vs. Tailplane Scale Area



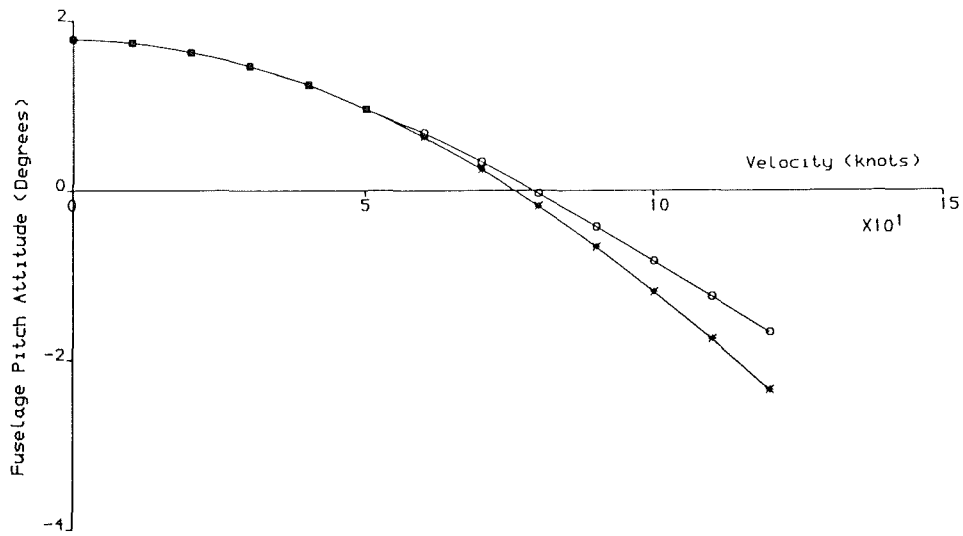
a) Fuselage Pitch Attitude vs. Flight Velocity



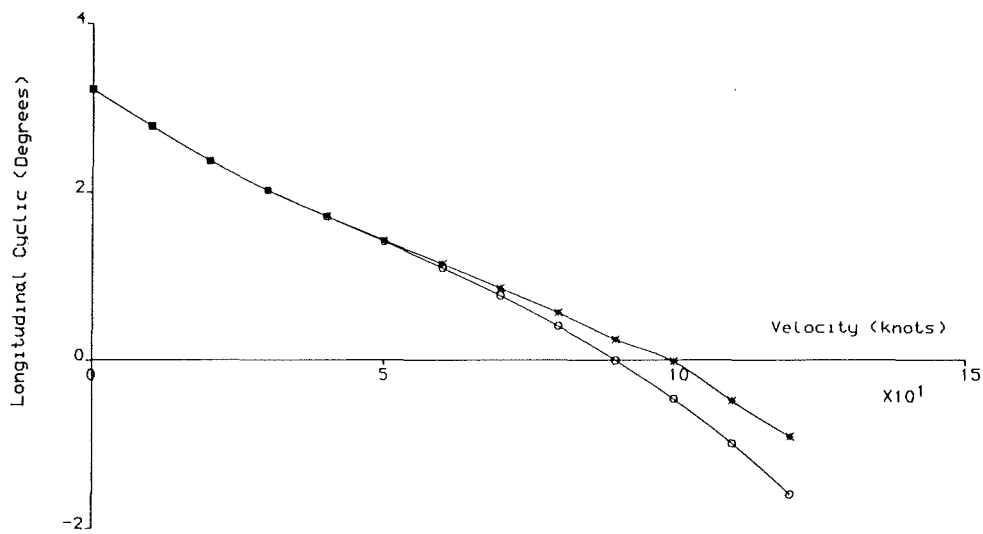
b) Main Rotor Longitudinal Cyclic vs. Flight Velocity

○ — ○ Standard Tailplane Area
 * — * Half Sized Tailplane

FIGURE 4.2 : Trim conditions for Straight and Level Flight
 BATTLEFIELD Configuration



a) Fuselage Pitch Attitude vs. Flight Velocity



b) Main Rotor Longitudinal Cyclic vs. Flight Velocity

○ — ○ Standard Tailplane Area
 * — * Half Sized Tailplane

FIGURE 4.3 : Trim conditions For Straight and Level Flight
 TRANSPORT Configuration

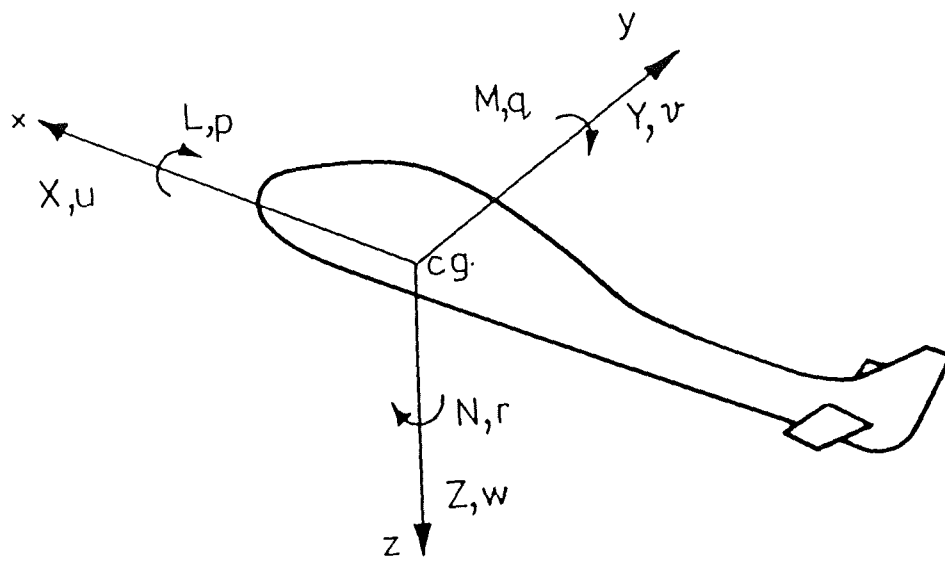


FIGURE A1 : Body Fixed Axes System

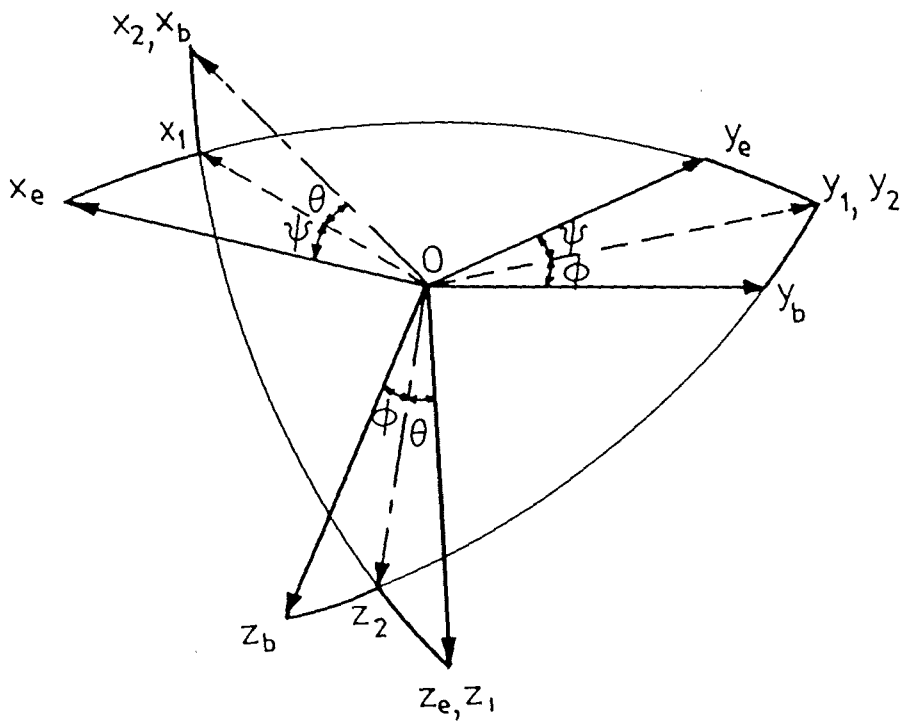
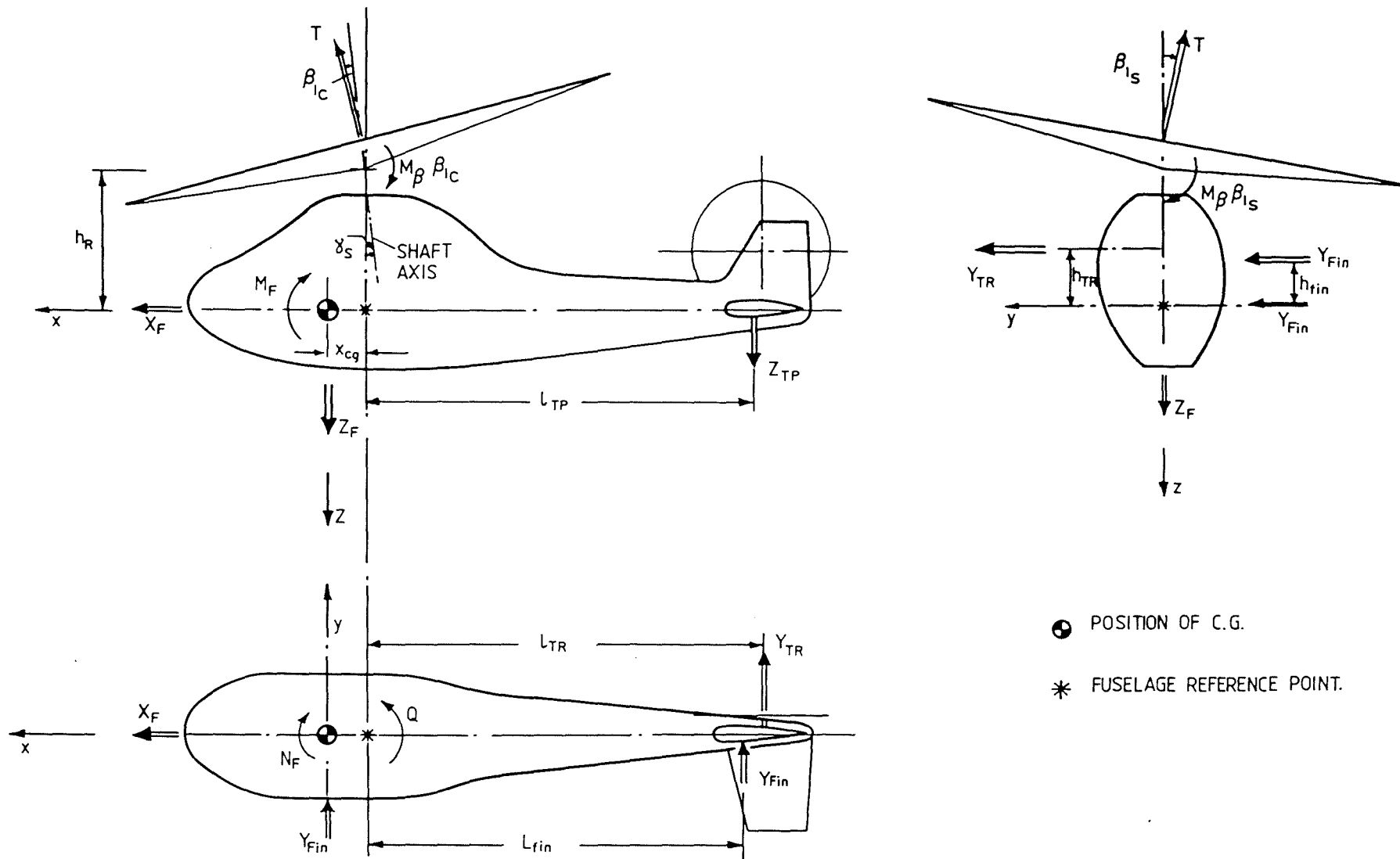


FIGURE A2 : Euler Angle Transformation



- POSITION OF C.G.
- * FUSELAGE REFERENCE POINT.

FIGURE A3 : Forces and Moments on Helicopter

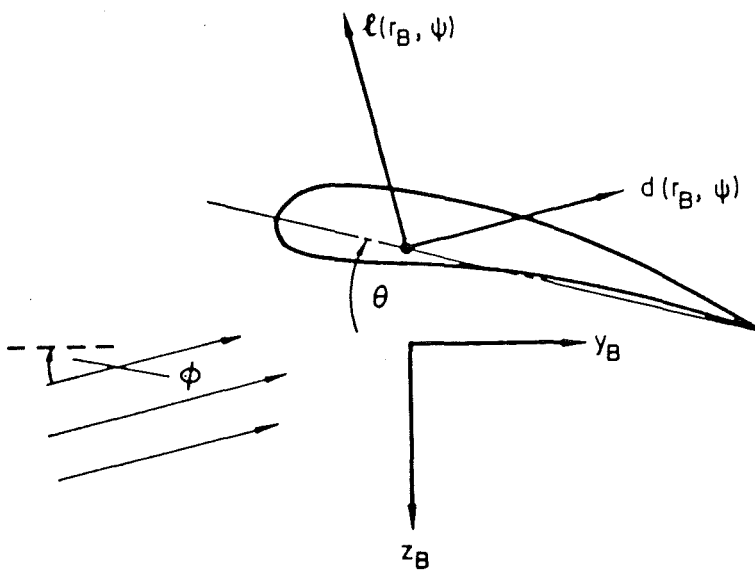


FIGURE A4 : Lift and Drag on Blade Element

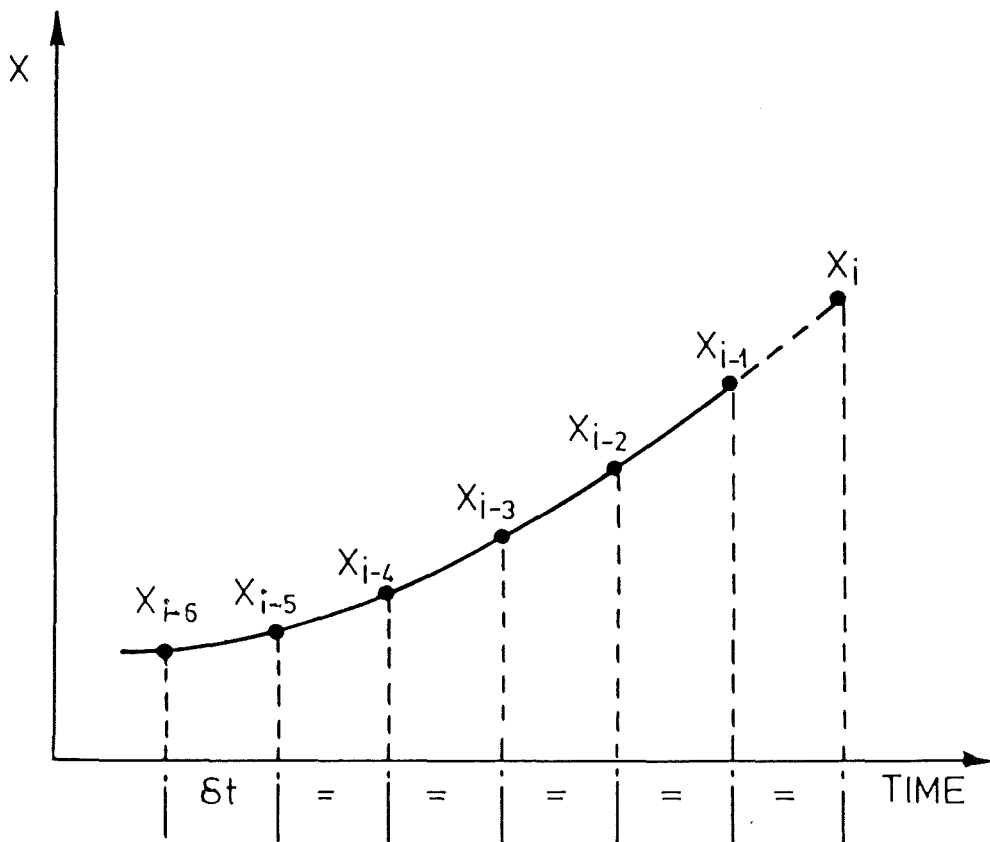


FIGURE A5 : Notation For Numerical Differentiation

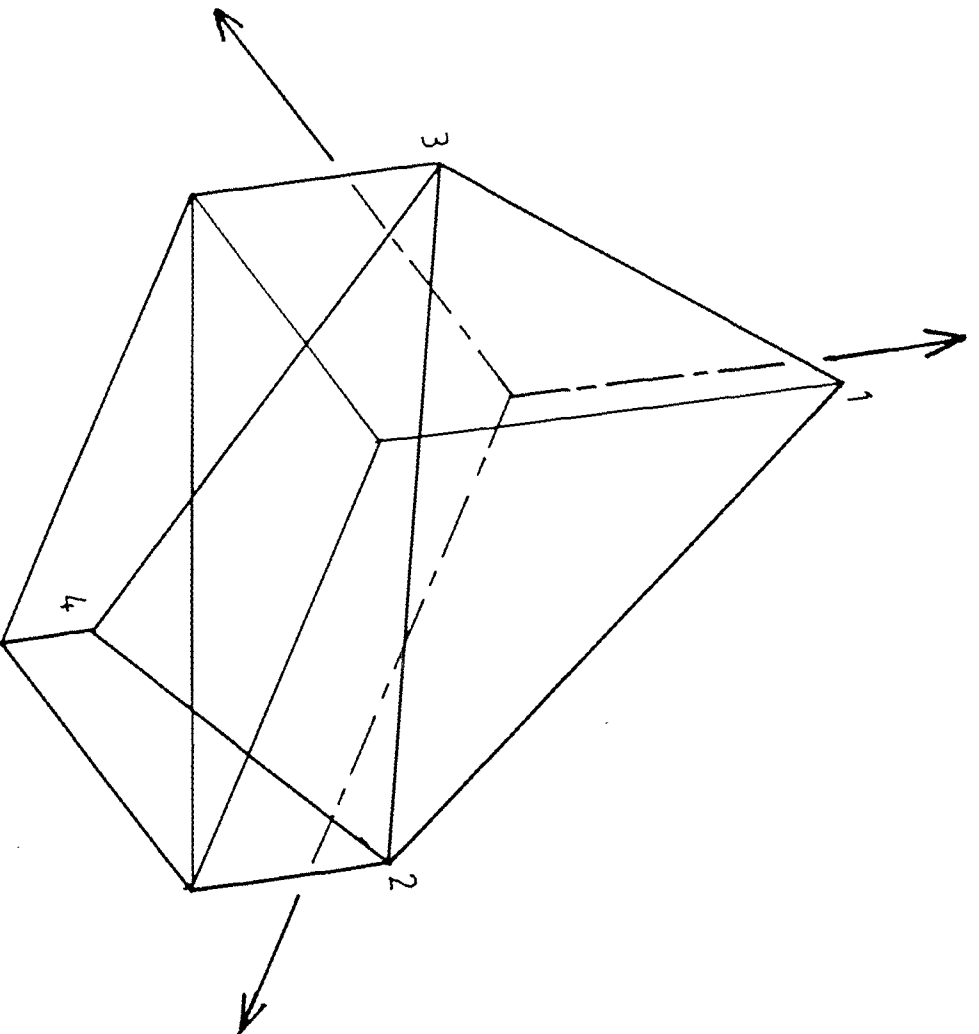


FIGURE A6 : Element of Agility Surface

